Studies on the photodynamic effects of photoactive fractions from *Fagopyrum tataricum* (L.) Gaertn and *Ficus auriculata* Lour. on skin cancer cells

Thesis submitted to the
University of Calicut in partial fulfilment of the
requirements for the award of the degree of

DOCTOR OF PHILOSOPHY IN BIOCHEMISTRY
under faculty of science

By

MERIN RINKY K

Under the guidance of
Dr. Gayathri Devi. D

DEPARTMENT OF LIFE SCIENCE
UNIVERSITY OF CALICUT
KERALA

MAY-2025

UNIVERSITY OF CALICUT
DEPARTMENT OF LIFE SCIENCES

Dr. Gayathri Devi. D
Assistant Professor
Department of Life Sciences
University of Calicut

Phone: 9447712539
E-mail: gayathrianith@gmail. com
Calicut University. P.O.,
Pin: 673635
KERALA(INDIA)

Date.....

CERTIFICATE

This is to certify that the thesis entitled **"Studies on the photodynamic effects of photoactive fractions from *Fagopyrum tataricum* (L.) Gaertn and *Ficus auriculata* Lour. on skin cancer cells."** is a bonafide research work done by **Ms. Merin Rinky K.,** under my supervision and guidance in the Department of Life Sciences, University of Calicut for the award of the degree of Doctor of Philosophy in Biochemistry, under the faculty of Science of the University of Calicut. I also certify that the same has not been submitted for any other degree, diploma or associateship in any other University.

University of Calicut
May, 2025

Dr. Gayathri Devi. D

DECLARATION

I hereby declare that the work presented in the thesis entitled **"Studies on the photodynamic effects of photoactive fractions from *Fagopyrum tataricum* (L.) Gaertn and *Ficus auriculata* Lour. on skin cancer cells."** is based on the original work done by me under the guidance of **Dr. Gayathri Devi. D**, Assistant Professor of Biochemistry, Department of Life Sciences and has not been included in any other thesis submitted previously for the award of any degree. The contents of the thesis are undergone plagiarism check using iThenticate software at C.H.M.K. Library, University of Calicut, and the similarity index found within the permissible limit. I also declare that the thesis is free from AI generated contents.

University of Calicut
May, 2025

Merin Rinky K.

Dr. Gayathri Devi. D
Assistant Professor of Biochemistry
Department of Life Sciences

CERTIFICATE

This is to certify that the suggestions recommended by the adjudicators have been incorporated in the thesis "Studies on the photodynamic effects of photoactive fractions from *Fagopyrum tataricum* (L.) Gaertn and *Ficus auriculata* Lour. on skin cancer cells" submitted by Ms. Merin Rinky K, Research scholar in Biochemistry, Department of Life Science, University of Calicut and the content of the thesis in both hard copy and soft copy are one and same.

University of Calicut

Date : 10.02.2026

Dr. Gayathri Devi D

Supervising Teacher

Head of the department
Department of Life Science
University of Calicut
Kerala, PIN- 673 635

UNIVERSITY OF CALICUT

CERTIFICATE ON PLAGIARISM CHECK

1.	Name of the Research Scholar	Merin Rinky K	
2.	Title of thesis / dissertation	Studies on the photodynamic effects of photoactive fractions from Fagopyrum tataricum (L.) Gaertn and Ficus auriculata Lour. on skin cancer cells	
3.	Name of the Supervisor	Dr.Gayathri Devi D	
4.	Department/Institution	Research Scholar, Department of Life Science, University of Calicut	
5.	Similar content (%) identified	Non Core	Core
		Introduction/ Theoretical overview/Review of literature/ Materials & Methods/ Methodology	**Analysis/Result/Discussion / Summary/Conclusion/ Recommendations**
		3	8
	Acceptable maximum limit (%)	10	10
6.	Software used	iThenticate	
7.	Date of verification	13.05.25	

**Report on plagiarism check, specifying included/excluded items with % of similarity to be attached.*

Checked by (with name, designation & signature) Dr. Nasirudheen. T
Assistant Librarian
University of Calicut, Kerala.

Name and signature of the Researcher Merin Rinky. K

Name and signature of the Supervisor. Dr. Gayathri Devi D.
Assistant Professor
Dept. of Life Sciences
Calicut University

The Doctoral Committee* has verified the report on plagiarism check with the contents of the thesis, as summarized above and appropriate measures have been taken to ensure originality of the Research accomplished herein.

Name & Signature of the HoD/HoI (Chairperson of the Doctoral Committee) 15-05-25. Dr. Gayathri Devi. D.

**In case of languages like Malayalam, Tamil etc. on which no software is available for plagiarism check, a report should be made by the Doctoral Committee, for which an additional certificate has to be attached.*

Head of the department
Department of Life Science
University of Calicut
Kerala, PIN- 673 635

ACKNOWLEDGEMENTS

I would like to take this opportunity to express my profound gratitude to all those who have supported and assisted me during my research journey.

I owe my deepest appreciation to my guide, ***Dr. Gayathri Devi D.****, Assistant Professor and Head of the Department, Department of Life Science, for introducing me to this fascinating field of study. Her scholarly recommendations, constructive critiques, continuous support, encouragement, and unwavering commitment to research have been instrumental in the completion of this thesis.*

I also extend heartfelt thanks to ***Dr. B. S. Harikumaran Thampi (Professor)****,* ***Dr. Denoj Sebastian (Professor)****,* ***Dr. E. Sreekumar (Associate professor)****,****Dr. Emmanuel Simon (Assistant Professor)****,* ***Dr. Punya Premraj (Guest Lecturer) and Dr. Sereena M.C (Guest lecturer)****, Department of Life Sciences, University of Calicut, for their guidance and encouragement.*

I wish to express my sincere gratitude to ***Mrs. Hairunneesa T.M.****, Librarian, Department of Life Sciences,* ***Mr. Jamsheer N.P.****, and* ***Dr. Nasirudheen.****, Research Desk, C.H.M.K. Library, University of Calicut, for their kind support in accessing essential resources.*

I am deeply thankful to my lab mates, ***Dr. Chanchitha Chandran****,* ***Mr. Sajil K.K.****,* ***Mr. Lijith K.P.****,* ***Ms.Vismaya K.V****,* ***Mrs. Neethu George****, and* ***Mrs. Sreeja R*** *for their constant support during my research work.*

I extend my heartfelt thanks to my friends ***Dr. Liji P.***, ***Dr. Rinju R.***, ***Dr. Chithra Pillai***, ***Mr. Kishore Haridas M.C.***, ***Dr. Rajendran N.S.***, ***Ms. Nithya Jayan***, ***Mr. Abdul Bari***, ***Dr. Abhini K. N.***, ***Dr. Bijesh K.***, ***Dr. Smitha Renganathan***, ***Mrs. Anusha T.P.***, ***Mr. Meghanath R.***, ***Dr. Sreena C.P.***, ***Dr. Ambili M.***, ***Dr. Akhila B. Rajan***, ***Dr. Rasiya K.T.***, ***Dr. Aparna Menon***, ***Mr. Ahammed Shahal***, ***Dr. Sreejesh P.G*** ,***Mrs. Sneha G.K.***, ***Ms. Aswathy, Ms. Shahala M, Ms. Renu I.C.,Ms. Kripa K., Ms. Bhasura K., Ms. Anjalikrishna M.B., Ms. Arya K.,Ms. Mahima M., Ms. Anjitha S., Mr. Vishnu Sathyan, Mrs. Vincy K Kalampalath,Ms. Akhila P.P., and Mrs. Bindu E.,*** *for their unwavering support and encouragement during research work. I would like to express my heartfelt gratitude to* ***Dr. Faisal Moosa Athikkavil***, ***Mrs. Ramya Johny, Mrs. Meghna Sudhesh, Mrs. Suhana Koothradan, Mrs. Anju V.V., Mrs. Surya P.H.,*** *and other research scholars in the Department of Biotechnology at the University of Calicut for their invaluable support throughout my Ph.D. journey. I am equally thankful to* ***Dr. Akhila A.K., Dr. Deepak Joshy, Dr. Lijin Rajan, Dr. Varsha Raveendran P.T.,*** *and fellow research scholars in the Department of Chemistry for their assistance and insightful discussions that enriched my research. My sincere appreciation extends to* ***Mr. Anadh P.P****. in the Department of Zoology, University of Calicut, for his help and encouragement during my doctoral studies. Additionally, I am grateful to* ***Mrs. Sneha Das****, research scholar at Amala Cancer Research Institute, for her support and guidance during my research endeavors.*

I extend my sincere appreciation to the staff and directors of CSIF, SAIF, CMPR, KVASU, and KFRI for their technical support in conducting various analyses critical to my study. I also extend my

thanks to Centre for Computational Biology and Bioinformatics (CCBB) university of Calicut for conducting docking studies.

I wish to express my sincere thanks to ***Mr. Rajesh*** *and other staff members of* ***Bina Photostat, Villunniyal****, for their help in printing and binding the thesis.*

I am profoundly grateful to my parents for their unwavering support and belief in me. Their sacrifices and encouragement have been the foundation of my journey. I also extend heartfelt thanks to my sister and brother-in-law for their understanding and support, and to my brother-in-law's mother for her kindness. My nephew's joy has been a source of happiness during challenging times.

To my husband, whose patience, love, and belief in me have been my anchor, I am deeply thankful. The blessings and support from my in-laws, including my sister-in-law, have provided strength and comfort.

To all my relatives, your prayers, love, and encouragement have been a constant source of motivation. I am blessed to have each of you in my life. Thank you for being my pillars of support.

I would also like to thank my friends and loved ones who have been supportive and have helped me face the most challenging situations with confidence.

Finally, I extend my thanks to everyone who has helped me during my entire work and whose names I have forgotten to mention.

Merin Rinky K

Abstract

Photodynamic therapy (PDT) represents a promising alternative to traditional cancer treatments, particularly for skin cancer, whose incidence is increasing in India. The study investigated the photodynamic potential of plant photosensitizers from *Fagopyrum tataricum* and *Ficus auriculata*, known for their content of fagopyrin and furan compounds, respectively. The photoactive fractions PAF1 (from *F. tatricum*) and PAF2 (from *F.auriculata*) were isolated by TLC fractionation of cold ethanol extracts of the aerial parts and leaves. The presence of photosensitizers was confirmed in crude extract by HPTLC. The efficacy of these fractions was investigated on A431 skin cancer cells using MTT assay, Trypan blue assay, caspase 3 assay and cell cycle analysis. They demonstrated dose and time-dependent cytotoxicity on cancer cells upon exposure to light, while exhibiting low toxicity compared to normal L929 cells. The photosensitizers present in PAF1 and PAF2 were detected using HRLCMS and GCMS analysis. Additionally, the interactions of key compounds with EGFR targets were supported by *in silico* docking studies. These results highlight the potential of plant-derived PDT agents for safer and more effective anticancer treatments. Further studies are needed to isolate the photosensitizers from the fractions and evaluate their photodynamic toxicity through further *in vitro, in vivo* and clinical studies.

Key words: Photodynamic therapy, Fagopyrum tataricum,Ficus auriculata,Fagopyrin,EGFR,Skin cancer

സംഗ്രഹം

മനുഷ്യരാശിക്ക് വെല്ലുവിളിയായി മാറിക്കൊണ്ടിരിക്കുകയാണ് അർബുദം എന്ന രോഗം. മനുഷ്യശരീരത്തിലെ എല്ലാ അവയവങ്ങളെയും ബാധിക്കുന്ന അർബുദങ്ങളോടൊപ്പം ഇന്ത്യയിൽ ചർമ്മ അർബുദവും വർദ്ധിച്ചുവരുന്നു. പരമ്പരാഗത ചികിത്സാരീതികൾ പലപ്പോഴും ദോഷകരമായ പാർശ്വഫലങ്ങൾ ഉണ്ടാക്കുന്നു. ഇതിന് ഒരു പ്രതിവിധിയായി ഉപയോഗിക്കാവുന്ന ഒരു ചികിത്സാരീതിയാണ് ഫോട്ടോ ഡൈനാമിക് തെറാപ്പി. വടക്കേ ഇന്ത്യയിൽ കാണുന്ന ഒരു തരം ഗോതമ്പ് (ഫാഗോപൈറം റ്റാറ്റാറിക്കം) എന്ന സസ്യത്തിന്റെ വേരൊഴികെയുള്ള ഭാഗവും എല്ലായിടത്തും സാധാരണയായി കാണപ്പെടുന്ന അത്തി (ഫൈക്കസ് ഓറിക്കുലേറ്റ) എന്ന സസ്യത്തിന്റെ ഇലയും ആണ് ഈ പഠനത്തിന് ഉപയോഗിച്ചത്. ഈ രണ്ട് സസ്യങ്ങളുടെയും എഥനോൾ സത്തിൽ നിന്നും വേർതിരിച്ചെടുത്ത രണ്ട് ഘടകങ്ങളായ പി. എ. എഫ് 1 ലും പി. എ. എഫ് 2 വിലും ഉള്ള ഫോട്ടോസെൻസിറ്റൈസറുകളുടെ സാന്നിദ്ധ്യം ടി. എൽ. സി, എച്ച്. പി. ടി. എൽ. സി തുടങ്ങിയ നൂതന സാങ്കേതിക വിദ്യകൾ ഉപയോഗിച്ച് സ്ഥിരീകരിച്ചു. ചർമ്മ അർബുദ കോശങ്ങളിൽ കോശങ്ങളെ നശിപ്പിക്കാനുള്ള ഈ ഘടകങ്ങളുടെ ശേഷി വിവിധ ശാസ്ത്ര പരിശോധനകളിലൂടെ (എം. ടി. ടി അസ്സെ, ട്രിപ്പാൻ ബ്ലൂ, കാസ്പെയ്സ് 3, സെൽ സൈക്കിൾ അനാലിസിസ്) പരിശോധിച്ചു. അർബുദം ബാധിച്ചിട്ടില്ലാത്ത കോശങ്ങളിൽ ഈ ഘടകങ്ങൾ ദോഷഫലങ്ങൾ ഉണ്ടാക്കുന്നില്ല എന്ന് ഈ പഠനത്തിൽ നിന്നും വ്യക്തമായി. പി. എ. എഫ് 1 ലും പി. എ. എഫ് 2 വിലും അടങ്ങിയിരിക്കുന്ന വിവിധ സംയുക്തങ്ങളെ കുറിച്ച് എച്ച്. ആർ. എൽ. സി. എം. എസ്, ജി. സി. എം.

എസ് തുടങ്ങിയ സാങ്കേതിക വിദ്യകളിലൂടെ മനസ്സിലാക്കി. കമ്പ്യൂട്ടറിൽ ലഭ്യമായ നൂതന ശാസ്ത്ര വിദ്യകൾ (ഡോക്കിംഗ്) ഉപയോഗിച്ച് ഈ ഘടകങ്ങൾ മനുഷ്യശരീര കോശങ്ങളിലെ ഇ. ജി. എഫ്. ആർ എന്ന പ്രോട്ടീനുമായി എങ്ങനെ രാസബന്ധനം ഉണ്ടാക്കുന്നു എന്ന് വിശകലനം ചെയ്തു. ഈ പഠനത്തിന്റെ ഫലങ്ങളിൽ നിന്നും പി. എ. എഫ് 1, പി. എ. എഫ് 2 എന്നീ രണ്ടു ഘടകങ്ങൾ ഫലപ്രദമായ രീതിയിൽ അർബുദരോഗ ചികിത്സക്കായി ഉപയോഗിക്കാൻ കഴിയുമെന്ന് മനസ്സിലാക്കി. എന്നാൽ ഈ ഘടകങ്ങളിൽ നിന്നും ഫോട്ടോസെൻസിറ്റൈസറുകളെ മാത്രമായി വേർതിരിച്ചെടുക്കാനും അവയുടെ ചികിത്സാരംഗത്തെ ഫലപ്രാപ്തി മനസ്സിലാക്കുവാനും കൂടുതൽ പഠനങ്ങൾ ആവശ്യമാണ്.

സൂചകപദങ്ങൾ: ഫോട്ടോഡൈനാമിക് തെറാപ്പി, ഫാഗോപൈറം റ്റാറ്റാറിക്കം, ഫൈക്കസ് ഓറിക്കുലേറ്റ, ഫാഗോപൈറിൻ, ഇ ജി എഫ് ആർ.

CONTENTS

LIST OF TABLES

LIST OF FIGURES

ABBREVIATIONS

ABTS	:	2,2′Azinobis(3ethylbenzothiazoline6sulfonic acid)
AIEPSs	:	Aggregationinduced emission photosensitizers
AK	:	Actinic Keratosis
AKT	:	Protein Kinase B
ALA	:	Aminolevulinic acid
ALFA	:	Crude extract of F. auriculata (After light exposure)
ALFT	:	Extract of F. Tataricum (after light exposure).
AO/EB	:	Acridine Orange/Ethidium Bromide
BCC	:	Basal Cell Carcinoma
BLFA	:	Crude extract of F. Auriculata (Before light exposure)
BLFT	:	Extract of F. Tataricum (before light irradiation)
BRCA 2	:	Breast Cancer 2
BRCA1	:	Breast Cancer 1
BSA	:	Bovine Serum Albumin
BSAAuNCs	:	Bovine Serum Albumin–Gold Nanoclusters
CART	:	Chimeric Antigen Receptor T Cell therapy
CB	:	Common Buckwheat
CBF	:	Common Buckwheat flowers
CDKN2	:	CyclinDependent Kinase Inhibitor 2A
CMPR	:	Centre for Medicinal Plants Research
CNS	:	Central Nervous System
CRISPR	:	Clustered Regularly Interspaced Short Palindromic Repeats
cSCC	:	Cutaneous Squamous Cell Carcinoma
CUR	:	Curcumin
CYS	:	Cysteine

Dex	:	Dextran
DMEM	:	Dulbecco's Modified Eagle Medium
DMSO	:	Dimethyl Sulfoxide
DNA	:	Deoxyribonucleic Acid
DOX	:	Doxorubicin
DPPH	:	2,2Diphenyl1picrylhydrazyl
DTT	:	Dithiothreitol
EDTA	:	Ethylenediaminetetraacetic acid
EGF	:	Epidermal growth factor
EGFR	:	Epidermal Growth Factor Receptor
EuCHE	:	EuropiumChelimic acid complex
F/DOX	:	Formamidino doxorubicin
FACS	:	FluorescenceActivated Cell Sorting
FBS	:	Fetal Bovine serum
FFF	:	FagopyrinFrich fraction
GAE/g DF	:	Gallic Acid Equivalent per gram of Dry Weight
GLU	:	Glutamic acid
HAS	:	Human Serum Albumin
HBEGF	:	HeparinBinding EGFLike Growth Factor
HEPES	:	4(2Hydroxyethyl)piperazine1ethanesulfonic acid
HER	:	Human epidermal receptor
HIS	:	Histidine
HpD	:	Hematoporphyrin Derivative
HPTLC	:	HighPerformance ThinLayer Chromatography
HPV	:	Human Papilloma Virus
IARC	:	International Agency for Research on Cancer
IC_{50}	:	Inhibitory Concentration 50
LCESIMS	:	Liquid Chromatography–Electrospray Ionization–Mass Spectrometry.
LD50	:	Lethal Dose 50%
LED	:	Light Emitting Diode
LEU	:	Leucine
lKyn	:	L Kynurenine

LYS	:	Lysine
MALT	:	Mucosa Associated Lymphoid Tissue
MAO	:	Monoamine Oxidase
MC1R	:	Melanocortin 1 Receptor
MDM2	:	Mouse Double Minute 2
MET	:	Methionine
MHC	:	Major Histocompatibility Complex
5 MOP	:	5Methoxypsoralen
8 MOP	:	8Methoxypsoralen
MTAD	:	Mixture of Tetracycline, Acid, and Detergent
MTT	:	3(4,5dimethylthiazol2yl)2,5diphenyltetrazolium Bromide
NFκB	:	Nuclear Factor kappalightchainenhancer of Activated
NIR	:	Near Infrared
NP	:	Nanoparticles
OD	:	Optical Density
PAF	:	Photoactive fraction
PBS	:	Phosphate Buffered Saline
PDD	:	Photodynamic Diagnostics
PDI	:	Photodynamic Inactivation
PDT	:	Photodynamic Therapy
PEEK	:	Polyetheretherketone
PI	:	Propidium iodide
PI3K	:	Phosphoinositide 3Kinase
pNA	:	ParaNitroaniline
Pp IX	:	Protoporphyrin Nine
PRO	:	Proline
PS	:	Photosensitizer
PTCH 1	:	Patched 1
PTT	:	Photothermal Therapy
PUVA	:	Psoralen and Ultraviolet A
PVA	:	Polyvinyl Alcohol
RCC	:	Renal Cell Cancer
RF	:	Riboflavin

Rf	:	Retention factor
ROS	:	Reactive Oxygen Species
RT	:	Radiation Therapy
SCC	:	Squamous Cell Carcinoma
SCGE	:	SingleCell Gel Electrophoresis
SER	:	Serine
$SnCe_6$	:	Sn(IV)chlorin e_6
STAT 3	:	Signal Transducer and Activator of Transcription 3
TB	:	Tartary Buckwheat
TBF	:	Tartary Buckwheat flowers
TGFα	:	Transforming growth factor alpha
THR	:	Threonine
TLC	:	Thinlayer Chromatography
TNF	:	Tumor Necrosis Factor
TPP	:	Tripolyphosphate
TRP	:	Tryptophan
TYR	:	Tyrosine
UA	:	Uric Acid
UV	:	Ultra Violet
VAL	:	Valine
WHO	:	World Health Organization

Chapter 1
Introduction

1.1 Statistics of cancer around the world

Cancer continues to be one of the biggest threats to world health, and it is anticipated that its effects will become much more intensified in the decades to come. According to the American Cancer Society, there will be over 600,000 cancer related fatalities (about 1700 per day) and over 2 million new cases (around 5600 per day) in the US in 2025. The most prevalent cancers in women are colorectal (7%), lung (12%), and breast (32%) cancers. They are the colorectal (8%), lung (11%), and prostate (30%) in men. For both men and women, lung cancer is the most deadly type (Siegel *et al*.,2025). In the year of 2022, the World Health Organization (WHO) stated that there were roughly 9.7 million deaths attributable to cancer and nearly 20 million new cases of cancer throughout the globe. According to the Institute (n.d.), it is anticipated that by the year 2040, these numbers will significantly increase to 29.9 million new cases and 15.3 million fatalities annually. This increase will be driven by population growth, ageing, and environmental factors (Sung *et al*., 2021). Figure 1.1 presents an all-encompassing compilation of statistics associated with cancer.

Figure 1.1: Cancer statistics-today and tomorrow

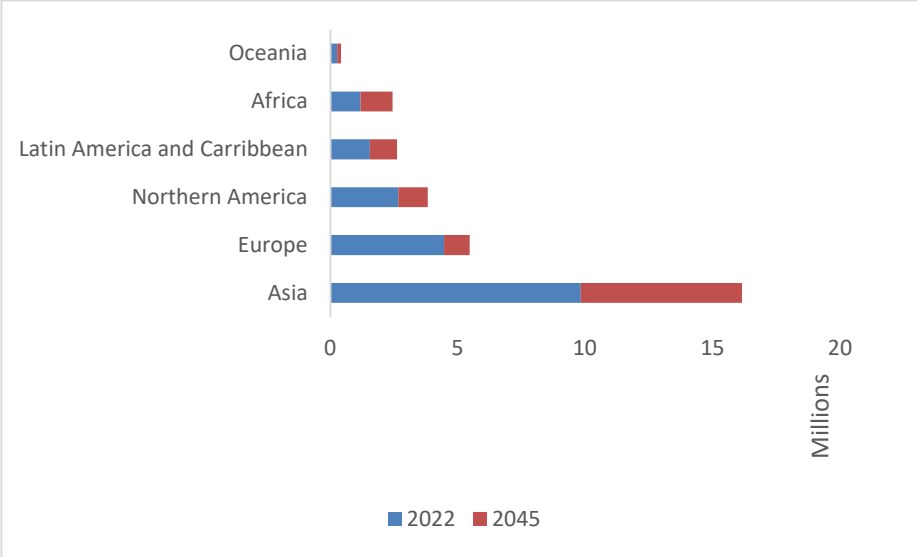

(Data sourced from https://gco.iarc.fr/en) Estimated number of new cancer cases (both sexes, age group 0–85+) projected from 2022 to 2045 for all cancer types.

1.2 Cancer in developed nations

Melanoma of the skin, breast cancer, prostate cancer, lung cancer, colorectal cancer, and lung cancer are some of the most common types of cancer that are diagnosed in wealthy countries like the United States. According to American Cancer Society, by the year 2024, approximately two million people in the United States will have been diagnosed with cancer, which would be the highest number of cancer diagnoses ever recorded. Concerns continue to be expressed regarding the rapidly increasing cancer rates among women, as well as disparities that have an effect on particular demographic groups (Dizon *et al*., 2024). Despite the fact that earlier diagnosis is growing and improving the rates of cure, this continues the case. There is a

significant amount of progress being made in the United States of America in relation to survivorship. As of January 2022, there are around 18.1 million cancer survivors in the United States. It is estimated that around 5.4% of the total population of the United States is represented by this percentage (Caffrey, 2023). This figure is projected to increase to 26 million by the year 2040, according to projections made by the American Cancer Society (2014). These projections are an indication of the success of improved treatments and early detection techniques.

1.3 Cancer in developing nations: India's growing crisis

Around 1.46 million new instances of cancer have been identified in India in 2022, and it is anticipated that the number of cancer cases will increase by 12.8% by the year 2025. There is an important rise in the incidence of children malignancies, particularly lymphoid leukemia, whereas the most prevalent forms of cancer in women are breast cancer and lung cancer in males. Alterations in lifestyle, environmental variables, high rates of tobacco use, and poor diet are all factors that contribute to the progression of the disease. In contrast to affluent countries, cancer cases in India are frequently identified at later stages, leading to an important reduction in the percentage of patients who overcome the disease (https:// ncdirindia.org/display/wcd.aspx).

1.4 Addressing the global cancer disparity

Public health policies, awareness campaigns, infrastructure improvements in healthcare, and interactions among each other

provide to minimizing the cancer load worldwide. Early assessment, immunotherapy, and precision medicine have greatly improved cancer outcomes in industrialized nations; nonetheless, there are difficulties to be addressed, especially in the goal of reducing inequality encountered by people who have fewer resources.

First goals for developing nations like India should be early identification, more access to high-quality medical treatment, and addressing of risk factors related with lifestyle choices. One cannot overestimate the importance of public health campaigns supporting better diets, stress the need of stopping smoking, and encourage more physical exercise. Especially in rural areas lacking more healthcare facilities than in metropolitan areas, the healthcare system also need major changes to close the treatment difference.

Still extremely important, though, are international organizations such as the World Health Organization (WHO) and the International Agency for Research on Cancer (IARC) in helping campaigns to decrease cancer rates worldwide. These organizations give technologies, funds, and policies to enable rich and underdeveloped nations have decreasing cancer rates.

1.5 What is cancer?

Cancer can be defined as a disorder that arises from modifications in somatic cells that are either genetic or epigenetic in nature, resulting in aberrant and unregulated cell growth. According to Sitki (2019), it is a type of neoplasm that is characterized by the production of tumors that may present as localized lumps or diffuse

masses and have the potential to spread to other parts of the body. In multicellular organisms, cancer relates to a category of disorders that are distinguished by genetic changes that disturb normal cell division and differentiation as well as other normal processes. An imbalance like this encourages the growth of tumors, which are characterized from benign malignancies by their capacity to penetrate tissues, disseminate to lymph nodes, and metastasize to organs that are located in remote locations. Cancer is characterized by a wide range of clinical and phenotypic characteristics, including heterogeneity in terms of invasiveness, proliferation, and responsiveness to treatment. In spite of these differences, it is important to note that malignancies share similar molecular characteristics, which are caused by changes in gene expression. Despite the fact that some indolent forms of cancer may remain undetectable without decreasing life expectancy, malignancies often cause dangerous morbidity and mortality if they are not treated by medical professionals.

1.6 Types of cancer

There are several over a hundred distinct forms of cancer, each of which behaves differently and responds differently to treatment. Cancer can be generated by the aberrant multiplication of different cell types in the body, which can lead to the development of cancer. Being able to differentiate between benign and malignant tumors is a critical component of the research field of cancer pathology (Khalaf *et al*., 2024).

1.6.1 Carcinomas

Carcinomas are tumors that originate in epithelial tissues, such as the skin, glands, and the linings of internal organs. Breast cancer,

prostate cancer, colorectal cancer, and lung cancer are all examples of solid tumors.

1.6.2 Sarcomas

Cancers that develop in connective and supporting tissues, such as nerves, tendons, joints, fat, blood vessels, bones, lymph vessels, muscles, and cartilage, are commonly referred to as sarcomas.

1.6.3 Leukemias

Cancers of the blood that are caused by the uncontrolled proliferation and change of healthy blood cells are referred to as leukemias. Acute myeloid leukemia, acute lymphocytic leukemia, chronic myeloid leukemia, and chronic lymphocytic leukemia are the types of malignancies that fall under this category.

1.6.4 Lymphomas

Beginning in the lymphatic system, which is a network of glands and containers that fights infection, lymphomas are the second type of cancer. Hodgkin lymphoma and non-Hodgkin lymphoma are the two types of lymphomas that they come under.

1.6.5 Central Nervous System Cancer

Cancers that develop in the tissues of the brain or spinal cord are referred to as cancers of the central nervous system (CNS). These cancers include brain tumors, primary CNS lymphomas, gliomas, pituitary adenomas, and meningiomas.

1.6.6 Multiple myeloma

The cancer of plasma cells, which are a type of immune cell, is commonly referred to as multiple myeloma. The accumulation of these myeloma cells in bone marrow results in the formation of tumors in the bones. This condition is also referred to as plasma cell myeloma or Kahler's disease.

1.6.7 Melanomas

Melanomas are cancers that develop in melanocytes, which are the cells of the skin that generate pigment. Despite the fact that they are most commonly found on the skin, melanomas may develop in other pigmented tissues, such as the eyes.

1.6.8 Other Tumors

Among the other types of cancers, germ cell tumors are those that develop from cells that create eggs or sperm. Any area of the body could be affected by these tumors, whether they are benign or malignant. Neuroendocrine tumors are formed when, in response to signals from the neurological system, cells generate hormones and release them into the bloodstream. Hormonal imbalances are caused by these tumors, which can be either benign or malignant. The symptoms of these tumors vary depending on the amounts of hormones.

1.7 Causes of cancer

There is a complex interaction between environmental, behavioral, and hereditary factors that leads to the development of

cancer. Each of these factors has an influence on the progression of the disease.

1.7.1 Genetic factors

Whether they are inherited or acquired, some genetic alterations considerably increase or decrease the probability of cancer: Inheritable Mutations: Some hereditary mutations, such those identified in the BRCA1 and BRCA2 genes, enhance a person's risk of becoming cancers including breast and ovarian cancer, claims King *et al*. (2003).

Somatic mutations: Conversely, somatic mutations are acquired mutations occurring within particular cells over the course of a person. Usually originating from either carcinogens or natural mistakes, these alterations result in the development of tumors (Stratton *et al*., 2009).

Oncogenes and Tumor Suppressor Genes :Vogelstein and Kinzler (2004) claim that cancer originates when oncogenes which are in charge of encouraging cell development are turned on or when tumor suppressor genes which are in charge of preventing growth are switched off.

1.7.2 Environmental factors

DNA damage and cellular alterations are two of the ways in which environmental exposures contribute to the occurrence of cancer. Tobacco smoke: According to Doll and Peto (1981), tobacco smoke is an important carcinogen that is responsible for 22 percent of all cancer

deaths worldwide. It is also closely associated to malignancies of the lungs, throat, and bladder.

UV-Radiation: Sunlight and tanning beds both contribute to an increased risk of developing skin malignancies such as melanoma and basal cell carcinoma (Armstrong & Kricker, 2001). UV radiation is a type of radiation that consists of ultraviolet light.

Occupational Exposures: Certain professions are at risk for exposure to carcinogens such as asbestos (which can cause mesothelioma), benzene (which can cause leukemia), and arsenic (which can cause lung and skin cancers) by Driscoll *et al*. (2004).

1.7.3 Lifestyle factors

One's chance of developing cancer is much changed by their choices on nutrition, level of physical activity, and alcohol intake: Diet*:* The World Cancer Research Fund (2018) links obesity, low fruit and vegetable consumption, and red and processed meat excess to colorectal cancer as well as other types of cancer. Physical activity: Regular physical activity has the ability to influence hormones, metabolism, and immune system, which in turn decreases the risk of acquiring cancers like breast, colon, and endometrial cancer, claims Friedenreich *et al*. (2016). Alcohol consumption: According to Bagnardi *et al.* (2015), drinking alcohol increases the risk of esophageal, breast, and liver cancers; the risk rises in direct proportion to the consumption of alcohol.

1.7.4 Infectious agents

It is possible for infections to play a role in the growth of cancer by causing persistent inflammation, lowering the immune system, or modifying DNA: Human Papillomavirus: According to Bosch *et al*. (2013), the Human Papillomavirus (HPV) is linked to numerous malignancies, particularly cervical cancer, as well as certain anogenital and head and neck cancers.

Hepatitis B and C: According to El-Serag (2012), chronic infection with the hepatitis B and hepatitis C viruses can result in the occurrence of liver cancer. Helicobactor pylori: According to Uemura *et a*l.'s 2001 research, Helicobacter pylori has been linked to both stomach cancer and MALT lymphoma.

1.7.5 Interactions between factors

The development of cancer is a complex process that frequently incorporates interactions between genetic material, environmental variables, and lifestyle choices. For example, people who have a genetic predisposition to melanoma are at a higher risk of developing the disease if they have been exposed to the sun for an extended period of time (Berwick *et al*., 2014).

1.8 Characteristics of cancer cells

Specific characteristics of cancer cells allow their survival, spread, and development. Many cite these features as the hallmarks of cancer. These include the ability to avoid programmed cell death (apoptosis), the capacity to generate angiogenesis to guarantee a supply

of oxygen and nutrients, and the capacity for growth uncontrolled in reaction to abnormalities in the management of the cell cycle. Genomic instability allows them to invade surrounding tissues and distribute to far-off organs by accelerating the mutation process and increasing the heterogeneity of tumors. Transforming their energy metabolism, cancer cells exhibit a preference for glycolysis even in environments rich in oxygen (a process frequently known as the Warburg effect). Moreover able to avoid immune surveillance by downregulating MHC molecules or producing immunological checkpoint proteins is cancer cells. Moreover, they maintain proliferative signaling by means of growth-promoting pathways triggered independent of outside cues. Knowing these characteristics enables one to have intelligent analysis of the evolution of cancer and establish the basis for the development of tailored treatments including immunotherapy and precision medicine, therefore improving findings for patients.

1.9 Skin cancer

The sixth most fast growing kind of cancer globally is skin cancer. Cells which make up the skin generate tissues; cancer results from aberrant or unchecked proliferation of these cells either inside the afflicted tissue or extending to nearby tissues. One may categorize this aberrant pattern of cell development as either benign or malignant. Typically benign and non-cancerous, benign tumors include moles. Malignant tumors, on the other hand, are cancerous and carry a life-threatening risk since they can spread to and destroy other body tissues (Pal *et al.*, 2020). Some skin cancer facts are listed in Figure 1.2.

Figure 1.2: Some skin cancer facts

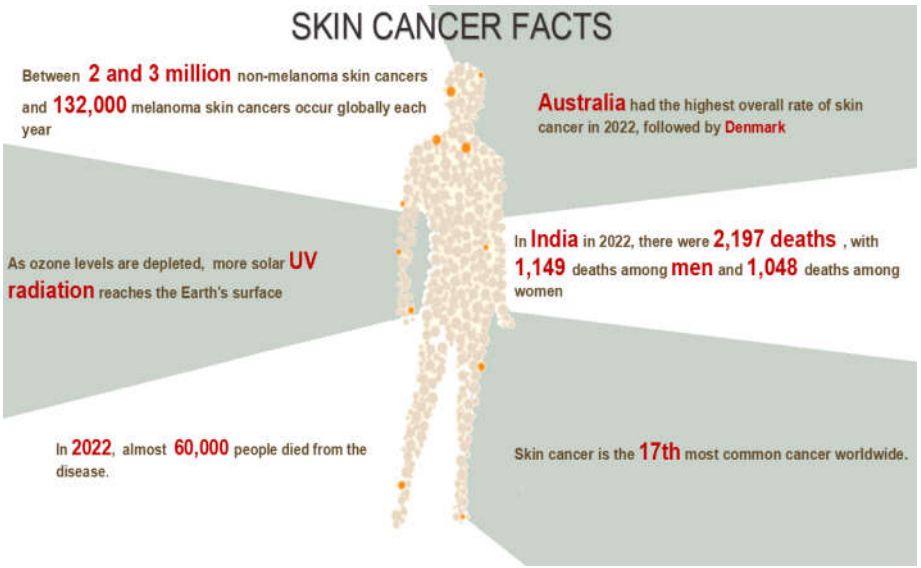

Data source: https://www.wcrf.org/cancer-trends/skin-cancer-statistics/, https://www.who.int/news-room/questions-and-answers/item/radiation-ultraviolet-(uv)-radiation-and-skin-cancer, https://www.iarc.who.int/cancer-type/skin-cancer/.

1.9.1 Causes of skin cancer (Craythrone *et al*., 2017)

The risk of developing skin cancer results from a combination of genetic and environmental factors, with prolonged exposure to ultraviolet (UV) light being the most common cause.

Genetic factors: Skin cancer risk is significantly influenced by a patient's skin pigmentation phenotype; those with low Fitzpatrick phototype are more likely to be diagnosed with skin cancer. Those with red hair and freckles who have two copies of the R allele form of the MC1R gene also run more risk of skin cancer. Rare autosomal recessive syndrome Xeroderma pigmentosa is a defect of DNA repair whereby UV-induced damage cannot be restored. This disorder raises one's vulnerability to early childhood skin malignancies, sunburn, and

freckling. Multiple basal cell carcinomas (BCCs) in affected individuals arise from uncontrolled cell proliferation carried on by an autosomal dominant condition known as basal cell nevus syndrome, which results from a mutation in the tumor suppressor gene PTCH1.

While 90% of melanomas are believed to occur sporadically, some inherited mutations have been identified. The most common genetic cause of inherited melanoma is a mutation in the CDKN2A gene. Additionally, mutations in the MDM2 gene increase the likelihood of women developing melanoma at an earlier age.

Environmental factors: The primary risk factor for melanoma is exposure to UV radiation, including sunlight and sunbeds. Additional risk factors include having more than 50 naevi, multiple atypical or dysplastic naevi, exposure to arsenic, immunosuppression (especially in transplant patients), and viral infections such as human papillomavirus.

1.9.2 Types of skin cancer

In the skin, there are three various kinds of cells: basal cells, squamous cells, and melanocytes. Each of these cells has the potential to transform into malignant cells. The most serious kind of skin cancer is melanoma, followed by basal cell carcinoma (BCC) and squamous cell carcinoma (SCC). Melanoma is the most widespread form of skin cancer.

1.9.2.1 Basal cell carcinomas

The most prevalent type of skin cancer is referred to as basal cell carcinoma (BCC), and it is frequently associated with prolonged exposure to the sun as well as mutations in the p53 gene or the PTCH1 gene. Patients over the age of 40 are frequently affected by them, and their progression is sluggish; nevertheless, certain types might be locally aggressive. BCCs seldom spread to other parts of the body, but left untreated, they can cause substantial morbidity. There are subtypes that are classed as low-risk and high-risk, accordingly.

The following are instances of low-risk subtypes of basal cell carcinoma:

- Superficial BCCs: These are well-defined plaques that are often red, pink, or brown in colour and usually appear on the trunk. . Pearly white, nodular lesions with telangiectasia are the most prevalent subtype of basal cell carcinoma (BCC) that are classified as nodular. The following are instances of high-risk subtypes:
- Infiltrative and morphoeic basal cell carcinomas: those that are aggressive, deeply infiltrating, and have an appearance equivalent to a scar. In addition to being yellow or white in colour, micro nodular basal cell carcinomas have a waxy and solid texture.

1.9.2.2 Squamous cell carcinoma

Squamous cell carcinoma, often known as SCC, is a type of cancerous tumor that originates from squamous keratinocytes that accumulate in the skin or inside the mucous membranes. The condition

is more common on skin that has been affected by photodamage, particularly in people who have fair Fitzpatrick skin types. When unfavorable prognostic markers are present, such as tumor size (more than 2 cm), depth (greater than 4 mm), position on the lower lip or ear, immunosuppression, and histological subtype, the spreading potential of squamous cell carcinoma (SCC) might increase to as much as thirty percent. In additional to chronic immunosuppression, scarring conditions, smoking, arsenic exposure, and human papillomavirus infection, ultraviolet radiation is a particularly significant predictor of the development of this disease.

1.9.2.3 Melanoma

The number of instances of melanoma that occur each year is dramatically rising. It is characterized by the development of a new or changing pigmented lesion, which often happens in sun-exposed areas in individuals with fair skin, and it can manifest in a number various subtypes. An excellent prognosis can be obtained with early discovery and treatment; however, this prognosis significantly deteriorates as the thickness of the lesion develops. Melanocytic nevus, actinic keratosis (AK), benign keratosis, dermatofibroma, and vascular lesions are some of the other types of keratosis.

1.9.3 Rising threat: The growing burden of skin cancer in India

While skin cancer rates are relatively low in India compared to countries with predominantly fair-skinned populations, it remains an important public health issue, particularly in regions with high UV exposure, such as high-altitude areas in the Himalayas. India's diverse population has varying degrees of melanin, which offers some natural protection against UV radiation. However, environmental factors,

occupational hazards, and lack of awareness contribute to the burden of skin cancer, especially in rural areas. Figure 1.3 indicates that the incidence of skin cancer in India is projected to increase in the future.

Figure 1.3: Skin cancer statistics-today and tomorrow in the Asia

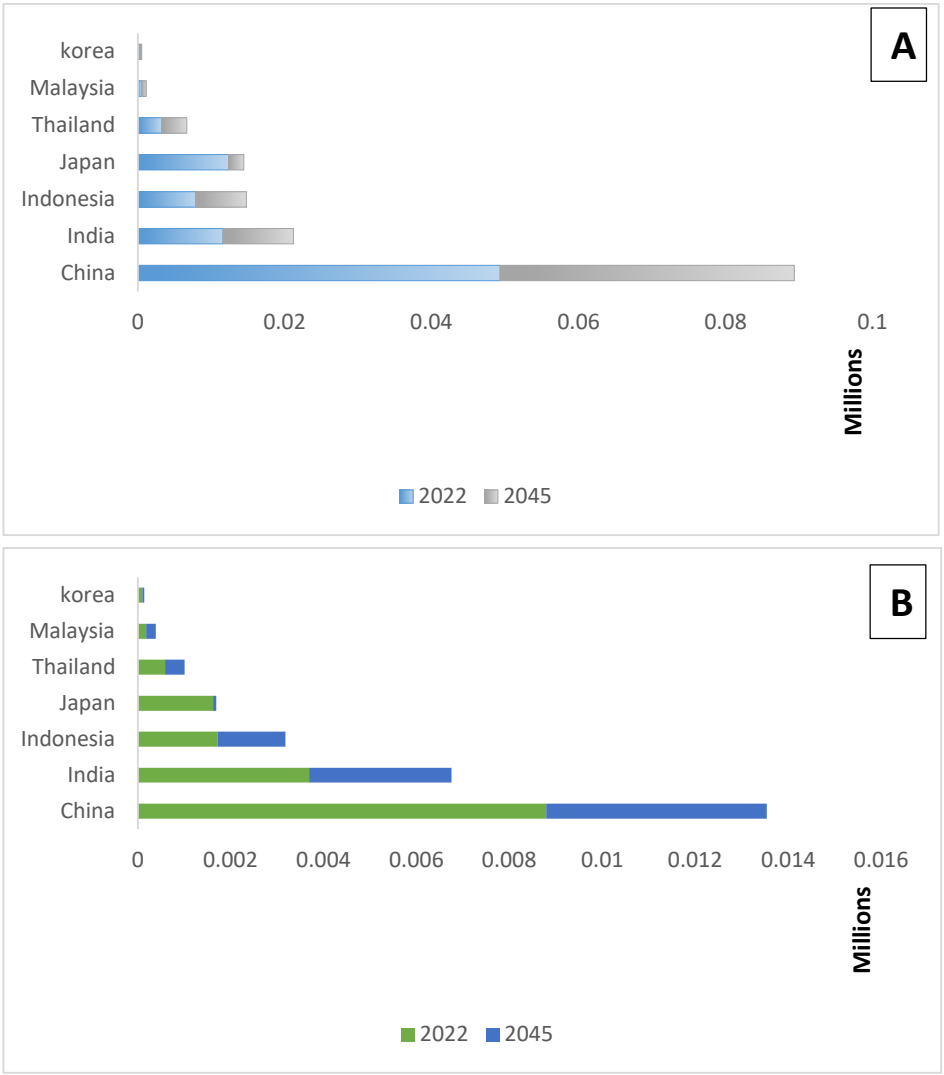

(Data sourced from https://gco.iarc.fr/en) Estimated number of new cancer cases (both sexes, age group 0–85+) projected from 2022 to 2045 for all cancer types (A) Non-melanoma skin cancer (B) melanoma.

The incidence of non-melanoma skin cancer has risen and continues to increase compared to melanoma.

1.9.4 Impact of skin cancer on public health and quality of life

One of the most important challenges to public health worldwide is cancer; its effects go so far beyond the simple discomfort the illness causes. At many levels, consequences of cancer affect individuals, families, and entire healthcare systems. Cancer disrupts general health as well as the quality of society in a major and different ways. When combined with the challenges of late-stage diagnosis and budgetary restrictions, the growing incidence of cancer poses serious public health issues in India that provide a considerable difficulty. various individuals are becoming increasingly concerned about cutaneous squamous cell carcinoma (cSCC), which has been connected to various aspects including prolonged UV radiation exposure.

Comprehensive efforts to improve public health with a particular emphasis on preventative measures, early identification, availability of treatment, and survivor care must be initiated to address these problems. India could be able to help to lower the cancer burden while improving the outcomes for millions of people worldwide if it were to try to solve the basic causes of cancer, upgrade the infrastructure promoting healthcare, fight antibiotic resistance, and provide complete treatment. Reducing the negative consequences of cancer on public health depends primarily on continuous spending on healthcare, legislative changes, and coordinated efforts to ensure that no patient falls behind in the course of treatment.

1.10 Emerging strategies for cancer treatment

By concentrating on the unique vulnerabilities of cancer cells, advances in cancer research have generated innovative approaches aimed to specifically and minimally combat the disease. Immunotherapy has revolutionised treatment with immune checkpoint inhibitors like pembrolizumab restoring the immune system's capacity to target cancer cells (Ghemrawi *et al*., 2024) and CAR-T cell therapy building T cells to attack particular tumors antigens (Hong *et al*., 2020). While precision medicine, guided by genomic profiling, customises treatments to the genetic makeup of individual tumors, improving efficacy while decreasing side effects, targeted therapies such EGFR (Manneling *et al*., 2019) and HER2 inhibitors (Oh.D.Y *et a*l., 2020) disrupt growth signalling pathways vital for tumor survival. Photodynamic therapy (PDT) is becoming more and more commonly destroying cancer cells with least harm on healthy tissues using photosensitisers activated by specific wavelengths of light generating reactive oxygen species (ROS). Although gene-editing technologies such as CRISPR offer the means to repair cancer-causing mutations, developments in nanotechnology enable precise medication delivery, thus decreasing off-target effects (Chehelrgedi *et al*., 2024). Combining treatments including immunotherapy with radiation or chemotherapy has shown good success in overcoming resistance and improving efficacy. Strategies exploiting metabolic vulnerabilities, modulating the tumors microenvironment, developing cancer vaccines (Saxena *et a*l., 2021), and integrating artificial intelligence for early detection (Patel D *et al*., 2020) and personalised care are redefining cancer treatment, so offering hope for more effective and less toxic therapies.

1.11 Illuminating hope: Photodynamic therapy in cancer treatment

Photodynamic therapy, commonly referred to as PDT, is a relatively new non-invasive treatment method which utilises a photosensitiser (PS), light, and endogenous molecular oxygen for the purpose to selectively target and eliminate cancer cells or microbes. Each component is harmless on its own; however, when the PS is exposed to light, it sets off photochemical procedures that result in the generation of extremely reactive singlet oxygen species. These species are responsible for cytotoxicity and result in the death of cells through the procedure of apoptosis. The photodynamic therapy (PDT) technique has not been generally adopted or utilised, despite the fact that it was discovered almost a century ago. The number of medications that have been licensed for use are still limited. According to Chilakamarthi *et al*. (2017), substantial research that is now being conducted is likely to drive the potential of photodynamic therapy (PDT) as a promising therapeutic option for both malignant and nonmalignant diseases.

1.12 Lighting the way to skin cancer cure: The success of photodynamic therapy

Skin, lung, head and neck, cervix, stomach, brain, and bile duct malignancies among other forms of cancer have demonstrated success with photodynamic therapy (PDT). By aiming targeted aberrant cells using a photosensitising chemical and light exposure, PDT is used to treat non-melanoma forms including basal cell carcinoma in skin cancer (Monfrecola *et al*., 2009). Particularly in cases when surgery is not a possibility, PDT is used to lower tumor size and relieve

symptoms for lung and head and neck tumors (Bredell *et al*., 2010; Simone *et al*., 2012). PDT helps to shrink tumors while decreasing symptoms such blockage or bleeding in cervical and stomach malignancies (Hassan *et al*., 2013; Wang *et al*., 2022). PDT can be used to target certain tumor locations, thereby either providing palliative care or enhancing the efficacy of other treatments, for brain (Bartusik *et al*., 2023) and bile duct tumors (Berr *et al*., 2000). Often in conjunction with other treatments to improve general treatment outcomes, PDT's adaptability and minimally invasive character make it a useful choice in managing various cancer kinds.

With 32% of the total patients treated with PDT having skin cancer, the pie chart (Figure 1.4) demonstrates that followed by cervical cancer patients, who make 24%.

Figure 1.4: Global distribution of patients treated with PDT from 1990 to 2024

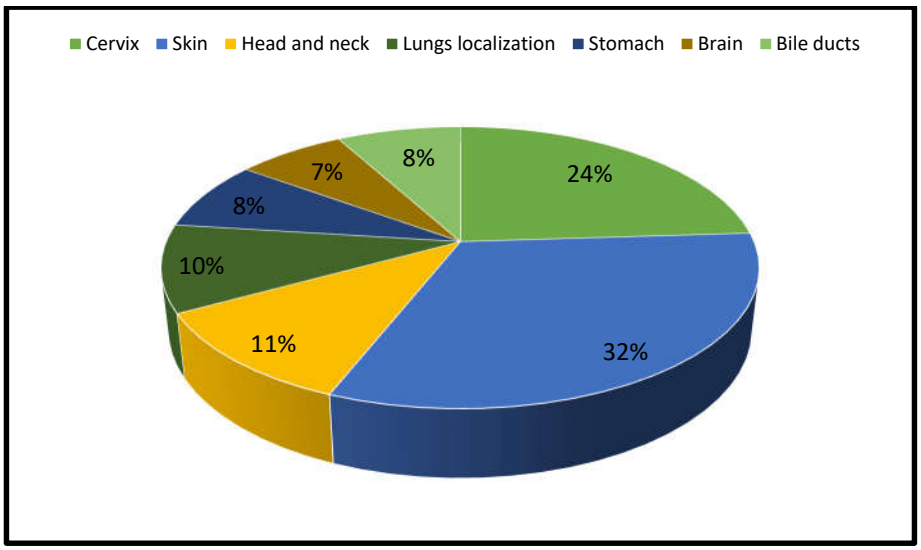

(Data Source: Alekseeva *et al*., 2024)

1.13 Impact of PDT on skin cancer treatment and public health

The novel uses of photodynamic therapy (PDT) in disease management and diagnostics have made significant improvements in public health. Photodynamic diagnostics (PDD) uses fluorescent photosensitisers that illuminate afflicted tissues under particular light wavelengths to enable early detection of disorders like skin malignancies and precancerous lesions. This enhances the results of treatment by enabling accurate and non-invasive diagnosis.

Apart from its diagnostic potential, PDT has transformed the battle against diseases by providing a powerful remedy for germs resistant to antibiotics through its antibacterial properties. It successfully kills bacteria without fostering the development of resistance by using photosensitisers that are activated by light to produce reactive oxygen species (ROS). Together, these uses highlight PDT's revolutionary influence on public health by offering more precise, safe, and potent diagnostic and treatment strategies.

1.14 Key elements of PDT (Correia *et al*., 2021)

For the purpose of to perform the photodynamic treatment, which is more often referred to as PDT, three fundamental components are utilised: light, oxygen, and a photosensitiser, also known as PS. During the process that leads to the creation of reactive oxygen species (ROS), which ultimately leads to an improvement in the treatment outcome, each and every action is important.

i) Light

Lasers, incandescent bulbs, and light emitting diodes (LEDs) are some of the light sources that are utilised utilising photovoltaic (PDT) technology. In spite of the fact that they offer a high degree of precision, lasers are quite pricey and require additional lenses in order to cover an expanded region. Conventional lamps and other non-laser light sources have the potential to cause detrimental heat effects that must be avoided. This is despite the fact that these light sources are compatible with optical fibres. The use of LEDs in PDT operations is highly recommended due to the fact that they are inexpensive, non-hazardous, and thermally safe.

When it comes to the ease with which light may travel through tissues, the texture of the tissue and the wavelength of the light work together. Longer wavelengths (600–1200 nm) of light, in particular red light, penetrate into the skin more deeply and enhance its sensitivity. Light of shorter wavelengths, such as 600 nm, is more easily absorbed by the skin and enhances its sensitivity. Within the range of wavelengths that are considered to be the "phototherapeutic window," the optimal range for photodynamic therapy (PDT) is from 600 to 850 tonne. It is guaranteed that this spectrum will have the highest possible tissue permeability.

Light fluence, which refers to the total quantity of energy that is delivered to a region, light fluence rate, which is the quantity of energy that is delivered per second, and exposure duration parameters are all important factors in determining the impact of photodynamic treatment (PDT). It is beneficial to have low light fluence rates because they

reduce the quantity of oxygen that is depleted in tissues. This, in turn, is beneficial because it encourages efficiency and induces apoptosis rather than necrosis. Additionally, there is the option of utilising natural daylight for photodynamic therapy (PDT), which offers patients a reduced level of discomfort and a reduction in the amount of time required for treatment. This is particularly advantageous for skin lesions that include actinic keratosis.

ii) Oxygen

Molecular oxygen is an essential component of photodynamic therapy (PDT) since it generates reactive oxygen species (ROS), which are needed for the therapeutic effects they generate. The success rate of PDT depends on the vascular density of the tumor and is usually limited in hypoxic cancers that are deeper. Oxygen concentration has a significant influence on this effectiveness. High light fluence rates can momentarily deplete oxygen, which may trigger disturbance of reactive oxygen species (ROS) synthesis and lower therapy effectiveness.

Real-time oxygen monitoring in PDT is crucial to maximise the effects by adjusting the light dosages. One of the techniques to increase the availability of oxygen is catalysed, which transforms hydrogen peroxide into oxygen. Other approaches entail supplying oxygen using carriers like perfluorocarbons and haemoglobin. Those methods are meant to lower tumor hypoxia's effects and raise PDT's effectiveness.

iii) Photosensitizer (PS)

Photodynamic treatment (PDT) relies heavily on photosensitisers as an essential individual component. In an ideal

scenario, these molecules would be able to selectively aggregate in tumours, experience a high singlet oxygen quantum yield, remain inactive when exposed to light, swiftly clear from the body, and show amphiphilic characteristics. In order to improve therapeutic efficiency while minimising damage to healthy tissue, PS molecules are often designed to be preferentially taken up by target tissues, such as tumour cells or infected cells. This is done in order to maximise the effectiveness of the treatment. In most cases, photosensitisers are given in a systemic manner and accumulate in the tissue that they are intended to affect. After being exposed to the right wavelength of light, the photosensitiser goes through a photochemical reaction, which results in the production of reactive oxygen species (ROS) that induce cytotoxic effects, ultimately leading to the killing of the cells that are being targeted. On the basis of their origin, photosensitisers, which serve as essential agents in photodynamic treatment (PDT), can be classified into two categories: synthetic varieties and natural variations.

1.15 Mechanism of PDT-Type I and Type II reactions

When the photosensitiser (PS) absorbs light in the target tissue, it sets off a chain reaction of photochemical processes that ultimately leads to the generation of reactive oxygen species (ROS) (Rocha., 2016). This is the beginning of the photodynamic consequence. When the photosensitiser (PS) is exposed to light, it undergoes a transition from its ground state, which is known as the singlet state (PS), to a singlet state that is electronically excited and has a brief duration of only a few nanoseconds or less (Lee *et al*., 2020; Dolman *et al*., 2003). Despite its high degree of instability, this excited state has the

capability of returning to its ground state by releasing surplus energy. This can be accomplished through either the emission of light (fluorescence) or the dissipation of heat (internal conversion). However, it is possible for the singlet state to experience intersystem crossing, which results in the transition to a triplet state (PS_{ET}) that is more stable and has a longer lifetime. This occurs when the electron undergoes spin conversion to a higher-energy orbital, as stated by Donnellt *et al*. (2008). In accordance with Dolmans *et al*. (2003), this triplet state has the ability of either returning to the ground state by the emission of light (phosphorescence) or taking part in two other kinds of processes. The lifespan of the triplet state is significantly longer (it can last for up to tens of microseconds), which allows for sufficient time for the direct transfer of energy to molecular oxygen (O2+). As a consequence of this transfer, singlet oxygen ($^1O_2$) is produced, and the photosensitiser (PS) is brought back to its initial state, so commencing the type II reaction. It is feasible for singlet oxygen to interact with a wide variety of biological substrates, which can result in oxidative damage and ultimately lead to the death of cells. Singlet oxygen is highly reactive. It is also possible for the type I reaction to take place if the excited state of the photosensitiser (PS) directly interacts with a substrate, which could be a cell membrane or a molecule. Free radicals and radical ions can be produced as a result of this interaction, which can also lead to the transfer of electrons or the abstraction of hydrogen atoms. As a result of the reaction between these radicals and molecular oxygen, reactive oxygen species (ROS) are developed. These ROS include superoxide anion (O2•), hydroxyl radical (HO•), and hydrogen peroxide ($H2O_2$). These ROS are

responsible for oxidative damage and have the potential to cause biological lesions (Correia *et al*., 2021). Figure 5 illustrates jablonski diagram of PDT mechanism.

Figure 1.5 Mechanism of PDT

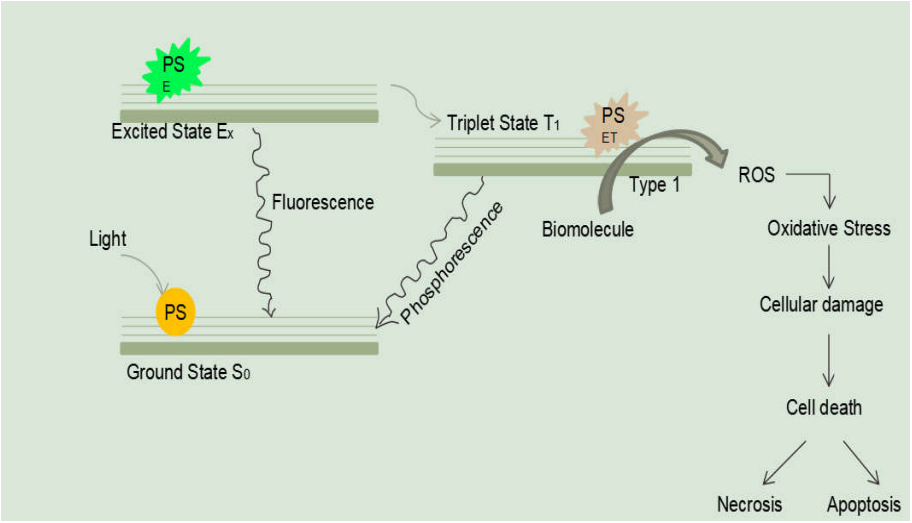

The products that are produced as a result of type I and type II reactions are the ones that are accountable for the beneficial effects of PDT, that involve the death of cells. Both processes are capable of taking place at the same time, and the equilibrium between them is affected by a number of parameters, including the photosensitiser (PS), the substrate, the oxygen concentration, and the binding affinity of the sensitiser to the substrate (Lee *et al*., 2020; Dolmans *et al*., 2003). According to Correia *et al*.'s research from 2021, the type II reaction is particularly prevalent during the process of photodynamic therapy (PDT). Singlet oxygen is the principal cytotoxic agent that is accountable for the biological effects. A significant characteristic of a photosensitiser (PS) is the quantum yield of singlet oxygen production, which is influenced by both the quantum yield and the lifetime of its

triplet excited state (Rocha.,2016). In addition, the quantum yield is influenced by the lifetime of the triplet excited state. As a result of the high reactivity and short half-life of reactive oxygen species (ROS), the photodynamic therapy (PDT) only has an effect on cells that are located in close proximity to the source of ROS formation, which is where the photosensitiser (PS) is located. According to Dolmans *et al*. (2003), the degree of damage and cytotoxicity that is caused by photodynamic therapy (PDT) is influenced by a number of factors. These factors include the type of photon source (PS), its extracellular and intracellular distribution, the total dose that is administered, the light dose (light fluence), the light fluence rate, the availability of oxygen, and the amount of time that passes between the administration of PS and the exposure to light. Due to the low oxygen levels and constrained light penetration into the tissue (due to light absorption by the photosensitiser and energy transfer to oxygen), photodynamic therapy (PDT) is more difficult to perform on deeper and hypoxic tumours. According to Dąbrowski (2017), superficial and well-oxygenated tumours are able to produce more reactive oxygen species (ROS), which results in a more successful photodynamic therapy (PDT) treatment.

1.16 Synthetic Photosensitizers

These are chemically designed and include porphyrins, phthalocyanines, and chlorins. They are tailored to have specific properties such as high singlet oxygen generation, tumor selectivity, and controlled pharmacokinetics. Synthetic photosensitizers offer versatility in modification, making them suitable for various applications and improved treatment outcomes.

1.17 Natural Photosensitizers

Chemicals derived from natural sources such plants, bacteria, or fungi are hypericin, derived from the plant *Hypericum perforatum*, and derivatives of chlorophyll. Usually highly biocompatible, this group of compounds is benign for the environment and has natural biological action. Still, additional alterations might be necessary to enhance the durability and therapeutic effectiveness of these drugs. These PSs were initially discovered in phototoxic plants, which have been known for a long time for the adverse effects that they have on both humans and animals (Kubrak *et al.*, 2022)**.**

1.18 Exploring Plant-Derived Photosensitizers for PDT

Scientists have been motivated to research natural photosensitisers for photodynamic treatment (PDT) mainly due to the reduced toxicity to healthy tissues and the lower rate of adverse effects. Additionally, the use of plant-based chemicals as photosensitisers (PSs) in photodynamic therapy (PDT) is still limited. We intended to investigate plant-derived photosensitizers for photodynamic therapy (PDT) in our research.

1.19 Fagopyrins and psoralens: potential natural photosensitizers with possible applications in PDT

Although many photosensitizers have been reported to be present in a variety of plant species, a major fraction remains unexplored with respect to their possible applications in PDT. Hypericin from *Hypericum perforatum* has been established as the only potent natural photosensitizer by virtue of a significant number of investigations. Fagopyrins are napthodianthrone derivatives that are structurally similar to hypericin (Figure 1.4). We have focused on

fagopyrin as natural photosensitizer, because of their similarity in structure to hypericin. Plants containing fagopyrins causes phytophotodermatitis in livestock and humans. Fagopyrism, is a severe photosensitivity reaction in animals and humans consuming buckwheat, owing to its fagopyrin content. In 2016, Sytar *et al*. demonstrated comparable anti-fungal activities between fagopyrin and hypericin suggesting a similar bioactivity for fagopyrin (Sytar *et al*.,2016). Moreover, compared to hypericin, fagopyrin is reported to be more phototoxic to *S. cereviciae* cells (Sytar *et al*.,2021). However, fagopyrins are not yet investigated for its photodynamic therapeutic efficacy.

Figure 1.6 Structure of hypericin and fagopyrin

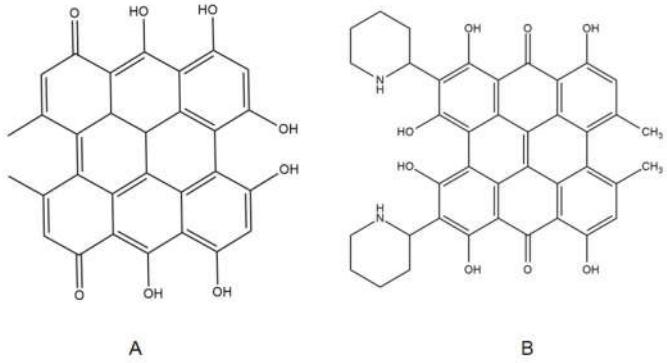

A) Hypericin B) Fagopyrin

Psoralens are furocoumarin derivatives that can act as natural photosensitizers owing to the cyclic structure with conjugated double bonds, a characteristic feature of photo active compounds (Figure 1.7). It is currently used for the treatment of vitiligo, psoriasis, and other skin diseases (Conforti *et al*.,2009). It has been isolated from many a plant species like celery (Aharoni *et al*.,1996), parsley (Beier *et al*.,1994), and citrus fruits (Peroutka *et al*.,2007).

Figure 1.7 Structure of psoralen

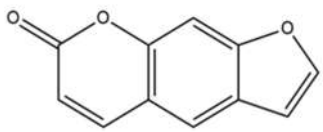

Members of Fagopyrum and Ficus species have been observed to be phototoxic due to the presence of fagopyrins and psoralens, respectively (Tavčar *et al*., 2015, Derraik *et al*., 2007). Hence we selected plants from these two species as the plant sources for the inquiry that we are undertaking.

1.20 *Fagopyrum tataricum*

Figure 1.8 *Fagopyrum tataricum* plant

Kingdom	Plantae
Order	Caryophyllales
Family	Polygonaceae
Genus	Fagopyrum
Species	*F.tataricum*
Common name	Buck Wheat

Common buckwheat and tartary buckwheat are two distinct kinds of buckwheats. Common buckwheat also termed sweet buckwheat is consumed extensively in Asia, Europe, North America, South Africa, and Australia (Li *et al*., 2001). Tartary buckwheat's bitter taste makes it less often consumed (Figure 1.8). Studies have demonstrated, however, that the general composition of crude protein, crude fibre, crude fat, and crude ash in ordinary buckwheat and tartary

buckwheat is practically exactly same (Bonafaccia *et al*., 2003). Moreover, compared to normal buckwheat, tartary buckwheat could have more beneficial components. For example, its flavonoid content is much higher 40 mg/g of tartary buckwheat seeds has more flavonoids than just 10 mg/g in normal buckwheat seeds (Li *et al*.,2001). Comparative research on the composition of common and tartary buckwheat expose higher quantities of thiamine, riboflavin, and pyridoxine, which makes them excellent choices for preventative diet (Bonafaccia *et al*., 2003). An anthraquinone secondary metabolite discovered in the green portions of Tartary buckwheat plants is fagopyrin. Although fagopyrin is among the secondary metabolites of buckwheat that could cause health problems when the green parts are consumed, buckwheat grains and their derived food items are regarded safe since their fagopyrin levels are minimal. Especially fagopyrin has phototoxic characteristics that could be used for PDT (Glavač, *et al*., 2017, Benković, *et al*., 2014).

1.21 *Ficus auriculata*

Figure 1.9: *Ficus auriculata*

Kingdom	Plantae
Order	Rosales
Family	Moraceae
Genus	Ficus
Species	*F. Auriculata*
Common name	Fig

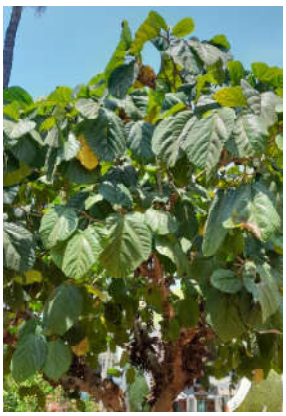

Comprising about 735 species, the genus Ficus L. (figs) falls within the family *Moraceae*. Rich in phytochemicals and antioxidants that provide essential nutrients to human health, figs are thought of as holy trees with many therapeutic uses (Jagadeesa *et al*., 2019). These plants range in temperate, tropical, and subtropical environments from 1,800 to 2,600 meters above mean sea level (Kala., 2007). The plant is dioecious morphologically and reaches a height of roughly 4–10 meters. White latex is rather plentiful in all areas of the plant (Wang *et al*., 2008; Schulz *et al*., 2000). Apart from curing menorrhoea, haemoptysis, diarrhoea, iron deficiency, cancer, and constipation, the fruits of *Ficus auriculata* are acknowledged as a great cure for diabetes.Ficus auriculata tree is shown in Figure 1.9. Emphasising potential therapeutic significance, the leaves of *Ficus carica cv. Dottato* have been found to contain greater amounts of psoralen and bergapten. Particularly on the leaves, these substances have been identified in rather high doses. Using these leaves could help to prevent disorders connected to oxidative stress, therefore upsetting homeostasis (Conforti *et al*., 2012). To the best of our knowledge, though, no research on the phototoxicity of *Ficus auriculata* exist. Umbelliferae (Apiaceae), Rutaceae, and Moraceae comprise the plant families with the highest phototoxic activity—that is, those with most phototoxic components. Ranunculaceae, Rubiaceae, Cruciferae, Mahonia, Capcium (Solanaceae), and Fabaceae (Fu *et al.*, 2013) follow these. We hypothesise that Ficus auriculata will likewise show phototoxicity and hence choose to investigate it further since other Ficus species and the Moraceae family have shown phototoxic qualities.

1.22 Non-melanoma skin cancer cell line for *in vitro* PDT research

A431 cells are a commonly used squamous cell carcinoma (SCC) cell line. They originate from human epidermoid carcinoma, a type of SCC. Squamous Cell Carcinoma (SCC) is a type of non-melanoma skin cancer that originates in the squamous cells of epidermis.

Objectives of the study

We felt inspired to investigate natural photosensitizers for the treatment of skin cancer in light of the awful impact of the disease and the amazing potential of Photodynamictherapy (PDT) in public health. We sincerely hope that our efforts may serve as a basis for further developments, even though this is a preliminary study. This study assessed the effects of PAF 1 and PAF 2 fractions from *F. tataricum* and *F.auriculata* respectively on skin cancer cells using PDT. The model for skin cancer (Non-melanoma) was A431 cells. To excite the photosensitizers in the PAF 1 and PAF 2 fractions, a 1000 W halogen tungsten lamp was used. The main objectives of the present study are:

- Extraction of photoactive fraction (PAF 1) from *F. tatricum* aerial parts
- Extraction of photoactive fraction (PAF 2) from *F. auriculata* leaves
- Evaluation of the effectiveness of isolated photoactive fractions in PDT on A431 cells
- Identification of photosensitizers in photoactive fractions
- *In silico* analysis

Chapter 2
Review of Literature

2.1 A Major focus of research on cancer

The main goal of continuously evolving cancer research is to understand the biological mechanisms that drive cancer development, progression, and recurrence. The researchers are dedicated to deciphering the molecular, genetic and environmental factors that contribute to the development and spread of cancer. This deeper understanding has led to revolutionary advances in treatment options, which have evolved from a "one-size-fits-all" approach to more precise and personalized therapies. One focus of today's cancer research is the development of personalized medicine, in which therapies are tailored to the genetic and molecular profile of the individual tumor. This has given rise to targeted therapies and immunotherapies that have revolutionized cancer treatment.

Targeted therapies target specific molecular changes in cancer cells and provide treatments that stop the growth and spread of cancer by targeting proteins or genes involved in tumor development. In contrast to conventional chemotherapy, which affects both healthy and cancer cells, targeted therapies aim to minimize damage to healthy tissue. This results in fewer side effects and improved effectiveness. Another significant advance is immunotherapy (Kirkwood *et al*., 2012), which uses the body's natural immune system to identify and attack cancer cells. These therapies include checkpoint inhibitors,

CAR-T cell therapies (Sterner *et al.,* 2021), and cancer vaccines (Saxena *et al*., 2021), all of which have shown remarkable success in treating cancers such as melanoma, lung cancer, and certain types of leukemia and lymphoma. Despite the early stage of development of CRISPR screening, it has great potential for identifying important cancer genes and therapeutic targets (Wang *et al*., 2022).

In addition to the development of these therapies, early detection and prevention remain central topics in cancer research. Early diagnosis is crucial to increase survival rates. Research is actively engaged in the development of new methods for early detection, such as liquid biopsies, which can identify cancer mutations in the blood before symptoms appear. Genetic screening and biomarkers are also valuable tools for identifying individuals at higher risk of cancer and enable early interventions (Mäbert, *et al*., 2014).

2.2 Cancer research in India: Progress and potential

In India, geriatric oncology research is still in its early stages. There are only a few specialized units, and geriatric examinations are used only occasionally. Future efforts should be aimed at increasing research output, developing India-specific guidelines, and promoting training programs to improve care for elderly cancer patients (Noronha *et al*., 2023). A polymer-based composite nanogel developed as a transdermal drug delivery system for the pH-sensitive, targeted, and controlled delivery of the cancer drug doxorubicin (DOX) (Mukkukada *et al*., 2024). A fluorescence probe using Eu(III)-incorporated BSA-AuNCs has been developed to selectively detect sarcosine, a biomarker

for prostate cancer (Sanjeevan *et al*.,2023). A luminescent europium-chelimic acid complex (Eu-CHE) has been developed to selectively detect the cancer biomarker L-kynurenine (l-Kyn), with a detection limit of 1.37 nM. This is applicable to serum, urine, and a paper-based sensor platform (Varghese *et al*., 2024).

2.3 Evolution of photodynamic therapy: Milestones and breakthroughs

Heliotherapy, i.e. the use of sunlight for healing, was adopted by ancient cultures such as the Greeks, Egyptians, Chinese and Indians. The Greeks, under the leadership of the physician Herodotus, were in favor of sunlight to restore health. Sunlight has been used to treat conditions such as rickets, psoriasis and psychosis. Egyptians even used sunlight to mask vitiligo symptoms by using amine fruit juice for a tanning effect (Agostinis *et al*., 2011; Correie *et al*., 2021). The PDT story tells of people's incessant quest to push the boundaries of what is possible. Although significant successes were achieved until 1990, it was only then that the field really gained momentum. In the decades that followed, researchers not only improved the technology, but also found surprising new medical uses for light. The time line of history of photodynamic therapy was prepared based on an article by David Aebisher in 2024 (Aebisher *et al*.,2024).

1800	Herschel discovered infrared radiation and described it.
1806	Ritter found ultraviolet radiation
18^{th} and 19^{th} century	In France, light therapy is used to treat conditions such as tuberculosis, psoriasis, scurvy and rheumatism. Discovery of bacterial properties of ultraviolet radiation revolutionized infection

	treatments
1893	Niels Finsen published a study on the use of light therapy in smallpox treatment.
1902	Oscar Raab found in Von Tappeiner's laboratory that light, acridine dyes and oxygen are required for photodynamic reactions.
1903	Niels Finsen used light therapy to treat skin tuberculosis and was awarded the Nobel Prize in Medicine. Eosin and light were used by Tappeiner and Jesionek to treat skin cancer, coining the term "photodynamic therapy".
1913	Friedrich Meyer-Betz conducted his own experiments with hematoporphyrin and sunlight and found swelling, pain and itching.
1924	Palokard perceived the selective affinity of hematoporphyrin to cancer cells.
1942-1948	Auler, Banzer, Figge and Weiland investigated the use of porphyrins in diagnostics and photodynamic therapy.
1955	Tumor localization was described by Rasmussen-Taxadal and colleagues using intravenously administered photosensitizers.
1972	In mouse models of gliomas, studies showed that tumor growth was inhibited for up to 20 days as a result of PDT.
1975	Kelly and his team were able to successfully use PDT for bladder cancer.
1978	Thomas Dougherty showed that porphyrin-based PDT in mice could completely cure cancerous tumors.
1980s-1990s	Because of the long-lasting phototoxicity of HpD, alternative photosensitizers have been researched.
2000s	In 1500 patients who received treatment with Photogem and PDT, 91% showed therapeutic effects, and 6% achieved complete tumor healing.

2.4 Development of PDT (2019-2024)

PDT technology has made significant advances since 1980 and improved its medical effectiveness. Among the most significant advances are improved photosensitizing drugs, advanced light sources, optimized dosing protocols and miniature devices. The increasing interest in PDT is reflected in the increasing number of publications, which has increased from 53 in 1982 to 3,381 in 2022. This underlines the dynamic growth of the field and the growing scientific attention.

Aggregation-induced emission photosensitizers (AIE-PSs) trapped in liposomes allow for controlled photosensitization, allowing PDT to be performed under normal lighting conditions instead of in a dark room (Yang *et al*., 2019). A novel NIR-responsive nanosystem has been developed to jointly provide oxygen and the cancer drug DOX. F/DOX nanoparticles showed significant therapeutic efficacy in vitro as well as in vivo by combining PDT and chemotherapy (Yang *et al*., 2019). In addition to killing bacteria, ALA-PDT promotes wound healing by regulating inflammatory factors, collagen remodeling, and macrophage activity (Yang *et al*., 2020). A Ru(II) polypyridine complex has been identified as phototoxic at clinically relevant 595 nm in monolayer cells as well as in multicellular 3D tumor spheroids, with efficacy in the low micro- to nanomolar range (Karges *et al*., 2020). The four curcuminoids demonstrated promising PDT efficacy, characterized by high ROS production and low LD_{50} levels, especially in compound 2. The biphasic dose responses in compounds 1 and 3 require further studies to treat persistent photosensitivity (Kazantzis *et al*., 2020). PpIX-IR-820@Lipo-NPs demonstrated a synergistic

efficiency of 70.5% in PDT/PTT on HeLa cells, highlighting their potential as a promising nanoplatform for the treatment of cervical cancer (Yan *et al*., 2022). According to Zhang *et al*. (2022), ALA-PDT has a comparable effectiveness to surgery, but with fewer side effects compared to local excision. The Ni(II) complex exhibits the PDT activity of red light and is the first first-row transition metal complex to exhibit combined PDT and PTT effects within the clinically relevant phototherapeutic window (Sarkar *et al*., 2023). Treatment of AK lesions with 20% ALA-PDT and LED red light has proven to be effective and also improves photoaging in Chinese patients. Fluorescence may be helpful in diagnosing AK with peripheral field cancerization and evaluating ALA-PDT efficacy (Li *et al*., 2024).

2.5 Combination therapy with PDT

Chemotherapeutic agents that act directly on DNA include alkylating agents, antitumor antibiotics, and topoisomerase inhibitors. Cisplatin and its derivatives are effective treatments against cancer, but they often have serious side effects. A combination with PDT can increase its effectiveness and reduce the dosage required. This combination has been shown to be effective against various cancers, including lymphoma (Nonaka *et al.,* 2002), esophageal carcinoma (Compagnin *et al*., 2010), breast cancer (Crescenzi *et al*., 2004), and head and neck cancer (He *et al*., 2009). A novel approach is to develop hybrid molecules that combine the cytotoxic properties of cisplatin with the photodynamic effects of a photosensitizer. By combining it with PDT, the effectiveness of antitumor antibiotics such as doxorubicin and mitomycin C against different types of cancer can be increased. Often, this combination leads to synergistic effects that

make it possible to use lower doses of chemotherapy while achieving better therapeutic outcomes. This approach has been tested in different cancer models, including bladder cancer (Datta *et al*., 1997) and colorectal cancer (Ma *et al*., 1992). Topoisomerases are indispensable enzymes for DNA replication and transcription. The inhibition can cause cell death, which makes it a promising starting point for the treatment of cancer. Drugs such as camptothecin and its derivatives, as well as etoposide, can target topoisomerases I and II. The effectiveness of these drugs can be increased by combining them with PDT and reducing their side effects. The therapeutic outcome can be further improved by innovative delivery systems such as micelles by increasing the accumulation of drugs in tumor tissues (Peng *et al*., 2009, Gantchev *et al*., 1996). Photoimmunotherapy uses photosensitizers that are linked to monoclonal antibodies and target specific tumor antigens. Although this approach has shown promise, it faces challenges such as complex chemical conjugation, reduced phototoxicity of the complexes, and limited tumor penetration (Mew *et al*., 1983). Apoptosis in bladder cancer can be increased by combining EGFR inhibitors such as Erbitux with PDT, resulting in an improvement in anti-tumor activity (Bhuvaneswari *et al*., 2009). The combination of radiation therapy (RT) and PDT has produced different results. The result can vary depending on the specific photosensitizer and the timing of the treatments (Berg *et al*., 1995, Ma *et al*., 1993).

2.6 EGFR combination with PDT

The A431 cells used in our study are characterized by EGFR overexpression. So it can be used in EGFR-targeted cancer therapy. The Gijsens study of 1998 aimed to combat tumors that overexpress EGF receptors with EGF-conjugated SnCe6. EGF-Dex-SnCe6 binds

specifically to EGF receptors, while EGF-PVA-SnCe6 has higher photocytotoxicity. PVA, in contrast to EGF, appeared to play a more important role in cellular uptake. According to the study, the photodynamic activity of EGF conjugates is highly dependent on the carrier used (Gijsens *et al*., 1998). In 2000, a study was conducted with the aim of combating tumors that overexpress EGF receptors with EGF-conjugated SnCe6(ED). The photocytotoxicity and the effectiveness of cellular uptake of EGF-HSA-SnCe6(ED) were higher than those of EGF-Dex-SnCe6(ED). The pronounced photocytotoxicity of EGF-HSA-SnCe6(ED) was attributed to its specific binding to EGF receptors and the subsequent intracellular accumulation, which led to increased formation of reactive oxygen species when exposed to light (Gijsens *et al.,* 2000). Chitosan/TPP nanoparticles loaded with curcumin represent a promising targeted photodynamic therapy for EGFR-overexpressing cancers (Tsai *et al.,* 2018). 21nm gold nanoparticles labeled with chlorine e6 and EGF effectively target and eliminate cancer cells without harming normal cells. This focused photodynamic therapy promises to be an effective treatment for cancer (Castilho *et al*., 2021).

2.7 Natural Photosensitizers used in PDT

There are only a small number of studies that deal with the identification of photoactive compounds from plant extracts as effective natural PSs. These drugs are often given in high doses to ensure that they have high bioavailability and are cytotoxic. A large number of pharmaceutically active compounds exist in nature, many of

which are documented in scientific publications. Table 2.1 lists various natural compounds with PS properties that are suitable for PDT.

Table 2.1 List of natural photosensitizers

Photosensitizer	**Absorption maxima**	**Description**
Pheophorbide A	670 nm	• Pheophorbide A extracted from Silkworm excreta showed photosensitizing efficacy against B16F10 melanoma in *in vivo* study (Lim *et al*., 2004). Used in PDT for cancers such as head and neck cancer (Chung et al., 2009)Leukemia (Lee *et al*.,2004),Prostrate cancer (Xu *et al*.,2013) Hepatocellular carcinoma (Tang *et al*.,2006) Uterine cancer (Tang *et al*., 2009) Glioblastoma multiformae (Cho *et al*.,2014) Bladder cancer(Bergstrom *et al*.,1994)Barrett's esophagus (Qumseya *et al*.,2013) Oesophageal (Wu *et al*.,2013)
Curcumins	420-480 nm	• Curcumins are present in *Curcuma longa rhizome* (Sontsa *et al*.,2022). • Broad anticancer activity Breast cancer cells (Askhbar *et al*.,2020), Skin cancer cells (Woźniak, *et al*., 2021),antibacterial(Lee *et al*.,2017),antiviral (Ambreen *et al*.,2020)
Anthraquinones	437 nm	• The anthraquinones are identified in several plant

		species and organisms as reported in various studies: *Polygonum cuspidatum* (Leu *et al*.,2008), *Heterophyllaea pustulata* (Comini *et al*.,2011), Aloe vera (Parvez *et al*.,2019), *Rheum palmatum* (Shia *et al*.,2009), *Rumex crispus* (Eom *et al*.,2020) *Dactylopius coccus* (Deveoglu *et al*.,2011), *Xanthoria parietina* (Manojlović *et al*., 2011) . • Soranjidiol, rubiadin and their methyl derivatives exhibit PDT activity against caspase-3-transfected MCF-7 cells from human breast cancer cells (Comini *et al*., 2011) • Natural anthroquinones exhibits phototxoic effects, produce ROS (Montoya *et al*.,2005)
Hypericin	590 nm	• Hypericin is identified in *Hypericum perforatum* (Čellárová *et al.,*1994). • PDT performed with hypericin has shown promise in the treatment of skin (Woźniak *et al*.,2023), cervical cancer (Vantieghem *et al*., 1998), bladder tumors (Zupko *et al*., 2001), nasopharyngeal (Xu *et al.,* 2009), and Pancreatic tumors (Liu *et al*., 2000).
Hypocrellins	Below 600 nm	• The presence of Hypocrellins in Hypocrella bambusae and Shiraia bambusicola are identified.And it has several

		potential applications (Bao *et al*., 2023). • Light-activated hypocrellins have antibacterial (Jiang *et al*., 2013) and antitumor properties (Miller *et al*., 1997, Jiang *et al.,* 2012).
Cercosporin	Below 532 nm	• Cercosporin is identified in *Cercospora kikuchii*, *(Upchurch et al.,1991).* • Photocytotoxicity of cyclosporine has been demonstrated against cell lines of glioblastoma (T98G, U87) and breast adenocarcinoma (MCF7) (Mastrangelopoulou *et al*.,2019).
Riboflavin	360 nm	• Source of riboflavin is leafy vegetables (Ismail *et al*.,2003) • Riboflavin-PDT may reduce the toxicity of cisplatin (Hassan *et al*., 2012, Hassan *et al*., 2013) and has been shown to be effective against cancers such as squamous cell carcinoma (Juarez *et al*., 2015), HeLa cells (Yang *et al*., 2017), and melanoma (Akasov *et al*., 2019).
Furanocoumarins	300-400 nm	• Psoralen, activated by UVA, is an effective treatment for skin diseases such as psoriasis and eczema and has an anti-cancer effect (Panno *et al*., 2009). (5-MOP, 8-MOP) block major cancer pathways (STAT3, NF-κB, PI3K/AKT) and lead to apoptosis in breast (Panno *et al*.,

		2012), leukemia (Kim *et al*., 2016) and melanoma cells (Menichini *et al*., 2010). PUVA therapy shows efficacy in melanoma (Sumiyoshi *et al*., 2014) and cutaneous T-cell lymphoma (Nagatani *et al*., 1990).
Fagopyrin	590 nm	• Presence of fagopyrin is reported in *F. tataricum* and *Fagopyrum esculentum* (Benković *et al*., 2014). • Fagopyrin showed photodynamic antibacterial activity (Kim *et al*., 2021).

2.8 Natural Photosensitizers in Clinical trial

2.8.1 Curcumin

Curcumin, a thoroughly researched natural photosensitizer, is the focus of clinical studies on its antimicrobial properties in PDT. The studies include applications for disinfection of the oral cavity, cleaning of the root canal, treatment of acne and mucositis in oncological patients. These show significant microbial reduction and safety without serious side effects. The specific results include:

1) Oral health: CUR-PDT proved to be an effective method for disinfecting the oral cavity and dentures, reducing candida and microbial counts, and improving oral hygiene in orthodontic patients. (Labban *et al*., 2021, Leite *et al*., 2014, Ricci *et al*., 2017)

2) Acne: Compared to light therapy alone, CUR-PDT achieved higher rates of lesion removal and had minimal side effects (Zhang *et al*., 2024)

3) Mucositis: In oncological patients, CUR-PDT in combination with photobiomodulation led to a cure of mucositis without adverse events (Pinheiro *et al*., 2019)

4) Root canals: CUR-PDT contributes to the optimization of dentin disinfection and adhesion strength in MTAD (Saini *et al*., 2022)

These results highlight curcumin's promise as a safe and effective photosensitizer in various clinical applications.

2.8.2 Hypericin

Hypericin-PDT has been investigated in three clinical trials, with a focus on the treatment of skin lesions with pure hypericin or an extract of Hypericum perforatum. The results include:

1) Mycosis fungoides (Cutaneous T-cell lymphoma): In a multicenter study, a 0.25% hypericin ointment activated by visible light (500–650 nm) showed a significant clinical response with mild local skin reactions but no serious side effects (Kim *et al*., 2022)

2) Skin lesions (Solar keratosis, basal cell carcinoma, Bowen's disease): Hypericum extract (32.5% hypericin) applied under red light (580–680 nm) showed complete response rates of 50%

in keratosis, 28% in basal cell carcinoma, and 40% in Bowen's disease. A burning sensation has been reported, but no serious side effects have been reported (Kacerovska *et al*., 2008).

3) Acne: Under red and green light, St. John's wort extract (0.5% H. perforatum) reduced acne lesions by 56.5%, with improvements in sebum, erythema and skin texture and no side effects (Kim *et al*., 2023)

2.8.3 Riboflavin

Three clinical studies investigated the application of riboflavin-PDT (RF-PDT) in dentistry, with a focus on surface conditioning.

1. **PEEK inlays:** RF-PDT with a 25 mol/L RF solution and green laser (540 nm) improved the surface conditioning of PEEK inlays bound to root canal dentin (Al Deeb *et al*., 2023)

2. **PEEK post:** The RF-PDT has effectively conditioned the surfaces of PEEK posts (Alkhudhairy *et al*., 2023)

2.8.4 Phycocyanin

In a clinical study by Hashemikamangar *et al*., the effect of phycocyanin as a photosensitizer in PDT on dentin binding strength was investigated. They applied a phycocyanin solution with a concentration of 1000 µg/mL for 5 min and then irradiated with a diode laser (220 mW, 635 nm, 61.2 J/cm²) for 3 min. According to the study, PDT with phycocyanin represents an effective antimicrobial method that does not interfere with dentin binding in a self-etching adhesion protocol (Hashemikamanagar *et al*., 2022).

2.8.5 Emodin

PDT with nano-emodin (n-emo gel) for wound healing at the donor site after surgery with free gum graft was investigated by Yaghobee *et al.* The scheme involved applying the gel for 5 min, followed by a 1-min LED irradiation (450 ± 10 nm, 1000 ± 1400 mW/cm², 60–80 J/cm²) from a distance of 1 mm. The results suggest that PDT with nano-emodin may be an adjunct to conventional wound care to reduce postoperative complications (Yaghobee *et al*., 2024).

Only a small number of natural photosensitizers have made their way into clinical trials, with hypericin being one of the few examples that has been tested on cancer cells. This highlights the urgent need for further research on natural photosensitizers. The discovery of more natural photosensitizers with anti-cancer properties could facilitate their move to clinical trials and potentially have lower toxicity compared to synthetic alternatives.

2.9 Exploring other sources of natural photosensitizers

In photodynamic applications, natural photosensitizers are of great value due to their ability to generate reactive oxygen species when light is activated. The aim of the study of alternative sources is to find new efficient compounds with improved photodynamic properties for medical, agricultural and environmental science applications.

2.9.1 *Fagopyrum tataricum* : potential source of Phototoxin

Six derivatives of Fagopyrin were isolated and characterized by UV-Vis absorption spectroscopy, NMR spectroscopy, and mass spectrometry (Benkovic *et al*., 2014). Naphthodian thrones such as

fagopyrin and hypericin, natural photosensitizers in cells, have been studied in the dark for their effects on *Saccharomyces cerevisiae*. Fagopyrin caused disturbances of the cell cycle and led to premature mitosis without budding, while hypericin had a triphasic growth reaction. Flow cytometry revealed reduced viability, with fagopyrine causing a 41% reduction at 100 μM and hypericin causing a 15% reduction. The biofilm structures of both compounds were altered, colony growth was restricted, and cell adherence was disrupted. These results highlight their high toxicity as well as their influence on multicellular growth, although efficiency can vary (Sytar *et al*., 2021). For the first time, Kim and colleagues investigated the production of reactive oxygen species (ROS) by a fagopyrin-F-rich fraction (FFF) of tartar buckwheat flower extract under the influence of light, as well as its antibacterial photodynamic inactivation (PDI) of Streptococcus mutans and its biofilm. With blue light (450 nm), a significant amount of ROS was formed in FFF, with type 1 ROS dominating. The viability and biofilm formation of S. mutans was significantly inhibited by PDI with FFF and blue light (10 J/cm²) compared to FFF without light. The destruction of the biofilm was confirmed by confocal microscopy and electron microscopy. (Kim *et al*., 2021). To the best of our knowledge, no additional studies have been carried out on the effect of fagopyrin in photodynamic therapy (PDT).

2.9.2 *Ficus auriculata :* Exhibits biological activities

The extraction conditions for phenolic and bioactive compounds from *F.auriculatata* fruits were optimized in a study using the response surface method and ultrasound-guided extraction.

Antioxidant capacity was determined by DPPH, ABTS, and reduction power assays. The best extraction parameters (ethanol 52.5%, temperature 40 °C, time duration 22 min) resulted in the highest DPPH scavenging activity (85.20%) and the highest total phenol content (31.65 mg GAE/g DF). The LC-ESI-MS analysis identified 18 bioactive compounds that may contribute to the antioxidant properties of the fruit (Shahinuzzaman *et al*., 2021). Phenolic compounds are associated with the antioxidant, antimicrobial, and phytotoxic properties of F. auriculatata leaf extracts (Bertoletti *et al*., 2018). As far as we are informed, no research has been carried out to prove the presence of photosensitizers in the leaves of the *F.auriculata*.

A promising, non-invasive approach to combat antibiotic-resistant infections, treat localized cancers, and treat skin conditions such as acne and psoriasis is PDT with natural photosensitizers. Because they are of natural origin, side effects are minimized and the risk of adverse environmental impacts is reduced – in line with sustainable health practices. PDT can help improve infection control and patient outcomes, as well as address the global challenges of antibiotic resistance and cancer, by integrating these compounds into health strategies. In the current study, we examined fractions containing natural photosensitizers from *F. tataricum* and *F. auriculata* for their effect on skin cancer cells.

Chapter 3
Extraction and Preliminary Phytochemical Analysis

3.1 Introduction

For generations, individuals used natural cures for medical problems, therefore starting the procedure of drug creation. Examining food micronutrients, medicinal herbs and bioactive cultures helped to pave the path for creation of pure, regulated-dose medications (Rishton *et al*., 2008). Plants are a wealth of chemicals and bioactive molecules with different pharmacological uses and few adverse effects as they are under investigation (Aye *et al*., 2019). Their great content of minerals and phytochemicals like polyphenols, which can help manage, treat, and prevent many medical conditions, including cancer, inflammation, liver diseases, and oxidative stress (Vujanovic *et al*., 2019), often describes their beneficial characteristics. Among these phytocompounds, natural photosensitizers occupy a particularly important role since they interact with light to produce reactive oxygen species (ROS). Particularly in the realm of photodynamic treatment (PDT), these ROS show great potential as they can target and destroy aberrant cells only. Based on literature review, we identified *F. tataricum* and *F. auriculata* as potential source of natural photosensitizers for Photodynamic therapy (PDT). These plant species were selected for further investigation. A detailed description of the plants can be seen in Chapter 1.

In this chapter the preliminary investigations done to examine the phytochemical content and antioxidant capacity of *F.tataricum* and *F.auriculata* are described. Carefully collected from their native environments, the plants guarantee sample authenticity and quality. To find main types of secondary metabolites in the plant extracts, preliminary phytochemical screening was carried out. Antioxidant activity was evaluated using the rather popular DPPH and ABTS methods.

3.2 Materials and Methods

3.2.1 Materials

2,2-Diphenyl-1-Picrylhydrazyl (DPPH) and 2,2'-Azino-bis(3-ethylbenzothiazoline-6-sulfonic acid (ABTS) were purchased from HiMedia laboratories.

3.2.2 Collection of plant materials and sample preparation

F.auriculata was collected from Thrissur during the April-May months. *F.tataricum* (Buckwheat) seeds were purchased from Vikaspuri local market, New Delhi and cultivated in the premises of our Department. The samples were authenticated and deposited in the library by Dr. Pradeep A. K from the Department of Botany, University of Calicut. The *F. auriculata* leaves and *F.tataricum* aerial parts were cleaned and air dried. The samples were shade-dried and powdered.

3.2.3 Extraction

Crude extract was obtained using the cold extraction procedure. For 48 h, 25 g of the dried powdered samples were steeped in 250 mL of ethanol. Filtrate obtained after filtering each plant extract using filter paper was concentrated to a small volume to eliminate ethanol. The gummy extract was stored in a refrigerated at 4° C (Villacorta *et al*.,2017).

3.2.4 Preliminary analysis of phytocompounds

Qualitative phytochemical evaluation of the extracts was carried out using standard procedures.

3.2.4.1 Test for Alkaloids

0.10 g of the plant extract was mixed with 2 ml of 5% HCl and filtered to determine the presence of alkaloids.

- **Mayor's Test** (Tracey *et al*.,1955): Six drops of Mayor's reagent (13.5 g of mercuric chloride and 5 g of potassium iodide in 1000 mL of distilled water) was added to 1mL of filtrate.Yellowish-white colored precipitate suggested the presence of the alkaloids.

- **Wagners Test** (Wagner., 1997) : To 1 mL of the previously prepared filtrate, a few drops of Wagner's reagent (1g of iodine and 3g of potassium iodide in 50 mL of distilled water) were added. The reddish brown precipitate was interpreted as proof of the presence of alkaloids.

3.2.4.2 Test for proteins

- **Million's Test** (Rasch and Swift.,1960) : When crude extract was combined with 2 ml of Millon's reagent, a white precipitate,and while heated turned in to crimson red that reveal the presence of protein.

- **Ninhyrin Test** (Yasuma and Ichikawa.,1953): Presence of protein and amino acid was shown by a violet colour developing when crude extract was heated with 2ml of Ninhydrin 0.2% solution.

3.2.4.3 Carbohydrates Test (Harborne *et al*.,1998)

- **Fehling's test** : 2 mL of Fehling A (7g of $CuSO_4 7H_2O$ in 100 mL of distilled water) and Fehling B (24 g of KOH and 34.6 g of potassium sodium tartarate in 100 mL of distilled water) reagents were combined in equal quantity (1:1) and subsequently added to crude extract before being gently heated.

- **Benedict's Test**: After boiling crude extract with 2ml of Benedict's reagent (17.3 g of $CuSO_4.5H_2O$, 100 g of Na_2CO_3 and 173 g of sodium citrate in 1000 mL of distilled water) a reddish brown precipitate appeared, indicating the presence of the carbohydrates.

- **Molisch's Test :** 2ml of Molisch's reagent (3.75g of alpha-naphthol in 25 mL of ethanol) was added to the crude extract, and the mixture was thoroughly agitated. 2ml of concentrated H_2SO_4 was gently added to the test tube's side. At the interphase, a violet ring formed which indicated the presence of carbohydrates.

3.2.4.4 Test for Phenols

- **Ferric chloride test** (Mage.,1963)**:** A 5% solution of $FeCl_3$ was dissolved in 2ml of crude extract. The presence of phenols was indicated by a dark green hue.

3.2.4.5 Test for Flavonoids (Trease.,1983) : A fraction of the crude extract was mixed with 5 ml of diluted ammonia solution before being mixed with concentrated H_2SO_4. Each extract had a yellow colouration that showed flavonoids were present. Standing made the yellow coloration disappeared.

3.2.4.6 Test for Phytosterols

- **Salkowski Test** (Harborne.,1998) : Chloroform was added to the extract and filtered. Filtrate was then treated with 3-4 drops of concentrated H_2SO_4 carefully and shake gently. The resulting filtrates were left undisturbed. The emergence of a vibrant golden yellow hue signifies the existence of triterpenes.

3.2.4.7 Test for Saponins (Harborne.,1998): A test tube containing crude extract and 5 ml of distilled water was vigorously shaken. It was assumed that the presence of saponins was indicated by the production of stable foam.

3.2.4.8 Test for Tannins (Soni *et al*.,2013) : In a test tube, 1 ml of the sample and 1 ml of 0.008 M potassium ferricyanide were added. After adding 1 ml of 0.02 M ferric chloride and 0.1 N HCl, the mixture was checked for blue-black colour.

3.2.5 Antioxidant Assays

3.2.5.1 DPPH Assay (Brand *et al*., 1995, Soltanian *et al*., 2019)

A 0.004% 2,2-diphenyl-1-picryl-hydrazyl (DPPH) solution was prepared in Methanol for the DPPH free radical scavenging assay. Various concentrations of the extracts (5-20 µg/mL) were added into the 96-well plate. Methanol was utilized to adjust the volume to 50 µL. Methanol served as the negative control. Each well received 150 µL of DPPH solution including a negative control well. The mixture of ingredients was shook on a microplate shaker and stored in a dark room for 30 min. With a plate reader, the degree of discoloration which indicated free radical scavenging activity was evaluated at 517 nm. Ascorbic acid (5-20 µg/mL) served as the positive control (Robinson *et al*., 2017). The inhibition percentage for various concentrations allowed one to determine the DPPH scavenging capacity of the extracts. The calculation was carried out using the following equation:

$$Percentage\ of\ inhibition\ of\ the\ DPPH\ radical = \left(\frac{Absorbance\ of\ Control - Absorbance\ of\ Sample}{Absorbance\ of\ Control}\right) X100$$

The IC_{50} values represent the concentration of the sample necessary to scavenge 50% of the DPPH free radicals.

3.2.5.2 ABTS assay (Miller *et al*., 1996, Hassouni *et al*., 2019)

The ABTS assay was conducted by utilizing a solution containing 7 mM of ABTS along with Ammonium persulphate (2.45 mM) (Bibi *et al*., 2020). Kept this solution in dark for 12-16 h at room temperature before the assay. After incubation the solution was diluted to 0.035 mM with methanol with an absorbance of 0.7 ± 0.02 at 734 nm. Various dilutions of the extract ranging from 5 µg/mL to 20

µg/mL were prepared in a 96-well plate, and each dilution was adjusted to a final volume of 50 µL using distilled water. Then in each well, 150 µL of ABTS solution was added. As a negative control, distilled water was served. The mixture was subjected to a 6 min incubation period in a dark room, after which the absorbance was measured at 734 nm using a spectrophotometer. As a positive control, ascorbic acid (Hussen *et al*.,2023) has been used. The experiments were conducted in triplicate. To calculate the percentage of radical scavenging activity for each extract, the following equation was employed.

$$Scavenging\ effect(\%) = \left(\frac{Absorbance\ of Control - Absorbance\ of Sample}{Absorbance\ of Control}\right) X100$$

The IC_{50} values indicate the concentration of the sample necessary to scavenge 50 % of the ABTS free radical.

3.2.6 Statistical Analysis

The statistical package for the social sciences (SPSS) program, version 20.0 for windows, was utilized for all statistical analyses not only in this chapter but also throughout the other chapters. One –way analysis of variance (ANOVA) was used to evaluate group differences. Post-hoc comparisons of means were performed using Duncan's Multiple Range Test at a significance threshold of $P<0.05$.

3.3 Results

3.3.1 Sample collection

Herbarium was prepared for the *F.auriculata* and *F.tataricum*. The accession numbers are 7297 for *F.auriculata* and 1482311 for *F.tataricum* .

3.3.2 Yield of extract

After the extraction we got 134.5 mg and 74.5 mg of extract per gram each plant samples of *F.tataricum* and *F.auriculata* respectively.

3.3.3 Preliminary Qualitative phytochemical analysis

The results of phytochemical analysis of *F.tataricum* and *F.auriculata* are given in table 3.1.

Table 3.1 Phytochemical analysis of *F. tataricum* and *F. auriculata*

Phytochemicals	***F. tataricum***	***F. auriculata***
Alkaloids	+	+
Flavonoids	+	+
Proteins	+	+
Carbohydrates	+	+
Phenols	+	+
Phytosterols	+	+
Tannins	+	+
Saponins	+	-

Phytochemical study of the ethanolic extracts of *F.tataricum* and *F.auriculata* helped to identify their bioactive moleules. Both extracts turned out to be rather rich in phyochemicals. Both extracts turned up alkaloids, flavanoids, proteins, carbohydrates, tannins and saponins. Still, phytosterols was absent in *F.tataricum*. These results imply that both plants contain several bioactive elements with possible medicinal uses. More research is required to separate and define these molecules and assess their biological action.

3.3.4 Antioxidant assays

3.3.4.1 DPPH Assay

The findings of the DPPH assay are displayed in Figure 3.1.

Figure 3.1 DPPH assay

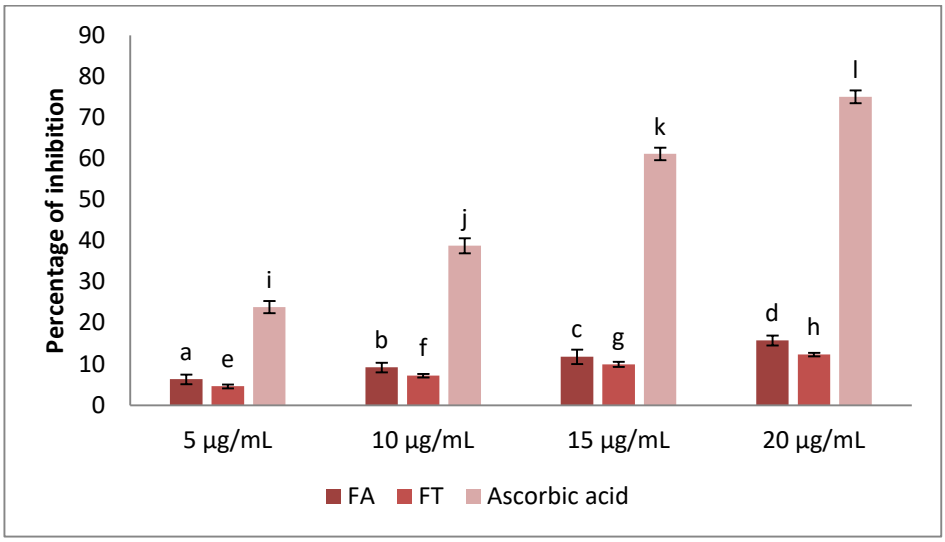

This bar graph depicts the percentage inhibition of DPPH (1, 1-diphenyl-2-picrylhydrazyl) radical by different concentrations (5, 10, 15, and 20 µg/mL) of *F.auriculata* and *F.tataricum* extracts. Error bars represent standard error (n=3). F value for DPPH Assay of FA, FT and Ascorbic acid are 27.087, 143.721, and 599.853 respectively. Different alphabets indicate the significant differences between the groups. P value < 0.05.

These results demonstrate that both *F. auriculata* and *F. tataricum* possess antioxidant properties; however, the antioxidant activity of *F.tataricum* is significantly higher than that of *F. auriculata*. In terms of inhibition, the highest degree was revealed by ascorbic acid, which is well-known for the antioxidant qualities it possesses. The antioxidant activity of *F.auriculata* and *F.tataricum*

appeared to increase with increasing concentration, which suggests that the intensity of the influence is depending on the concentration.

3.3.4.2 ABTS assay

The results of antioxidant analysis by using ABTS of *F.tataricum* and *F.auriculata* are given in Figure 3.2.

Figure 3.2 ABTS Assay

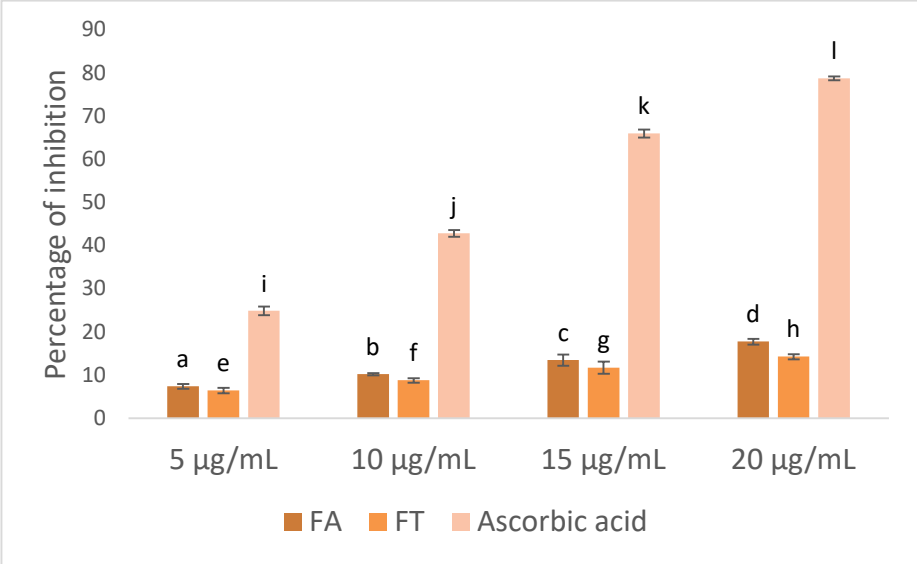

This bar graph depicts the percentage inhibition of ABTS by different concentrations (5, 10, 15, and 20 µg/mL) of *F.auriculata* and *F.tataricum* extracts. Error bars epresent standard error (n=3). F value for ABTS of FA, FT and Ascorbic acid are 95.809, 47.292, and 2671.476 respectively. Different alphabets indicate significant differences between the groups. P value <0.05.

The results of the ABTS experiment demonstrated that extracts of both *F. auriculata* and *F. tataricum* contained a high amount of antioxidant activity. This was proved by the fact that both extracts were able to neutralize the ABTS radical with their respective

properties. When the quantity of the extracts was raised from 5 µg/mL to 20 µg/mL, there was a considerable rise in the proportion of the ABTS radical that was inhibited. This leads one to believe that the antioxidant activity increased in a manner that is dependent on the concentration of the extracts. Taking into consideration the fact that both extracts demonstrated favorable outcomes, it was discovered that the *F. tataricum* extract consistently demonstrated a higher degree of antioxidant activity in contrast to the *F. auriculata* extract throughout all concentrations. Considering all of these data, it is obvious that both *F. auriculata* and *F. tataricum* possess antioxidant properties, which could potentially play an important part in the medical applications of both of these species.

IC_{50} of the extracts in DPPH and ABTS method are given in table 3.2.

Table 3.2 IC_{50} values of Antioxidant assays using DPPH and ABTS methods

Sample name	IC_{50} value from DPPH assay	IC_{50} value from ABTS assay
F.auriculata (FA)	75.93 ± 1.722	67.47 ± 0.932
F. tataricum (FT)	92.58 ± 2.877	87.71 ± 1.099
Ascorbic acid	12.59 ± 0.335	11.66 ± 0.208

Values are expressed in µg/mL ± SD (n=3)

The DPPH and ABTS assays have been used in order to determine the quantity of antioxidant capabilities possessed by the extracts of both *F. tataricum* and *F. auriculata*. During the DPPH and

ABTS experiments, the median inhibitory concentration (IC_{50}) values for *F. auriculata* were determined to be 75.93 ± 1.722 µg/mL and 67.47 ± 0.932 µg/mL, respectively. Furthermore, the IC_{50} values for *F. tataricum* in the DPPH and ABTS assays were 92.58 ± 2.877 µg/mL and 87.71 ± 1.099 µg/mL, respectively. These values were found to be comparable. Ascorbic acid, a well-known antioxidant that served as a reference in our research, exhibited IC_{50} values of 12.59 ± 0.335 µg/mL and 11.66 ± 0.208 µg/mL in the DPPH and ABTS assays, respectively. In general, these results indicate that both *F.auriculata* and *F. tataricum* extracts possess antioxidant activity. However, *F. auriculata* extracts showed a somewhat higher capacity for antioxidant activity than *F. tataricum* extracts in both trials. The antioxidant activity of both extracts, on the other hand, was found to be much lower than that of ascorbic acid.

3.4 Discussion

India's mainly mountainous northern and northeastern states including Jammu & Kashmir, Uttarakhand, Himachal Pradesh, and the northeastern states (Rana *et al*., 2012, Joshi *et al*., 1999) have buckwheat farming concentrated primarily. Arunachal Pradesh, Assam, Bihar, Jammu & Kashmir, Jharkhand, Maharashtra, Manipur, Meghalaya, Mizoram, Orissa, Sikkim, Karnataka, and West Bengal (Singh *et al*., 2023) additionally demonstrate *F. auriculata* in India. Kerala is beginning to know *F.auriculata* as an ornamental plant really well. These plant species are readily accessible because of home cultivation.

Using 90 % ethylene glycol or methanol with 10% glacial acetic acid, Chick *et al* successfully eliminated all of the photosensitizing material including all extractable constituents from *Fagopyrum esculentum* (Chick *et al*., 1941). Pre-extraction with ether followed by acetone/water/acetic acid (Brockman *et al.*, 1952) allowed Brockmann *et al*., to extract up to 270 mg of partially purified fagopyrins per Kg of *Fagopyrum esculentum* dried flowers. For *in vitro* phototoxicity experiments, Theurer employed ethanol/water (1:1) extracts (Theurer *et al*., 1997). Tartary buckwheat typically flowers later than common buckwheat. According to Fabjan *et al.* (2003), TB flowers bloom around the 50th day after sowing (DAS) and begin forming seeds, though this timing can vary with cultivation conditions. Jacheol's study indicated that TBF started blooming on the 40th DAS. We observed flowering after two months of growth, specifically at 60 days after sowing.

Jacheol Kim (2020) reported the detection of fagopyrins in the stems, leaves, and flowers of Tartary buckwheat (TB), with concentrations in Tartary buckwheat flowers (TBF) being significantly higher than in other parts. Both TBF and common buckwheat flowers (CBF) exhibited greater fagopyrin levels than other plant parts, as noted by Eguchi *et al.* (2009) and Stojilkovski *et al*. (2013). Additionally, various studies indicate that fagopyrins are generally higher in buckwheat leaves than in seeds or hulls (Eguchi *et al*., 2009; Stojilkovski *et al*., 2013; Benković *et al*., 2014). Jacheol also highlighted that the highest concentrations of fagopyrins were found in the flowers of both CB and TB, followed by leaves and stems. This is

why we selected the aerial parts of Tartary buckwheat during flowering, for fagopyrin extraction.

Using ethanol as the solvent, Villacorta and colleagues efficiently recovered natural photosensitizers from the aerial sections of *L. racemosa*, *C. odorata*, and *A. procera*. We chose this approach to extract photosensitizers from our chosen plants as their performance with other plant species (*L. racemosa*, *C. odorata*, and *A. procera*) suggested ethanol as the most suitable solvent. Heating can reduce fagopyrin content (Glavac *et al*., 2017). Consequently, we believe that a method without heating is more advantageous for our study.

Buckwheat is rich in protective flavonoids, such as quercetin and quercitrin which helps to withstand UV-B rays and other stresses (Zhang *et al*.,2017) Because of the strong sunlight and high temperatures tatary buckwheat, that particularly grown in high-altitude areas like Liangshan, China contains high concentration of flavonoids (Wang *et al*.,2022., Aubert *et al*.,2022). Different plant parts of the Buckwheat have these flavonoids that possess antioxidant activity (Borovaya *et al*.,2020., Matsui *et al*.,2020., Park *et al*.,2017). In our study we found the presence of flavonoids which are probably responsible for the antioxidant activity shown by the ABTS and DPPH method. This correlation is supported by existing literature.

Phenolic acids such as neochlorogenic, chlorogenic, vanillic, caffeic, and ferulic acids are present in both native and germinated buckwheat (Bhinder *et al*.,2022., Ren *et al*.,2022). Tatary buckwheat typically has higher quantities of phenolic acid than regular

buckwheat; however, fermentation raises this quantity (Podolska *et al*.,2021). Enzyme activity causes neochlorogenic acid levels to drop during dough production at low temperatures, while they remain stable at temperatures over 80ºC (Germ *et al*.,2020). Neochlorogenic and chlorogenic acids show potential as chemopreventive agents inhibiting breast and colon cancer cells growth (Noratto *et al*.,2009., Thurow *et al*.,2012).

F. auriculata leaves contained alakloids, phenols, flavonoids, tannins and terpenoids. The plant extract also exhibited antioxidant activity. This may be due to the presence of phenols and flavonoids (Kumari *et al*.,2018). Our study also found the presence of these phytochemicals.

This chapter comprehensively analyzed *F.auriculata* and *F.tataricum*, revealing their chemical composition and bioactivity. The plants are rich in essential minerals and contain functional groups. The presence of the phytochemicals such as alkaloids, flavonoids, and other compounds, aligning with the observed antioxidant activities measured by DPPH and ABTS assays. These findings suggests that both plants possess valuable bioactive compounds with potential medicinal applications, warranting further research to isolate and characterize specific molecules and explore their therapeutic efficacy.

Chapter 4

Phototoxicity assessment and chromatographic separation of photoactive fractions

4.1 Introduction

The study of phototoxicity and the identification of phototoxic compounds are critical areas of research in pharmacology and toxicology, as they help to understand the mechanism of photosensitizers when exposed to light. This chapter focuses on the isolation of potential phototoxic compounds from the crude extracts of *F. tataricum* and *F. auriculata*, specifically designated as PAF 1 and PAF 2.

Our approach begins with a preliminary assessment of the crude extract's phototoxic potential using the uric acid test, a method that detects the depletion of uric acid due to the generation of reactive oxygen species upon light exposure. Subsequently, thin-layer chromatography (TLC) is employed for the chromatographic separation of the crude extract, aiming to isolate photosensitizer-containing fractions. TLC's simplicity and efficiency make it a pivotal tool for purifying these compounds.For the TLC separation, hypericin and psoralen are used as standard photosensitixing compounds,based on previous reports.

Following TLC separation, the isolated fractions, PAF 1 and PAF 2, underwent further scrutiny to confirm their phototoxic

properties. This involves repeating the uric acid assay on the individual fractions, providing evidence of their ability to induce photochemical reactions. To further validate their photosensitizing activity, the linoleic acid assay is conducted, which measures the light-induced oxidation of linoleic acid. This dual approach, utilizing both uric acid and linoleic acid assays, provides a comprehensive understanding of the phototoxic potential of PAF 1 and PAF 2, shedding light on their interaction with light and their ability to generate reactive species. We aim to contribute to the broader knowledge of phototoxicity of PAF 1 and PAF 2 fractions from *F. tataricum* and *F. auriculata* respectively.

4.2 Materials and methods

4.2.1 Materials

1000 W halogen tungsten lamp (L05100, Wipro Ent [P] Ltd) It can cover a wavelength range of 350 nm to 3500 nm which can span the absorption maximum of reported photosensitizers from the selected plant species. Uric acid is purchased from Scisco Research Laboratories (SRL).

4.2.2 Uric acid photodepletion assay (Fischer *et al*., 1998)

Comparing the photodynamic activity of various photosensitizers is best accomplished using the uric acid test, which stands out as the most suitable method. Because of photosensitization, uric acid, which acts as a singlet oxygen scavenger, demonstrates a reduction in its absorption at a wavelength of 293 nm.

Requirements:

1. Phosphate buffered saline solution (1M, pH 7.4)
2. Uric acid solution: 10 µg/mL

Procedure

All the test tubes were kept under the dark to avoid light, other than that from the halogen lamp. An irradiation process lasting 5 min was performed on 1 mL of a solution of uric acid that contained photosensitizers. When the illumination being was performed, the light source was kept at a distance of between 30 cm from the light source. Using a UV-Visible Spectrophotometer, the samples' optical density (OD) was measured at a wavelength of 293 nm, before and after the irradiation.

4.2.3 Thin Layer chromatography (TLC) (Eguchi *et al*., 2009)

TLC plate preparation: To make silica gel slurry, combined 4 g of TLC silica gel with 8 mL distilled water. Evenly spread this slurry over a glass slide that was 16 x 8.2 cm in size to create a layer, precisely 0.50 mm thick. After allowing the silica gel layer to air dry for 30 min, it was heated for another 30 min at 110 ºC to activate it.

Sample and standard loading: The capillary tube was used to spot the plant extracts (5 mg/mL), psoralen (50 µg/mL) and Hypericin (10 µg/mL) reference standards to the TLC plate from a distance of 1 cm from the end.

Chromatogram development: Toluene, ethyl acetate, formic acid, and pyridine were properly blended in a precise ratio of 50:40:10:20 to serve as the solvent system for chromatogram development. The chromatographic chamber was filled with the solvent system first, then it was covered and let to saturate. TLC plates with samples on them were allowed to develop in the saturated chamber.

Chromatogram visualisation: After the TLC plate developed completely, it was taken out of the chamber and the solvent front was noted. After drying, the spots on the plates were seen under a UV trans-illuminator (Syngene G: Box).

Spot collection: Collected the spot by lightly scratching the silica gel where the target compound is located. After being collected, the silica gel was carefully dissolved in methanol for PAF 1 spot and acetone for PAF 2 spot. Following that, the solution was centrifuged at 1500 rpm for 5 min. This effectively separated the solid remains, producing a supernatant that was clear and homogenous. The supernatant was then concentrated and used for further analysis.

Standards used in TLC: *F.tataricum* has been reported to possess fagopyrin. Hence hypericin was used as a standard for fagopyrin, due to its structural similarity and commercial availability. Ficus species has been reported to contain furanocoumarins. Hence psoralen was chosen as a standard for furanocoumarins.

4.2.4 HPTLC

The HPTLC analysis was carried out at the Centre for Medicinal Plants Research (CMPR) in Arya vaidyasala, Kottakkal, Malappuram. Sample solution was prepared and applied to the silica gel HPTLC plate using a capillary tube. The plate was then developed in a developing chamber containing a 50:40:10:20 mixture of toluene, ethyl formate, formic acid and pyridine as the mobile phase (Eugchi *et al*., 2009). Once the solvent front reached the desired height, the plate was removed and allowed to dry. The developed spots were visualized under ultraviolet (UV) light at a wavelength of 288nm, 302nm and 346 nm.

4.2.5 Linoleic acid test (Castell *et al*., 1994)

Highly reactive lipid hydroperoxides are produced when photo-induced lipid peroxidation of linoleic acid occurs. The rise in absorbance at 233 nm can be used to quantify this.

Requirements

1. Phosphate buffer (0.01 M pH 7.2)
2. 0.05% Tween 80 (v/v): 100 mL of distilled water is mixed with 0.5 mL of Tween 80, and heated in a boiling water bath until it dissolves completely.
3. 0.01 M phosphate buffer with 0.35% linoleic acid (pH 7.2)

Method: Filled test tubes with 1 mL of the 0.35% linoleic acid solution. The reaction mixture which contains photosensitizers in

different concentrations is exposed to irradiation for 5 min. Absorbance at 233nm was measured before and after irradiation for each photosensitizer. Linoleic acid's photosensitized peroxidation level is determined by measuring the absorbance rise at 233 nm.

4.3 Results

4.3.1 Uric acid photodepletion test

The results of Uric acid test with crude extract of *F. tataricum* and *F. auriculata* are given in Figure 4.2.

Figure 4.1 UV-Visible absorption spectra of uric acid in PBS

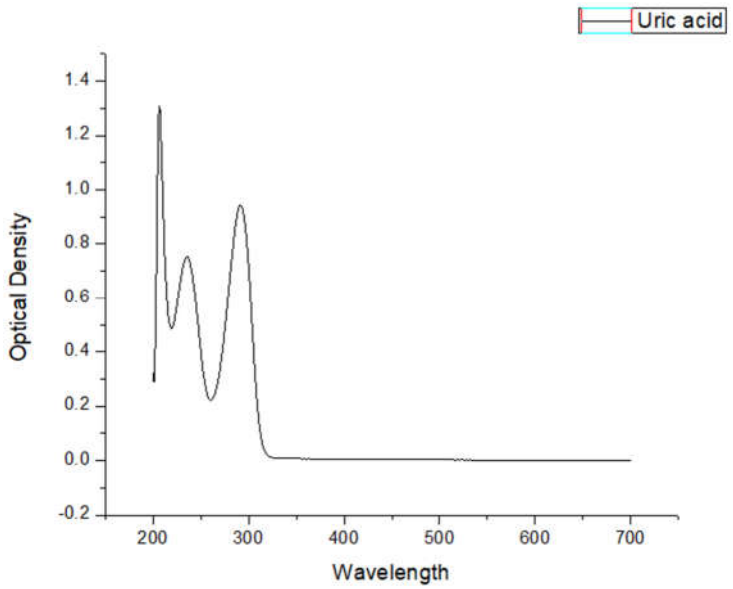

UV-Visible spectrum of uric acid shows a peak at 292 nm.

The UV-Visible spectrum in figure 4.1 illustrates absorption peak for uric acid in PBS. Under the presence of phototoxic chemicals from *F.auriculata* and *F.tataricum*, the UV-visible spectra of uric acid show a decrease in peak intensity at 292 nm (Figure.4.2). The phototoxic chemicals included in both *F.auriculata* and *F.tataricum* clearly show photodynamic activity based on UV-Visible spectra and uric acid behavior. Reduced uric acid peak intensity at 292 nm after irradiation indicates the synthesis of singlet oxygen, a fundamental reactive oxygen species engaged in photodynamic reactions.

Figure 4.2 UV-Visible spectrum of uric acid test

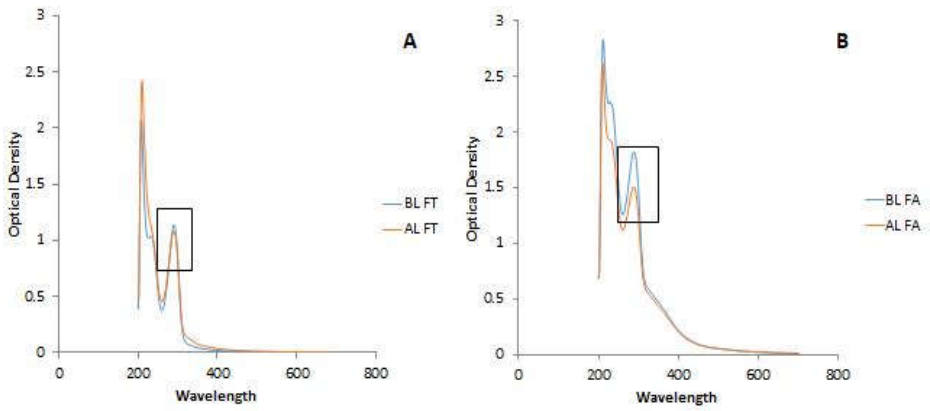

Uric acid test of samples exhibiting a decrease in peak at 292 nm. The peak intensity decreases in the presence of phototoxic compounds from *F. tataricum* at 300 µg/mL concentration (A) and *F. auriculata* at 300 µg/mL concentration (B). The following abbreviations are used – BLFA: crude extract of *F.auriculata* (before light exposure), ALFA: crude extract of *F. auriculata* (After light exposure), BLFT: Extract of *F.tataricum* (before light irradiation), ALFT: extract of *F.tataricum* (after light exposure).

The crude extract of *F.auriculata* demonstrates a greater phototoxic breakdown activity of uric acid compared to *F. tataricum.* A greater decrease in the 294 nm peak in *F.auriculata* indicates a more

significant reduction in uric acid concentration compared to *F.tataricum.* This suggests that *F.auriculata* crude extract possess more phototoxic compounds.

4.3.2 TLC

The result of TLC separation is given in figure 4.3.

Figure 4.3. TLC chromatogram

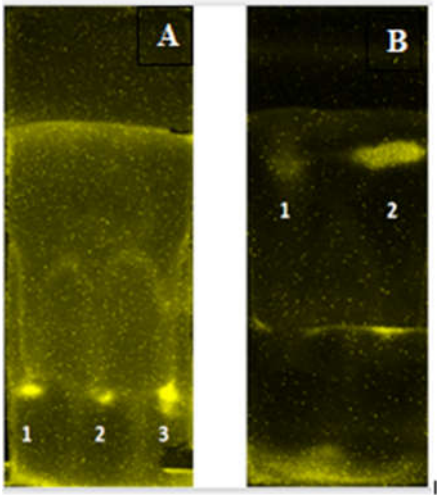

[A] *F. tataricum* (Lane 1and 2) Hypericin (Lane 3)

[B] *F. auriculata* (Lane 1) Psoralen (Lane 2)

In accordance with Figure 4.3, the TLC chromatogram analysis demonstrated that the *F.tataricum* exhibited a band where Rf value that was identical to that of the standard, hypericin (Figure 4.3A). When compared to its standard, psoralen, the corresponding TLC fraction derived from *F. auriculata* had an Rf value that was precisely the same figure as psoralen. Based on these findings, it is highly probable that

F.tataricum extract consists of a naphthodianthrone with similar structure as hypericin; and *F. auriculata* extract possesses a furan, structurally related to psoralen. These isolated fractions from the *F. tataricum* and *F. auriculata* are termed hereafter as Photoactive fraction 1 (PAF 1) and Photoactive fraction 2 (PAF 2) respectively.

4.3.3 HPTLC

The results of HPTLC of *F.tataricum* extract and hypericin are given in Figure 4.4,Table 4.1 and Table 4.2.

Figure 4.4 HPTLC chromatogram of *F.tataricum* and hypericin

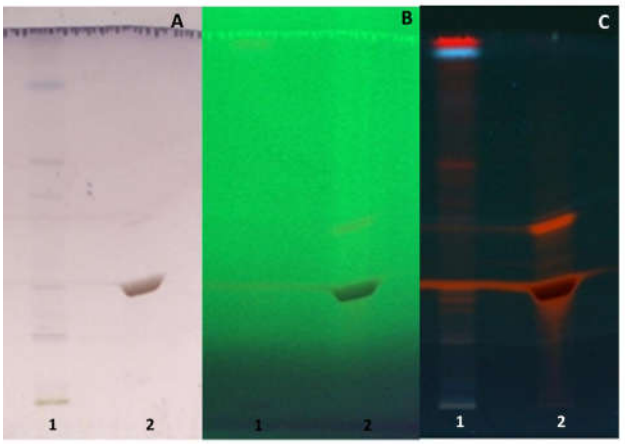

HPTLC chromatogram visualization under (A) Visible light, (B) 254 nm (C) 366 nm.
Lane 1: *F.tataricum* extract
Lane 2: Hypericin

Hypericin (Lane 2) appears as a spot under all three wavelengths: visible light, 254 nm and 366 nm. The *F. tataricum* extract (lane 1) shows spot under visible light and 366nm wavelength light, which corresponds to the hypericin standard, as well as several other fluorescent spots with different retention factors.

Table 4.1 Rf values of *F. tataricum* spots observed under 366nm

Peak	Start Rf	Start Height	Max Rf	Max Height	Max %	End Rf	End Height	Area	Area %
1	0.02	0.2	0.04	26.7	10.55	0.05	1.9	275.5	5.26
2	0.14	4.9	0.17	46.3	18.30	0.20	14.9	1039.5	19.84
3	0.26	14.5	0.27	22.2	8.75	0.29	11.8	349.4	6.67
4	0.29	12.3	0.32	60.3	23.82	0.36	8.8	1275.5	24.34
5	0.47	14.8	0.50	27.9	11.02	0.51	8.1	625.6	11.94
6	0.52	9.2	0.53	13.8	5.47	0.56	5.3	337.7	6.45
7	0.63	7.5	0.65	18.1	7.15	0.68	1.7	453.1	8.65
8	0.74	1.1	0.76	13.2	5.20	0.78	4.2	207.8	3.97
9	0.88	6.2	0.91	24.7	9.73	0.93	16.0	675.9	12.90

Table 4.2 Rf values of Hypericin spots observed under 366 nm

Peak	Start Rf	Start Height	Max Rf	Max Height	Max %	End Rf	End Height	Area	Area %
1	0.04	2.3	0.06	12.3	1.68	0.07	4.5	262.5	1.09
2	0.14	3.2	0.17	16.4	2.26	0.18	15.2	394.7	1.64
3	0.20	16.3	0.23	26.0	3.57	0.23	22.8	581.2	2.42
4	0.25	31.7	0.30	585.4	80.37	0.36	13.5	20057.2	83.49
5	0.46	11.9	0.49	71.8	9.86	0.54	6.3	2093.0	8.71
6	0.78	7.9	0.80	16.5	2.26	0.85	2.6	633.5	2.64

The chromatogram exhibits several prominent peaks characterized by their retention factor (Rf), height and area, indicating different compounds. Table 4.1 shows the identification of nine peaks. With an area of 1275.5, peak 4 is the largest, representing 24.34% of the total area. Its maximum Rf is 0.32 and its maximum height is 60.3. Six peaks were observed in table 4.2. Peak 4 in particular clearly dominates, accounting for 83.49% of the total area (20057.2), has a maximum Rf of 0.30, and reaches a remarkably high maximum height of 585.4. The remaining peaks in this chromatogram have areas of significantly smaller extent, accounting for 1.09% to 8.71 % of the

total area. The Rf value of the spot in the *F.tataricum* extract is similar, indicating the presence of fagopyrin in this extract.

The results of HPTLC analysis of *F.auriculata* and psoralen are observed under visible light, under 254 nm and 366 nm are given in figure 4.5.

Figure 4.5 HPTLC chromatogram of *F.auriculata* and psoralen

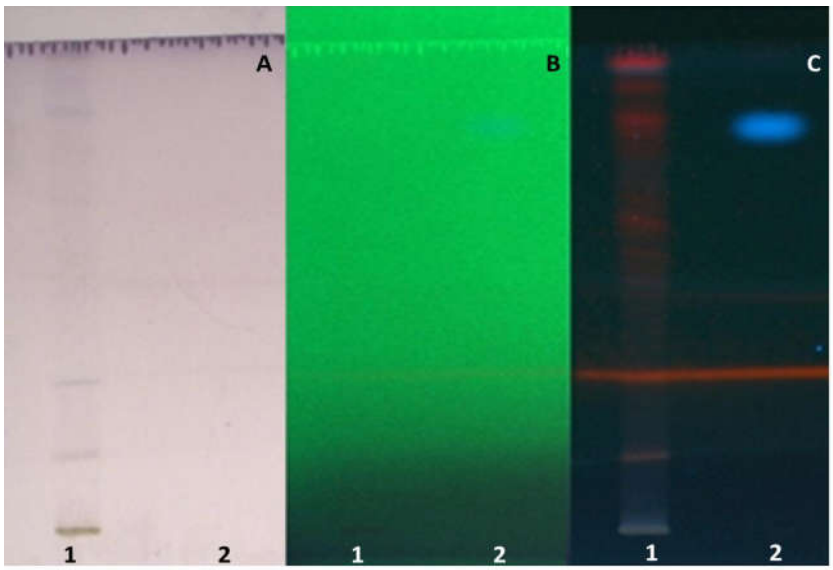

HPTLC chromatogram visualization under (A) visible light (B) 254 nm (C) 366 nm
Lane 1: *F.auriculata* extract
Lane 2: Psoralen

The HPTLC plate revealed that the psoralen lane was not visible under normal light. However, a spot was visible under 254 nm and 366 nm. A fluorescence spot in PAF 2 chromatogram corresponding to the reference psoralen was clearly visible under 366 nm. This indicates the presence of furan compound in the plant extract. In addition, additional fluorescent spots were detected, indicating the presence of other compounds in the extract.

Table 4.3 Rf values of *F.auriculata* plant extract

Peak	Start Rf	Start Height	Max Rf	Max Height	Max %	End Rf	End Height	Area	Area %
1	0.11	1.0	0.13	67.9	26.46	0.17	7.6	1148.3	21.70
2	0.29	2.9	0.31	16.7	6.51	0.32	6.2	317.8	6.01
3	0.49	14.2	0.50	23.2	9.03	0.52	11.5	516.9	9.77
4	0.60	10.4	0.63	19.1	7.45	0.64	9.0	479.7	9.07
5	0.65	8.1	0.67	24.0	9.33	0.69	6.2	503.2	9.51
6	0.83	21.3	0.84	25.8	10.03	0.85	15.0	504.6	9.54
7	0.89	11.7	0.91	26.2	10.21	0.93	17.5	562.7	10.64
8	0.94	16.9	0.96	53.9	20.98	0.99	7.3	1257.6	23.77

Table 4.4 Rf values of psoralen

Peak	Start Rf	Start Height	Max Rf	Max Height	Max %	End Rf	End Height	Area	Area %
1	0.13	1.3	0.16	11.5	4.31	0.17	7.0	238.6	2.77
2	0.29	9.9	0.31	40.6	15.18	0.33	10.4	688.7	8.00
3	0.47	10.7	0.49	16.5	6.15	0.53	5.1	590.4	6.85
4	0.78	3.8	0.83	199.0	74.36	0.88	3.3	7095.5	82.38

TLC analysis of the *F.auriculata* extract (Table 4.3) revealed eight distinct peaks, indicating multiple compounds separated by their Rf values ranging from 0.11 to 0.94. The compounds differed in their peak heights and the proportions they represented in the total area. The psoralen had four discernible peaks, with Rf values ranging from 0.13 to 0.78 (Table 4.4). Peak 4 was the dominant compound in the psoralen lane with a maximum Rf value of 0.83 and a proportion of 82.38 % of the total area. A maximum Rf value 0.82 was also found in the *F.auriculata* extract lane.

4.3.4 Uric acid test of PAF 1 and PAF 2

The results of uric acid test of PAF 1 and PAF 2 is depicted in Figure 4.6.

Figure 4.6 UV-Visible spectrum of uric acid test of PAF 1 and PAF 2

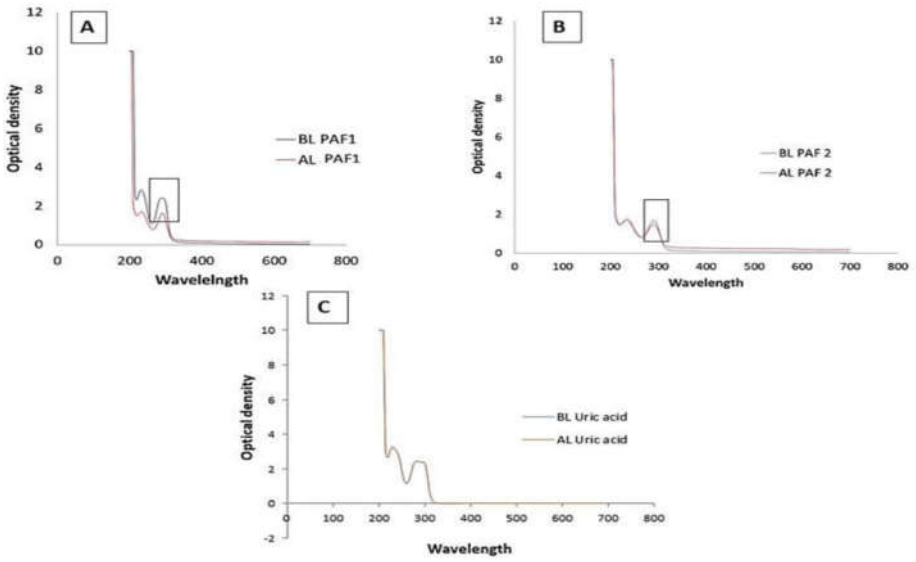

The test exhibits a decrease in peak at 292 nm. The peak intensity decreases in the presence of phototoxic compounds from PAF 1 at 300 µg/mL concentration (A) PAF 2 at 300 µg/mL concentration (B) and uric acid (C). BL: Before light treatment AL: After Light treatment

Figure 4.6 illustrates UV-Visible spectrum of uric acid, characterized by a peak at 292 nm, which signifies its concentration. Upon exposure to phototoxic compounds from PAF 1 and PAF 2, both at a concentration of 300 µg/mL, a reduction in the 292 nm peak intensity is observed, indicating uric acid degradation. Notably, PAF 1 demonstrates a more decrease in peak intensity compared to PAF 2, suggesting a greater capacity for phototoxic breakdown of uric acid. Furthermore, PAF 1 exhibits a higher depletion of uric acid than the crude extract it was derived from, highlighting the effectiveness of the fraction in inducing this phototoxic effect. Moreover, this confirms that the photoactive compound from the plant is present in this particular TLC fraction.

4.3.5 Linoleic acid photo-peroxidation assay

The result of linoleic acid photo-peroxidation is given in figure 4.7.

Figure 4.7. Relative photoperoxidation ability of PAF 1 and PAF 2

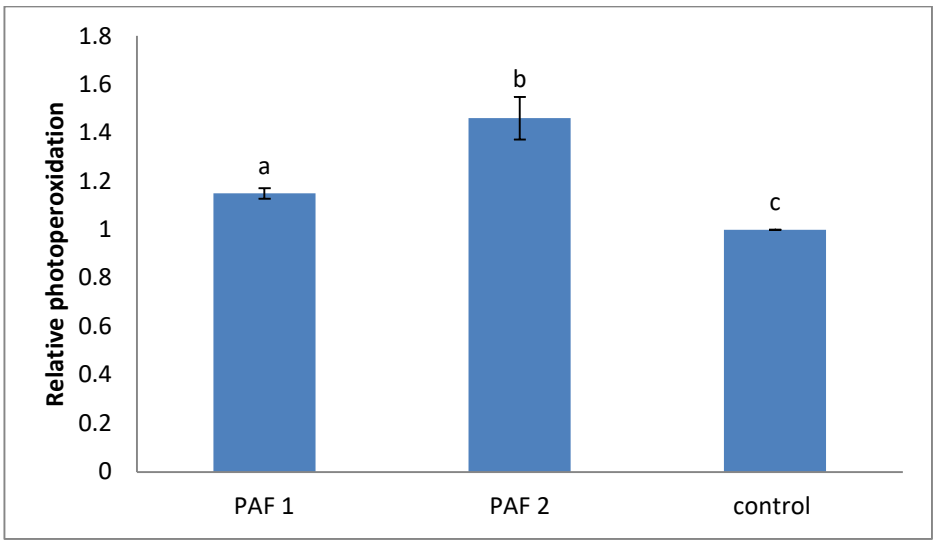

Linoleic acid was exposed to 1000 W halogen lamp irradiation for 1 min at 300 µg/mL concentration and the formation of conjugated dienic hydroperoxides was quantified by absorbance at 233 nm. Values are mean of three estimations. Error bar indicates standard error. Different alphabets indicate significant differences between groups. F value for linoleic acid photoperoxidation is 61.274 .P <0.05.

Figure 4.7 illustrates the relative photoperoxidation ability of PAF1 and PAF2, demonstrating that both compounds induced linoleic acid peroxidation under 1000W halogen lamp irradiation for 1 min at 300 µg/mL concentration. The observed increase in absorbance at 233 nm for both PAF1 and PAF2 confirms the formation of conjugated dienic hydroperoxides, a direct indicator of lipid peroxidation.

Notably, the data suggests that both PAF 1 and PAF 2 possess linoleic peroxidation activity.

4.4 Discussion

In the present work, we discovered that the uric acid (UA) peak at 292 nm dropped following addition of *F. auriculata* and *F. tataricum* to a UA solution and subsequent 5 min illumination of the solution. This produced the noted drop in the UA peak. The mechanisms that were found for established photosensitizers (PS) in the UA test match this decrease. This indicates that among the plant extracts are molecules acting as type II photosensitizers. Two sensible theories explain the drop in UA absorbance: either singlet oxygen production or quenching of the excited triplet state of the photosensitizer. One can find both of these justifications feasible. Fischer *et al.* (1998) claims that both of these mechanisms participate in photodynamic reactions. The molecules of the photosensitizer in the extracts definitely go through the process of excitation to a singlet state after being exposed to light; this is subsequently followed by intersystem crossing to the triplet state, which is more stable. Following that, this triplet state can interact with molecular oxygen, which produces reactive oxygen species (ROS), specifically singlet oxygen, a feature of Type II photochemical reactions (Foote. 1968, Abrahamse *et al*., 2016). Triplet state interacts with molecular oxygen in this way. Following that, the produced reactive oxygen species (ROS) could be in charge of uric acid degradation in solution, therefore causing the observed decrease in absorbance. This investigation provides proof that the plant extracts comprise active photosensitizers

able to induce photodynamic activity under light. The observed drop in UA absorption helps to show this fact. More noteworthy is the consistency of this approach with the function photosensitizers have been shown to perform in quenching excited triplet state process, generating singlet oxygen. Given the results, it seems that natural photosensitizers could come from extracts of *F. tataricum* and *F. auriculata*. Two fields where the use of these extracts could be quite beneficial are the field of photodynamic treatment and oxidative stress research. When comparing *F.tataricum* and *F. auriculata*, the extract of *F. auriculata* revealed a more significant drop in the peak of uric acid. When compared to the amount found in the extract of *F. tataricum*, the extract of *F. auriculata* contains rather more chromophores.

The observed phototoxicity of the crude extract prompted us to isolate photosensitizer-containing fractions using thin-layer chromatography (TLC). The appearance of red spots on the TLC plates of *F. tataricum* extracts is consistent with Euguchi *et al*. (2009), who reported the distribution of fagopyrin in buckwheat cultivars. Their study showed that the intensity and presence of red spots, indicative of fagopyrin, varied across different plant parts. Similarly, our results suggest the presence of fagopyrin in *F. tataricum* extracts, as the red spots on silica gel TLC plates indicate compounds with similar chromatographic properties. Euguchi *et al.* (2009) also demonstrated that fagopyrin concentration, visualized by red spot intensity, differs significantly across plant tissues, with leaves and flowers typically showing higher concentrations. The red spots observed in the present analysis of *F. tataricum* extract suggest the likely presence of

fagopyrin. Further analysis is required for definitive confirmation. Due to the limited availability of pure fagopyrin, hypericin, which shares structural similarities, was used as a standard. Hypericin is also known to be used as a standard compound for fagopyrin identification.

PAF 1 and PAF 2 were further tested for their phototoxic property using uric acid test and photo-lipid peroxidation test. We found phototoxicity for both PAF 1 and PAF 2. Our findings demonstrated a significant increase in linoleic acid photo-peroxidation, as evidenced by a heightened absorbance at 233 nm, following exposure to 1000 W halogen tungsten lamp for 1 min. This observation aligns with the established principle that the formation of conjugated dienes, a hallmark of lipid peroxidation, results in a characteristic absorption peak near 233 nm (Recknagel *et al.,* 1983). As highlighted by Maurer (1987), linoleic acid photo-peroxidation serves as a valuable *in vitro* test system for detecting potentially phototoxic compounds. Its simplicity, cost-effectiveness, and sensitivity make it a convenient tool for early-stage photosensitizer drug development.

The increase in absorbance at 233 nm in our experiments indicates a substantial rise in conjugated diene formation, thereby confirming the susceptibility of linoleic acid to photo-peroxidative damage under the applied conditions. This is consistent with the general observation that unsaturated fatty acids, such as linoleic acid, are readily peroxidized upon exposure to light and photosensitizers, due to the presence of methylene groups between double bonds, which are susceptible to free radical attack (Miranda *et al*., 1993).

While the linoleic acid photo-peroxidation assay offers a rapid and sensitive method for detecting phototoxic potential, it is crucial to

acknowledge its limitations. As noted by Maurer (1987) and Miranda *et al*. (1993), this assay may produce false positives due to its inability to account for cellular antioxidant defenses. Furthermore, it may not detect phototoxic compounds acting through alternative mechanisms, such as DNA damage. Therefore, complementing this assay with other techniques capable of assessing photodamage to diverse biological targets is essential for a comprehensive evaluation of phototoxicity.

In the present study, the use of a non-peroxidized linoleic acid sample as a control, allowed for the accurate determination of the difference in 233 nm absorbance, effectively isolating the contribution of photo-peroxidation from the inherent end absorption of non-peroxidized lipids. This approach ensures that the observed increase in 233 nm absorbance is directly attributable to the formation of conjugated dienes resulting from the applied experimental conditions.

In conclusion, this chapter demonstrates that extracts from *F. auriculata* and *F.tataricum* contain photosensitizing compounds capable of inducing photodynamic activity, as evidenced by the reduction of uric acid absorbance and the photo-peroxidation of linoleic acid. These findings suggest potential applications for these fractions (PAF 1 and PAF 2) in photodynamic therapy and oxidative stress research, warranting further investigation into the specific photosensitizing compounds and their mechanisms of action.

Chapter 5

Effect of PAF 1 and PAF 2 on skin cancer (A431) cells *in vitro*

5.1 Introduction

Photodynamic therapy (PDT) is an emerging treatment for various cancers, including skin cancer, utilizing a light-activated compound known as a photosensitizer. Upon activation, the photosensitizer generates reactive oxygen species (ROS) that induce cell death. Before progressing to *in vivo* experiments and clinical trials, *in vitro* cytotoxicity assessments are crucial for determining the effectiveness of photosensitizers, particularly against cell lines like A431. This chapter focuses on the methods used to evaluate the cytotoxicity of phototoxic fractions PAF 1 and PAF 2 against A431 cells. These techniques include subcellular localization assessments to determine drug placement within cells, AO/EtBr staining to differentiate between apoptosis and necrosis, Comet assay to assess DNA damage, Caspase 3 assay to investigate apoptotic activity, and cell cycle analysis to examine the impact of PAF 1 and PAF 2 on cell cycle progression. Collectively, these experiments contribute to a comprehensive understanding of the mechanisms underlying the cytotoxic effects observed in A431 cells treated with PAF 1 and PAF 2.

5.2 Materials and Methods

5.2.1 Materials

The study employed a 1000 W tungsten halogen lamp ((L05100, Wipro Ent [P] Ltd) as the light source for PDT. The human epidermoid carcinoma cell line A431was purchased from the National Centre for Cell Sciences (NCCS) in Pune, India. For cell culture experiments, essential materials, including Dulbecco's Modified Eagle Medium (DMEM), 0.25% Trypsin - EDTA, and Antibiotic-antimycotic solutions and 3-(4,5-dimethylthiazol-2-yl)-2,5-diphenyltetrazolium bromide (MTT) were purchased from Himedia, India. Fetal Bovine serum (FBS) was purchased from Gibco, Life Technologies Limited, UK. 5-Amino Levulinic acid (ALA) was acquired from Sisco Research Laboratories Pvt. Ltd, Mumbai, India. Acridine orange, Ethidium bromide, DAPI, DCFDA, low melting agarose, agarose, propidium iodide, caspase 3 substrate, BSA all are purchased from SRL, India. Softwares used are: Casp-1.2.3b1.exe for comet assay analysis, Floreado.io for flowcytometry analysis.

5.2.2 Cell culture

5.2.2.1 Maintenance of cell lines

The A431 human epidermoid squamous carcinoma cell line and L929 mouse fibroblast cell line was purchased from the National Centre for Cell Sciences (NCCS) in Pune. These cells were cultured in Dulbecco's Modified eagle Medium (DMEM) supplemented with 10 % Fetal Bovine Serum (FBS) and 1 % of antibiotic-antimycotic

solution. The cell cultures were maintained in a humidified atmosphere at 37 ºC with 5 % CO_2 .

The cell lines are grown as a monolayer, adhering to the surface of the culture flask. In culture, cells undergo proliferation, gradually forming a continuous layer on the seeded surface. Once the surface is entirely covered by a monolayer of cells, the culture is considered "confluent". When cells reach around 80-90 % confluence in a culture flask, it is advisable to perform sub-culturing by reseeding them at lower density.

5.2.2.2 Subculture

For the subculture, first verified the cell culture flask for confluent cell growth and discarded the spent media. Subsequently, performed two washes with 1ml of Phosphate Buffered Saline (PBS) containing 137 mM NaCl, 2.7 mM KCl, 8 mM Na_2HPO_4, and 2 mM KH_2PO_4 at a pH of 7.4 to eliminate residual serum that might interfere with trypsin activity. Added 1 ml of trypsin-EDTA solution to the flask and let it incubate for 5-10 min to facilitate cell detachment. Neutralized trypsin by adding fresh culture media, followed by centrifugation of the cell suspension at 1500 rpm for 5 min. discarded the supernatant and dissolved the pellet with 1 ml of fresh media. Transferred a 1/10 aliquot of the cell suspension into a new flask with an appropriate amount of culture medium. After that placed the cell culture flasks into a CO_2 incubator. After 24 h, verified cell reattachment and confirmed the medium pH is around 7.4. Changed the media as needed until the next subculture. To determine cell

viability, employed trypan blue dye and a hemocytometer for cell counting.

5.2.2.3 Cell counting

For the cell counting mixed 100 µL of trypsinized cells which are already mixed with 1 mL of fresh media with 100 µL of 0.4% trypan blue dye and let the mixture stand at room temperature for 5 min. 10 µL of this mix was placed on a hemocytometer and observed under microscope. Viable cells will repel the dye, while damaged cells will absorb it.

5.2.2.4 Cryopreservation

To preserve the cells, they were frozen and stored at -80ºC. The cell suspension was diluted to a 1:1 ratio with a freezing medium consisting of DMEM media with 5 % DMSO (serving as the cryoprotectant).

5.2.2.5 *In vitro* cytotoxicity assay

In vitro cytotoxicity assessments of samples were done using MTT assay, trypan blue exclusion method and NRU assay. Based on the samples and treatment methods applied, we took eight experimental groups which are as follows:

Group I (G-I): Cells

Group II (G-II): Cells + Light (267.81 W/m^2, 90 S)

Group III (G-III): Cells + PAF1

Group IV (G-IV): Cells + PAF2

Group V (G-V): Cells + ALA

Group VI (G-VI): Cells + PAF1+ light (267.81 W/m^2, 90 S)

Group VII (G-VII): Cells + PAF2 + light (267.81 W/m^2, 90 S)

Group VIII (G-VIII): Cells +ALA+light (267.81 W/m^2, 90 S)

- **MTT assay**

The MTT (3-[4,5-dimethylthiazol-2-yl]-2,5 diphenyl tetrazolium bromide) assay relies on the transformation of MTT (a water-soluble tetrazolium salt in yellow form) into water insoluble dark blue formazan crystals through the reductive cleavage of the tetrazolium ring by viable cells, reflecting their mitochondrial activity. Given that for most cell populations, total mitochondrial activity correlates with the number of viable cells, this assay finds widespread application in assessing the *in vitro* cytotoxic impact of samples on cell lines.

Requirements:

1. MTT - 5 mg/1 mL (PBS)
2. DMSO- 100%
3. 96 well plate

Procedure:

Cells were plated in a 96 well plate at a density of $5x10^3$ cells per well and incubated for 24 h at 37 ºC with 5 % CO_2. Once cells attached, they were treated with samples at final concentrations of 6.25

µg/mL, 12.5 µg/mL, 25 µg/mL and 50 µg/mL (Dissolved in 0.1% DMSO and then diluted with PBS). Following a1 h incubation, the cells were irradiated with a 1000 W tungsten-halogen lamp for 90 s. Another plate was kept in dark to evaluate the dark toxicity of those fractions. Positive controls involved cells treated with ALA, while an untreated set served as the control. After each incubation interval (24,48 and 72 h), the medium was replaced with fresh medium, and 10 µL of MTT solution was added to each well. The plates were incubated for 4 h during which viable cells reduced the yellowish MTT to a dark - colored formazan. Subsequently, the medium was removed, and 100 µL of DMSO was added to dissolve the formazan. The microplate was shaken, and optical density values were measured at 492 nm using plate reader (Alere 2100). The percentage inhibition were calculated by the formula:

$$Percentage\ of\ growth\ inhibition = \left(\frac{Absorbance\ of\ control - Absorbance\ of\ sample}{Absorbance\ of\ control}\right) \text{X } 100$$

- **Trypan Blue exclusion method**

The dye exclusion test is employed for assessing the quantity of viable cells within a cell suspension. This method relies on the fundamental principle that viable cells maintain intact cell membranes, preventing the uptake of specific dyes like trypan blue, Eosin or propidium. Conversely, non-viable or dead cells lack this membrane integrity and readily incorporate such dyes.

Requirements :

1. Trypan blue - 0.4 % in PBS
2. PBS
3. Hemocytometer

Procedure :

Approximately 15x 10^3 cells were seeded in 12 well plates. Following a 24 h incubation period, the cells were treated with the IC_{50} concentration of the samples, incubated for 1 h, and subjected to photo-irradiation using halogen lamp for 90 s. Another plate was kept in dark without any light exposure, and a control group consisted of cells without dye treatment. After an additional 24 h of incubation, the cells were trypsinized, centrifuged for 10 min at 1500 rpm, and the supernatant was discarded. The cell pellet was then resuspended in 1 mL of serum-free medium. A mixture of 0.4 % trypan blue and the cell suspension was prepared in a 1:1 ratio. 10 uL of the mixture was placed on a hemocytometer, and the unstained (viable) and stained (non-viable) cells were counted separately. The percentage of dead cells was calculated as follows:

$$Percentage\ of\ dead\ cells = \frac{Number\ of\ dead\ cells}{Total\ number\ of\ cells} \text{ x } 100$$

5.2.2.6 Cell Morphology analysis

15 X 10^3 cells were cultured in tissue culture 6 well plate with the IC_{50} concentration of samples for 24 h. After the incubation, the media was removed carefully, and the cells were washed with PBS. Again, added fresh media in to each well.

Morphological alterations in the cells were examined under a phase-contrast inverted microscope (Optika, IM3) at a magnification of 20X.

5.2.2.7 Subcellular fractionation

Accumulation of PAF 1 and PAF 2 in cellular compartments were assessed through subcellular fractionation by using method by Kunwar *et al*., 2008 with some changes.

Requirements:

1. Lysis solution: 2.5M NaCl, 100mM EDTA, 10Mm Tris buffer, 90mM Sodium Sarcosinate, 1% TritonX100, 10% DMSO

2. Methanol

Procedure

Cells in a 25cm^2 flask were incubated with PAF 1 and PAF 2 at its IC_{50} concentration for 1 h. After the incubation subcellular fractionation was carried out. The treated cells were suspended in 0.5 mL of lysis solution which also contained detergents. In Kunwar method they used lysis buffer and and then Nonidet P-40 (0.6%). Instead of this we used lysis solution to breakdown the cells. Then the cells were subjected to centrifugation at 2000× g for 10 min,10,000 × g for 15 min, and 100,000 × g for 45 min to isolate nuclear, mitochondrial, and membrane fractions respectively as pellets, after centrifugation at each velocity. The cytosolic fraction remained in the supernatant after collecting the pellet corresponding to the membrane fraction. Each pellet fractions were washed three times with cold PBS,

air dried, and resuspended in 0.5 mL of methanol, followed by sonication to completely extract our compounds. The supernatant was also subjected to fluorescence measurement.

5.2.2.8 Acridine orange (AO) and Ethidium Bromide (EB) dual staining

The morphological identification of apoptotic and necrotic cells was conducted using DNA-Binding dyes Acridine orange (AO) and Ethidium bromide (EB). Acridine orange, capable of penetrating both viable and nonviable cells,emits green fluroscence when intercalated into double-stranded nucleic acid (DNA) or red fluroscence when bound to single-stranded nucelic acid (RNA). Ethidium bromide,on the other hand, is exlusively taken up by nonviable cells emitting red fluroscence through intercalation into DNA.

Requirements:

1. Ethidium bromide - 5 µg/mL
2. Acridine orange - 5 µg/mL
3. Chilled PBS
4. 12 well plate

Procedure

Acridine orange and ethidium bromide dual staining was done by Mustafa *et al*., 2021 with some modifications. A431 cells were cultured in DMEM and reaching 60-70% confluency, underwent

treatment with the IC_{50} concentration of the dye. Following a 1 h incubation, the cells were exposed to light for 90 s and then further incubated for 24 h. Another plate was kept in dark to assess dark toxicity. After the incubation period, cells were rinsed with chilled PBS and stained with a mixture of Acridine orange and Ethidium bromide (1:1) at room temperature for 10 min in dark. The stained cells immediately underwent two or three washes with PBS and were subsequently examined under a fluorescence microscope with in 20 min using a blue filter. Proper washing step is mandatory during the staining techniques.

5.2.2.9 Assessment of Reactive Oxygen Species (ROS) levels

DCFH-DA, a stable nonfluorescent compound, easily crosses cell membranes and becomes integrated into the hydrophobic lipid regions of cells. Inside the cell, cellular esterases remove the acetate moiety, leading to the formation of the polar 2',7'-dichloroflurescin (DCFH), which is then trapped within the cell. DCFH, initially nonfluorescent, undergoes rapid oxidation by various reactive oxygen species (ROS) to yield the highly fluorescent 2',7'-dichlorofluorescein (DCF). The detectable green fluorescence serves as an indicator of ROS formation.

Requirements:

1. PBS
2. 10 μM DCF-DA
3. 12 well plate

Procedure

Assessment of ROS was done by the method described by Mustafa *et al*., 2021. A431 cells were seeded in a 12 well plate and subjected to the IC_{50} concentration of the samples. Following 1 h incubation, the cells were exposed to light and then incubated for 24 h. Media was removed, and cells were washed with PBS. Control and treated cells were stained with 10 µM DCFDA for 10 min at 37ºC in dark, followed by a wash with cold PBS to remove the remaining part of the stain. Examined under a fluorescent microscope within short time period.

5.2.2.10 DNA damage analysis by Comet assay

The comet assay, also known as single-cell gel electrophoresis (SCGE), identifies DNA damage by observing that, when exposed to an electric field, cells with compromised DNA display enhanced migration of genetic material from the nucleus towards the anode, creating a comet-like tail. The extent of this migration id directly proportional to the level of DNA damage. Utilizing nucleotide staining, the analysis of the "comets" formed during single-cell electrophoresis allows for the quantification of DNA damage.

Requirements:

1. Low melting point agarose- 0.5 % and 1% low melting point Agarose

2. Normal agarose -0.5% Agarose

3. Microslides

4. Cover slips

5. PBS- NaCl: 0.8g, KCl: 0.02g, Na_2HPO_4: 0.144g, KH_2PO_4 : 0.024g Dissolved it in 100 ml distilled water.

6. Lysis solution- 2.5M NaCl, 100mM EDTA, 10Mm Tris buffer, 90mM Sodium Sarcosinate, 1% TritonX100, 10% DMSO

7. Neutralization buffer - 400mM Tris HCL.

8. Electrophoresis buffer- 300Mm NAOH, 1.2Mm EDTA, dissolved in 1000ml distilled water

9. Ethidium bromide – 20 µg/mL

10. Fluorescent microscope

Procedure

To assess DNA damage, comet assay was performed on A431 cells treated with the IC_{50} concentration of PAF 1 and PAF 2. Following a 1 h incubation, the cells were exposed to light for 90 s. After 24 h of further incubation, cells were harvested by trypsinization, and the cell suspension was centrifuged at 1500 rpm for 5 min. The resulting pellet was re-suspended in 5 ml PBS. Microslides were prepared by applying 1 % normal agarose in PBS, covered with a coverslip, and allowed to solidify at 37 ºC. After removing the cover slip, a mixture of 50 µL of cell suspension and 50 µL of 1 % low melting agarose was applied on top of the gel-covered microslide.

Following a 10 min incubation at 4ºC, the coverslip was removed. A third coating of 50 µL of 0.5% low melting agarose was placed on the gel and allowed to set at 4ºC for 15 min. After agarose solidification, slides were kept at a refrigerating temperature along with ice cold lysis solution for 1 h. All procedures were conducted under low lighting conditions to minimize additional DNA damage. Slides were then placed horizontally in an electrophoresis chamber, which is filled with electrophoresis buffer and allowed to unwind for 30 min. Electrophoresis was then carried out at 25 V and 300 mA for 20 min. Following electrophoresis, slides were removed, washed in a neutralization buffer, and then in distilled water before being left to dry. Cells were stained with 20 µL of ethidium bromide, covered, and kept in the dark for 20 min. After removing the coverslip, slides were washed in chilled distilled water to eliminate excess stain. Analysis of comet tail was conducted under a fluorescence microscope.

5.2.2.11 Caspase 3 Assay

The quantification of Caspase-3 activity was conducted through a colorimetric method. The assay relied on detecting the quantity of Ac-DEVD-p-NA substrate cleaved by caspase 3 in cell lysates, resulting in the liberation of the colored p-NA (para-nitroaniline) molecule.

Requirements:

1. Lysis buffer : 50 mM HEPES, P^H 7.4, 5 mM Triton X100, 5 mM DTT

2. Assay buffer :20 mM HEPES, P^H 7.4, 0.1% Triton X100,5 mM DTT, 2 mM EDTA

3. Caspase 3 Substrate 0.07 mM

4. Bradford reagent

5. BSA

Procedure

Caspase 3 assay was conducted by the method prescribed by Pattayil L *et al*., 2019. Cells were cultured in a 25 cm^2 cell culture flask. The cells were then exposed to the IC_{50} concentration of the PAF1 and PAF2. Untreated cells served as the control group. Following a 1 h incubation, the cells were subjected to light exposure for 90 s and further incubated for 24 h. Subsequently, the cells were washed in PBS and suspended in ice-cold lysis buffer for 15 min. The lysed cells were centrifuged at 16,000 X g, 4ºC for 15 min. Protein concentrations in the lysate were determined using the Bradford assay. For the Caspase 3 assay, each tube containing 0.07 mM substrate in assay buffer received 10-60 µl of cell lysate, bringing the total volume in each well to 100 µl. Caspase 3 activity was assessed by measuring the optical density at 405 nm using a microplate reader. Activity is expressed as µmol p-NA released per min per milligram of protein.

5.2.2.14 Cell cycle analysis

Cell cycle analysis evaluates cell distribution across different stages by measuring DNA content. After fixing cells with ethanol,

Propidium iodide (PI), a nuclear staining dye is used. Cells undergoing division exhibit high amount of DNA leading to increased fluorescence. The differences in fluorescence intensity serve as indicators for the percentage of cells in distinct phases of the cell cycle.

Requirements:

1. 1X PBS
2. 70% ice cold Ethanol
3. RNAase A - 100 mg/mL
4. Propidium Iodide - 50 mg/mL

Procedure

Cell cycle analysis was done by the method described by Athikkavil *et al*., 2023. The A431 cells were treated with PAF1 and PAF2 at their IC_{50} concentrations. After the irradiation of light incubated them for 24 h. Subsequently the cells were collected, rinsed with 1X PBS. Permeabilized cells for 30 min by adding 70 % ice cold ethanol drop by drop and continuously vortexed the cell suspension. The permeabilized cells were then treated with 100 mg/mL RNAase A and 50 mg/mL propidium iodide (PI) before undergoing flow cytometric analysis using a FACS instrument (BD FACS Melody).

5.3 Results

5.3.1 MTT assay

To assess the cytotoxicity of PDT, skin cancer cells were subjected to MTT assays at different doses and time intervals. The results of the study were used to analyse the time and dose dependent responses of the cells to PDT (figures 5.1, 5.2 and 5.3).

Figure 5.1 MTT Assay 24 h

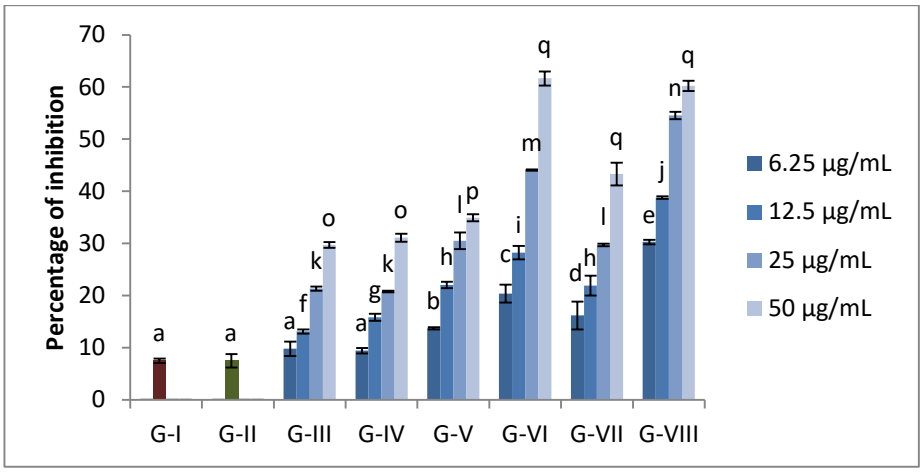

Dose dependent response was found in all groups. The groups without light treatment showed lower inhibitory activity compared to light treated groups Values are mean of three estimations. Error bars represent standard deviation (n=3). Different alphabets indicate significant difference between the groups. F value for 6.25 µg/mL,12.5 µg/mL,25 µg/mL and 50 µg/mL are 77.882,197.041,404.157 and 998.781 . P value <0.05

Figure 5.2 MTT Assay 48 h

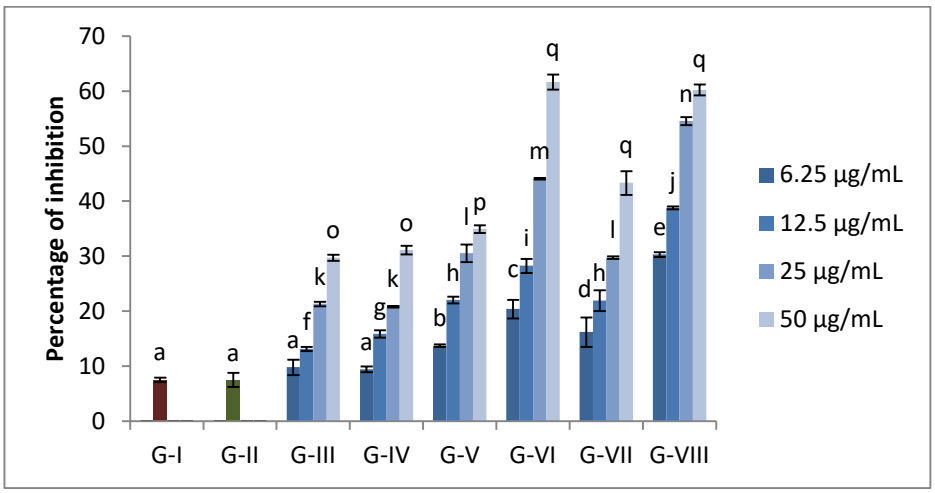

Dose dependent response was found in all groups. The groups without light treatment (Group I-Group III) showed lower inhibitory activity compared to light treated groups (Group IV-VI). Error bars represent standard deviation (n=3). Different alphabets indicates significant differences between the groups. F value for 6.25 µg/mL,12.5 µg/mL,25 µg/mL and 50 µg/mL are 103.464,334.872,1211.129 and 951.579. P value < 0.05

Figure 5.3 MTT Assay 72 h

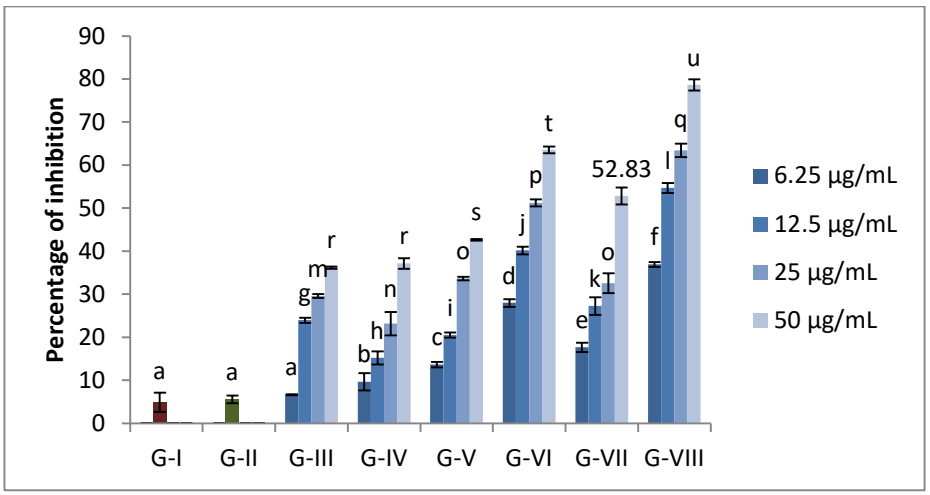

Dose dependent response was found in all groups. The groups without light treatment (Group I-Group III) showed lower inhibitory activity compared to light treated groups (Group IV-VI). Values are mean of three estimations. Error bars represent standard deviation (n=3). Different alphabets indicates significant differences between the groups. F value for 6.25 µg/mL,12.5 µg/mL,25 µg/mL and 50 µg/mL are 257.382,449.911,445.171 and 1164.325. P value <0.5

The MTT assay results obtained at different intervals showed a significant rise in the inhibitory activity of the PDT group in a dose and time dependent manner. The concentration of photosensitizers directly relates to an increase in the percentage of cell inhibition. Similarly, the duration of the incubation period influences the viability of the cells; a longer incubation period after treatment causes higher inhibitory rate. These findings suggest that the inhibitory effect of PDT is directly influenced by the photosensitizer concentration and the duration of the incubation time. Furthermore, in contrast to the other groups, the cells in group II that were simply exposed to light did not exhibit any discernible inhibitory activity, indicating that light treatment by itself is insufficient to inhibit the proliferation of A431 cells.

Table 5.1 IC_{50} values of Groups III- VIII.

Group name	24 h	48 h	72 h
Group III	88.82 ± 2.250	92.73 ± 0.688	69.53 ± 0.961
Group IV	88.43 ± 2.563	88.93 ± 3.869	70.49 ± 2.337
Group V	76.96 ± 0.980	79.12 ± 1.022	58.06 ± 0.258
Group VI	37.38 ± 0.717	35.65 ± 1.077	29.08 ± 0.234
Group VII	65.54 ± 2.120	60.19 ± 2.924	46.45 ± 1.192
Group VIII	33.68 ± 0.424	29.56 ± 0.650	13.51 ± 0.254

The values are expressed as µg/mL ± SD.n=3.

The inhibitory activity of the six experimental groups varied significantly,as Table 5.1 shows,with groups VI,VII and VIII displaying the greatest inhibitory effects. These are the PDT groups. Furthermore, the IC_{50} values in these groups decreased gradually over time, suggesting a higher time dependency effect.

5.3.2 Trypan blue exclusion

Trypan blue exclusion assay was used to assess the cytotoxicity of photosensitizers.

Figure 5.4 Trypan blue exclusion assay.

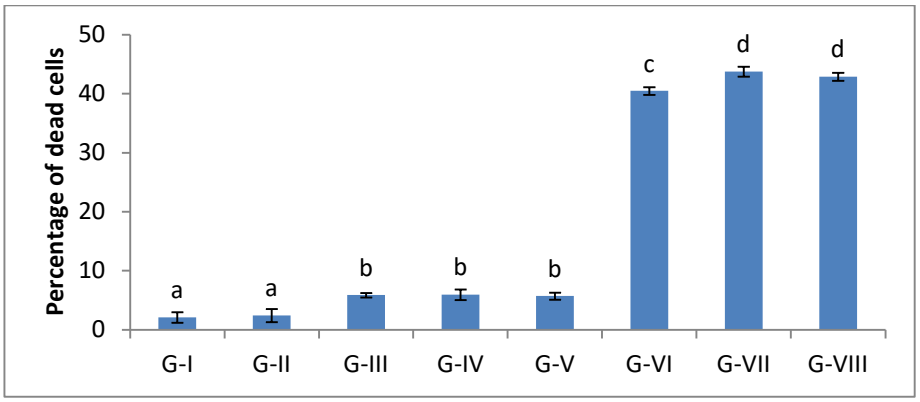

All values are mean of 3 estimations. Error bar indicates standard error.Different alphabets indicate significant difference between groups. F value for trypan blue exclusion assay is 2277.733. P value <0.05.

Cell viability in eight experimental groups including the control group was evaluated using the Trypan blue exclusion test, and the results are shown in Figure 5.4. As shown in the results, the percentage of dead cells in groups I-V ranged from 2%-5%. These levels were comparable. By comparison, the percentage of cell death in groups VI, VII and VIII were much higher, ranging from 40% -45%.

5.3.4 Analysis of cell morphology

Visual examination of A431 cells' structure and appearance under a microscope was done to analyze their morphology.

The morphological analysis of A431 cells treated with PAF1 and PAF2 is shown in Figure 5.5. Within groups VI, VII and VIII we found a considerable decrease in the number of cells, indicating a strong cytotoxic effect of the treatments. These cells also showed distinct morphological changes, which were indicated by the presence of apoptotic bodies. These features point to programmed cell death, a common process brought on by coming into contact with cytotoxic substances. The photosensitizer-alone and the light-alone treated groups, on the other hand, showed only slight changes in their cellular morphology suggesting that there had been no significant damage or adverse effects.

Figure 5.5 Morphological analysis of A431 cells

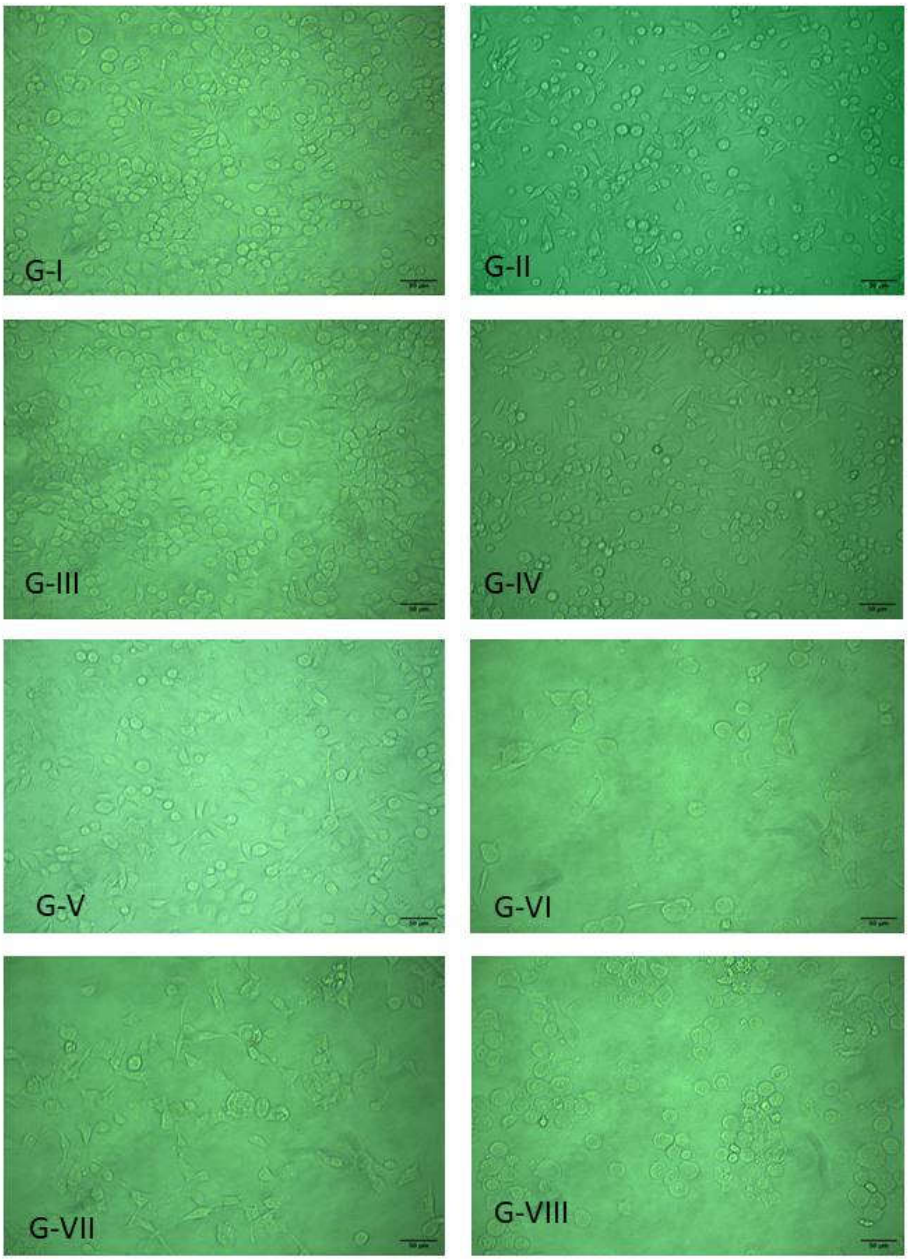

Cells were observed under 20x magnification. PDT groups show reduced cell number and morphological alterations in the cells.

5.3.5 Subcellular fractionation

The results of subcellular fractionation are given in Figure 5.6.

Figure 5.6 Subcellular distribution in different fractions

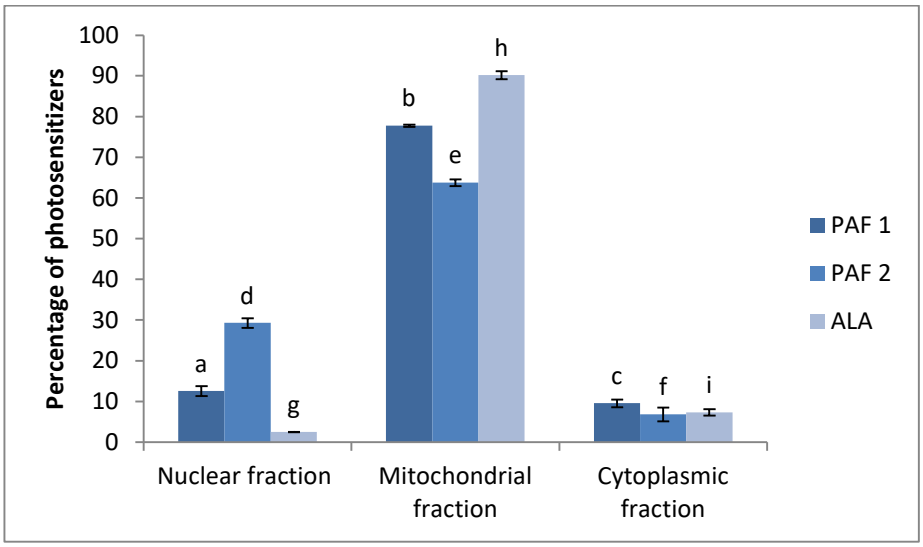

The bar graph shows the percentage of components found in the nuclear, mitochondrial, and cytoplasmic fractions for PAF 1, PAF 2, and ALA. The mitochondrial fraction shows the highest concentration for all treatments, with ALA exhibiting the most pronounced enrichment. The nuclear and cytoplasmic fractions contain relatively lower levels, indicating differential localization across subcellular compartments. Values are means of three estimations. Error bar indicates standard error. Different alphabets indicate significant difference between the groups. F value for PAF 1,PAF 2 and ALA is 4693.787, 4415.043 and 4987.395 respectively. $P < 0.05$.

The subcellular distribution analysis in figure 5.6 revealed distinct localization patterns of components across nuclear, mitochondrial, and cytoplasmic fractions for the treatments PAF1 and PAF2, and ALA. The mitochondrial fraction consistently exhibited the highest concentration of components across all samples, indicating a

preferential accumulation in this compartment. Among the treatments, ALA showed the most pronounced enrichment in the mitochondrial fraction, suggesting a stronger association or targeting of components to the mitochondria under this condition. In contrast, the nuclear and cytoplasmic fractions contained relatively lower levels of components, indicating differential localization and a lesser accumulation in these compartments compared to the mitochondria. This pattern implies that mitochondrial targeting plays a significant role in the cellular distribution of these components across the different treatments.

5.3.6 Acridine orange/Ethidium bromide dual staining

Figure 5.7 presents the results of acridine orange/ethidium bromide dual staining, a method used to visualize cell death, in different photodynamic therapy (PDT) groups.

Group I and group II displayed no signs of apoptosis. Groups III-V exhibited a small number of apoptotic cells, which could be attributed to normal physiological cell death. In contrast, groups VI-VIII, all part of the PDT regimen, demonstrated a range of apoptotic responses. These groups showed a clear presence of orange staining and membrane blebbing, characteristic features of apoptosis. The variation in the extent of apoptotic features among these groups suggests that the efficacy of PDT in inducing apoptosis is not uniform. Some groups appear to be more susceptible to PDT-induced apoptosis than others.

Figure 5.7 Acridine orange/ethidium bromide dual staining

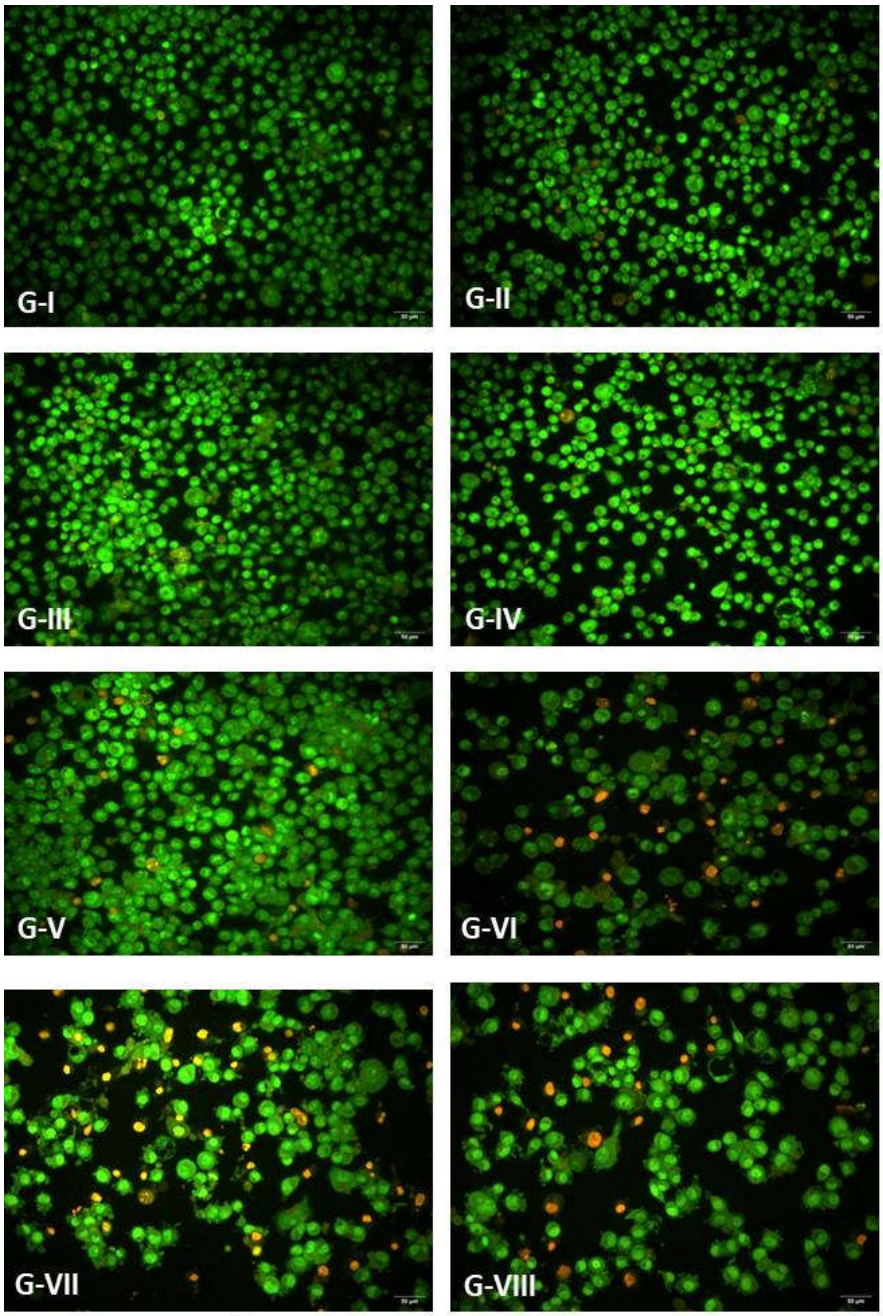

Experimental groups demonstrating varying degrees of apoptotic features, including noticeable orange staining and membrane blebbing.Cells were observed under 20x magnification.

5.3.7 ROS generation assessment

Figure 5.8 illustrates the results of Reactive oxygen species generation which is a key process of PDT.

Figure 5.8 ROS generation assessment

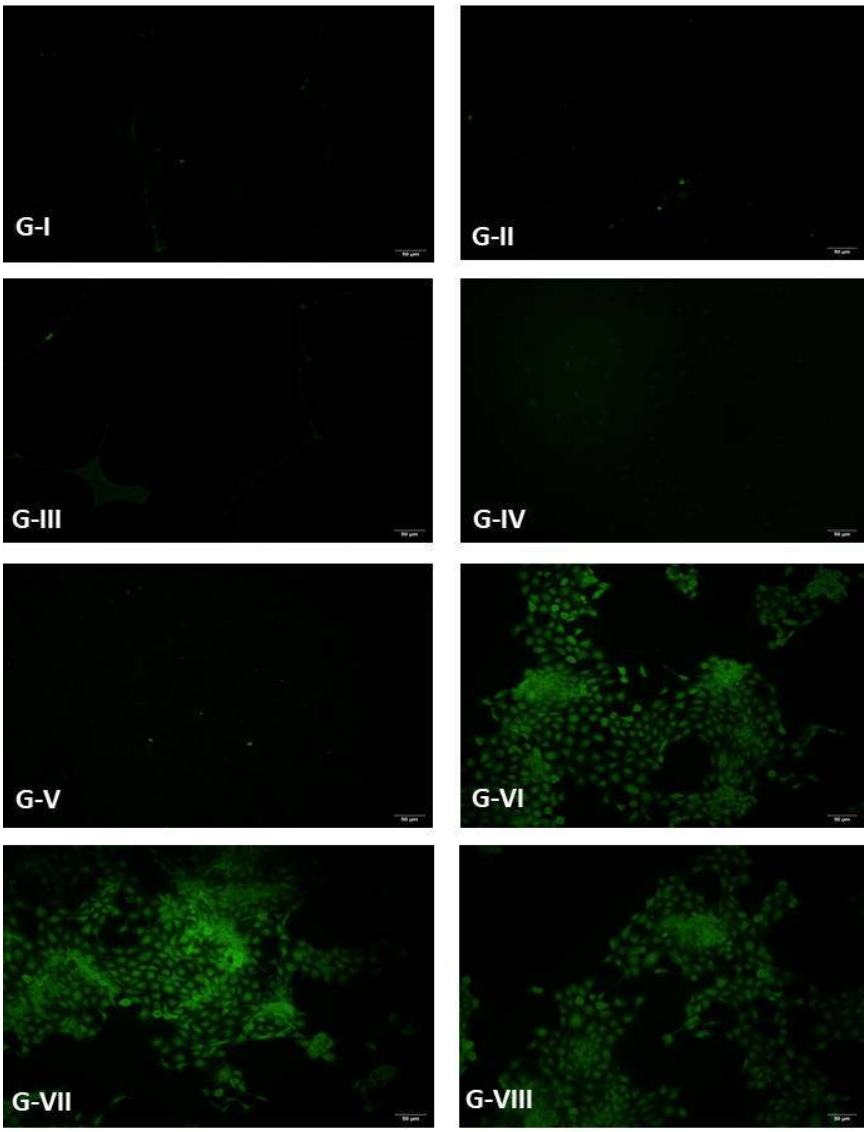

The PDT groups (Groups VI-VIII) showed ROS generation. Cells were observed under 20 x magnification

The PDT groups (VI-VIII) exhibited presence of ROS. This finding suggests that the treatment or conditions associated with these groups led to increased production of reactive oxygen species. In contrast, the control groups (Group I and Group II) did not show a similar level of ROS generation.

5.3.8 Comet assay

The results of comet assay are given in figure 5.9.

Figure 5.9 Comet assay

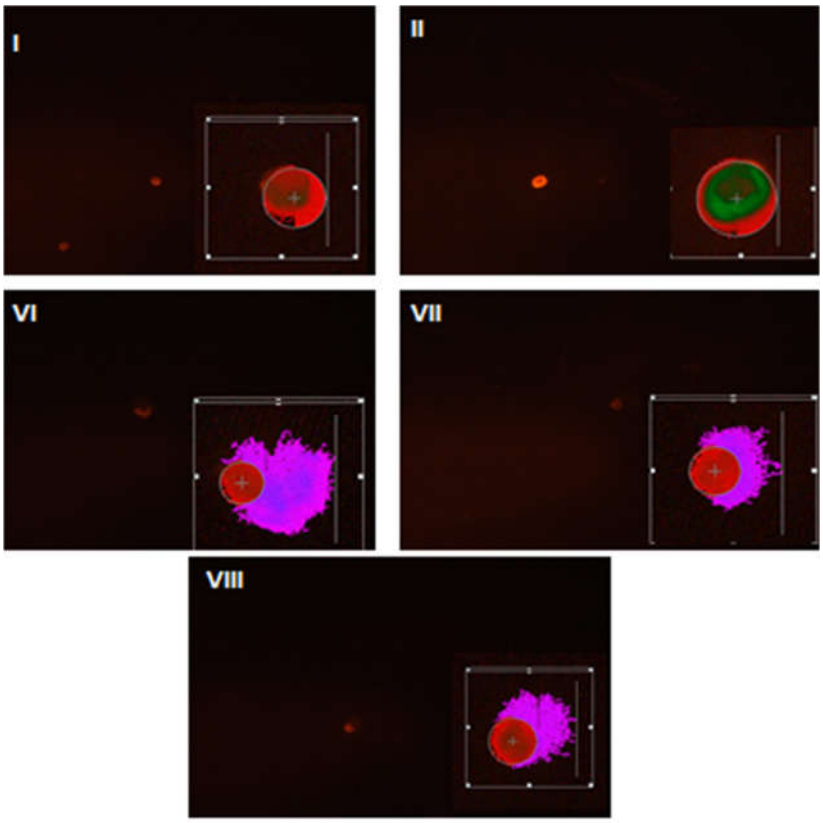

Control groups, showing minimal DNA in the comet tail, indicating low DNA damage. Groups VI-VIII, showing higher percentages of DNA in the comet tail, indicating increased DNA damage. Each image includes a small inset box displaying analysis results from CaspLab software, which quantifies the percentage of DNA in the tail and head regions.

Based on Figure 5.9, the comet assay results reveal varying levels of DNA damage across the different groups. The control groups, Group I and II, show minimal DNA in the comet tail, indicating low levels of DNA damage and maintaining DNA integrity. In contrast, Groups VI-VIII display a higher percentage of DNA in the comet tail, suggesting a significant increase in DNA damage. The greater tail DNA percentage in these groups indicates more extensive DNA fragmentation, which may be due to the treatment conditions applied (Table 5.1). The analysis by CaspLab software confirms these observations, quantifying the distribution of DNA in the head and tail regions for each group.

Table 5.2 DNA percentage in tail and head.

Groups	**Head DNA %**	**Tail DNA %**
Group I	99.95	0.049
Group II	99.99	0.004
Group VI	22.35	77.64
Group VII	54.66	45.33
Group VIII	68.81	30.18

5.3.9 Caspase 3 Assay

Figure 5.10 depicts the caspase-3 assay results indicate significant variations in apoptotic activity among the groups.

Figure 5.10 Caspase-3 assay

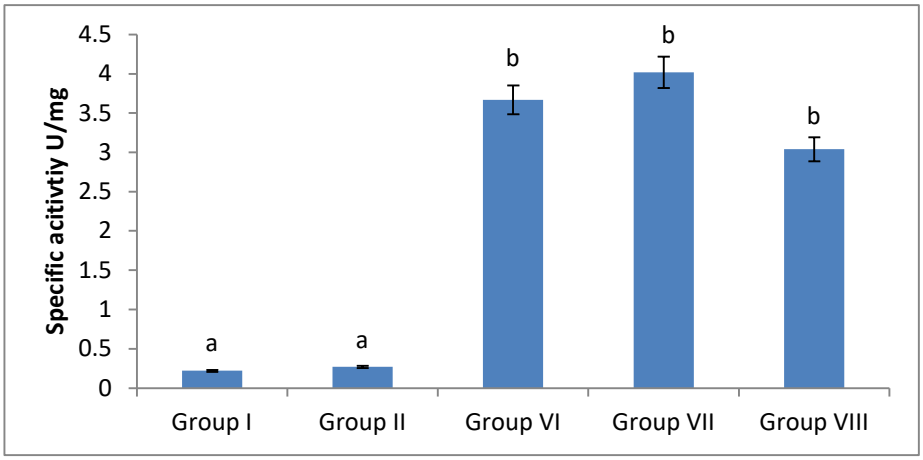

Groups I and II show reduced caspase-3 activity, indicating lower levels of apoptosis. In contrast, other groups exhibit higher caspase-3 activity, suggesting increased apoptotic processes. Values are mean of three estimations. Error bar indicates standard error. Different alphabets indicate significant difference between the groups. F value for caspase 3 is 14.564. $P < 0.05$.

The control groups, I and II, show lower caspase-3 activity, suggesting minimal apoptosis and stable cellular conditions. This indicates that the baseline apoptotic response is low in these untreated groups. In contrast, the PDT-treated groups exhibit markedly higher caspase-3 activity, indicating an increase in apoptotic processes. The elevated levels of caspase-3 activity in these groups suggest that the photodynamic therapy (PDT) effectively induces apoptosis, highlighting its impact on promoting cell death compared to the control groups. These findings suggest that PDT treatment leads to varying levels of cellular apoptosis across the treated groups.

5.3.11 Cell cycle analysis

The percentage of cells shown in each phase are given in table 5.3.

Table 5.3 Percentage of cells present in different phases

Sample name	% G_1 Phase	% S Phase	% G_2 Phase
Group I	40.88 %	39.24 %	19.88%
Group II	37.87%	30.68%	31.45%
Group VI	31.53%	56.39%	12.07%
Group VII	33.84%	60.94%	5.22%
Group VIII	27.96%	32.48%	39.56%

The flow cytometric analysis of the cell cycle across different treatment groups (Figure 5.11) revealed distinct effects on cell cycle progression. The control group (Group VIII) exhibited a typical distribution of cells across the G1, S, and G2 phases, serving as a baseline for comparison. Group VII showed a similar cell cycle distribution to the control, with no notable changes in phase proportions which is light control. In contrast, Groups VI and VII demonstrated a marked increase in the percentage of cells in the S phase, indicating a cell cycle arrest at this stage. This suggests that the treatments applied to these groups led to impeded progression through the S phase. Meanwhile, Group VIII showed a significant rise in the number of cells in the G2 phase, indicating that the treatment caused cell cycle arrest in the G2 phase. These findings highlight the differential impact of treatments on cell cycle regulation, with Groups VI and VII arresting in the S phase and Group VIII arresting in the G2 phase.

Figure 5.11 Cell cycle analysis

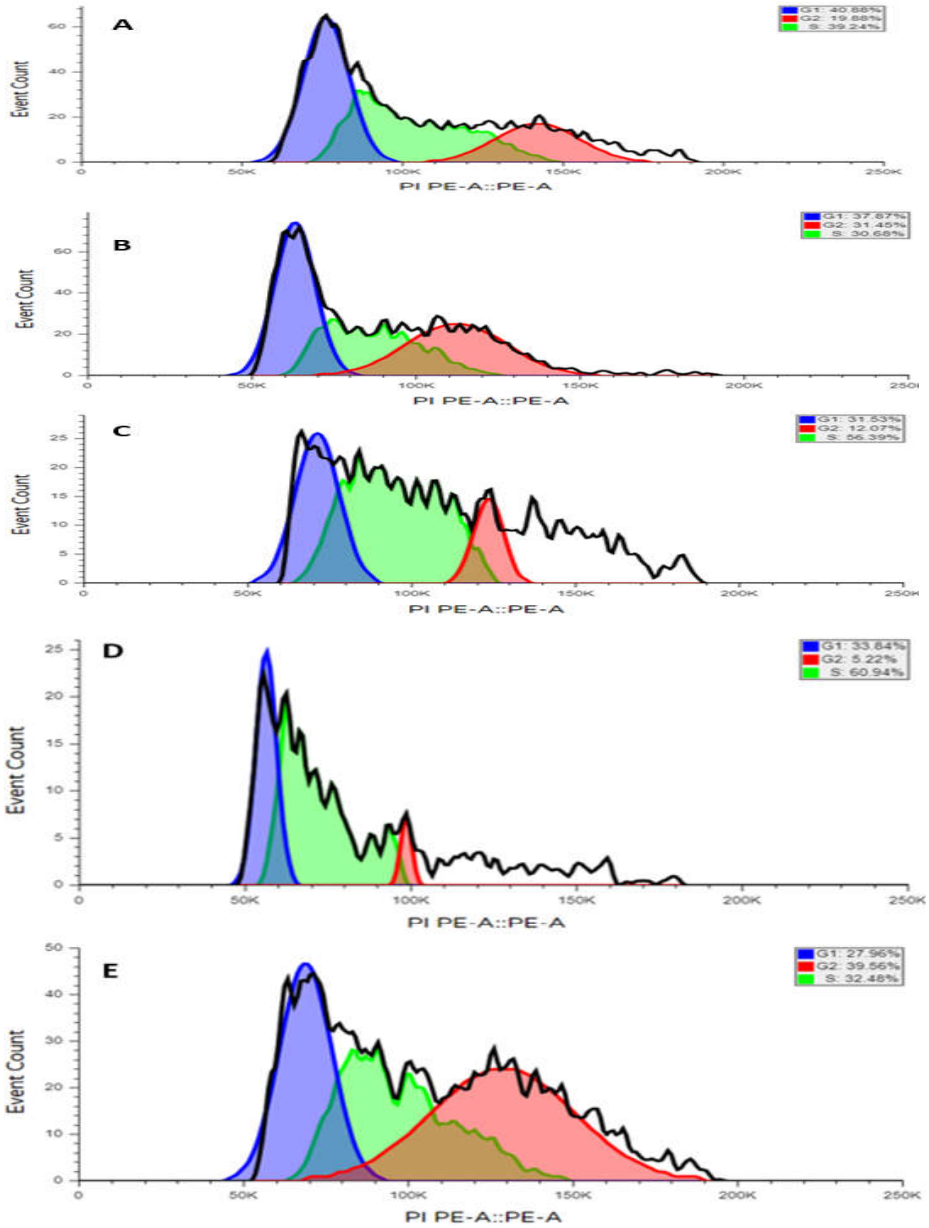

Flowcytometry analysis was performed to assess the distribution of cells across different phases of the cell cycle. (A) Group I and (B) Group II control groups showing typical distribution of cells across G1, S and G2 phases. (C) Group VI and (D) Group VII showed increased percentage of cells in the S phase, indicating cell cycle arrest at this stage. (E) Group VIII showed a significant increase in cells at the G2 phase, indicating cell cycle arrest in the G2 phase.

5.4 Discussion

SCC has been becoming more common, especially as a result of increased sun and tanning bed exposure to ultraviolet (UV) radiation. This pattern highlights the necessity of efficient treatment and preventive plans (Jemal *et al* 2003, Kyriazi 2006). For actinic keratosis, basal cell carcinoma, squamous cell carcinoma, and squamous cell carcinoma in situ, among other cutaneous neoplasia PDT is a potentially effective treatment option. According to Zahao *et al*., 2010, the two topical photosensitizers for PDT in dermatology that are currently approved are Levulan® and Metvix ®. Although these artificial photosensitizers work well for PDT, natural photosensitizers derived from microbes, plants or other sources may be a superior choice because of their increased compatibility and decreased toxicity.

In comparison to the groups that did not receive light treatment, the plant fractions PAF1 and PAF2 demonstrated increased cytotoxicity against the A431 cells after photodynamic therapy with a 1000 W light source.

A lux meter (Figure 5.12) is a device used to measure illuminance, which is the amount of light falling on a specific surface area from a given light source at a certain distance. Lux meters are commonly used across various fields, including industrial settings, hospitals, museums, and photography, to ensure optimal lighting conditions (Sonar *et al*., 2021).

Figure 5.12 Light intensity measuring using Digital lux lumen meter

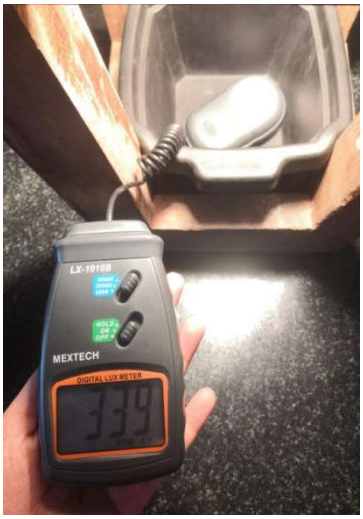

The measurement of light intensity can vary significantly depending on the unit used. In the literature, it is often expressed in lux, µmol m^{-2} s^{-1}, or W m^{-2}, but there is no single conversion factor between these units because the conversion depends on the wavelength of the light. Without knowing the spectral composition, direct conversion is not possible. However, for sunlight, some approximate conversions are available: 1 lux $\approx$ 0.0079 W m^{-2}, 1 µmol m^{-2} s^{-1} $\approx$ 0.22 W m^{-2}, and 1 lux $\approx$ 0.036 µmol m^{-2} s^{-1}(Ruigork T *et al*.,2015). Although there is no universal conversion factor, we used these approximations when converting lux to W m^{-2}, as our halogen tungsten lamp emits a broad range of wavelengths (Price *et al*., 2003), similar to sunlight. Therefore, we applied the solar conversion factor to estimate the light intensity in W m^{-2}.

1 lux $\approx$ 0.0079 W/m^2

Measured lux = 33900 lux

So the fluency rate W/m^2 $\approx$ 33900 X 0.0079 = 267.81 W/m^2 = 0.026781 W/cm^2

Another approach to calculate the dose of light in J/cm^2 manually.

Total light dose (J/cm^2) = fluence rate (W/cm^2) X treatment time (S)

Area illuminated by the lamp : when placed at 24 cm away = 90 cm X 200 cm = 18000 cm^2 (Calculated by measuring the average length and breadth of the illuminated rectangular region when the light source was kept at 24 cm)

The dose of light incidence per cm^2 = 1000 W/18000 = 0.0555555556 W/cm^2

So for the 90 s illumination the total dose of light was 0.0555555556 X 90 = 5 J/cm^2.

In 2021, Mugas *et al*. experimented with blue light at doses of 2 J/cm² and 8 J/cm² to treat K562 leukemic cells using the natural photosensitizer anthraquinone parietin. Demethoxycurcumin (DMC)-PDT was also effective against MCF-7 breast cancer cells at a light dose of 30 J/cm² (Lin *et al*.,2015). Various light doses are used in *in vitro* cancer cell testing. However, we chose a 90-second irradiation time in this study to minimize the risk of contamination. Here we used A431 cell lines.

A431 human epidermoid carcinoma cells, a popular *in vitro* model for studying skin cancer, was used in this work to examine the cytotoxic properties of photosensitizers as possible treatment agents. The mechanism of Photodynamic therapy for skin cancer cells depends on the interaction between a photosensitizer, light, and oxygen to produce reactive oxygen species (ROS), which cause cells to become selectively fatal (Allison *et al*.,2013). This mechanism was confirmed by the MTT assay results, which showed that the fractions (PAF1 and PAF2) had cytotoxicity on A431 skin cancer cells in a time and dose dependent manner. The presence of other secondary metabolites in the fractions may have shown the cytotoxic effects when there is no light, which would explain the little dark cytotoxicity seen. Furthermore, there was no discernible cytotoxicity in the group that was only exposed to light, proving that light exposure cannot cause cell death on its own. This highlights the way in which light and photosensitizer work in tandem during PDT to effectively suppress cancer cells (Kwiatkowski *et al*., 2018). The IC_{50} value for the PDT groups during dark toxicity test trypan blue exclusion assay shows low toxicity towards A431 cells. This suggests that the photosensitizer remains inactive until it is exposed to light; only becoming active after light exposure.

Following PDT treatment with PAF1 and PAF2 at their respective IC_{50} concentrations, 35-45% of cells died in the Trypan blue exclusion assay which is comparable with the fundamental concepts of these assays. The ability of mitochondrial dehydrogenases in living cells to convert MTT into formazan is the basis for the MTT assay

(Berridge and Tan., 1993). On the other hand, the Trypan blue (Strober W., 1997) evaluate membrane integrity and lysosomal function, respectively. Given that the experiments showed a comparable percentage of cell death, it appears that the PAF1 and PAF2 affect the integrity of the cellular membrane as well as mitochondrial function. In accordance to the Trypan blue assay, the samples damaged the integrity of the cell membrane, allowing the dye to penetrate and stain dead cells in a way that is consistent with cell death.

Due to their plant-based nature, PAF1 and PAF2 are excellent choices for PDT. These molecules have a number of advantages, one of which is their natural origin, which makes them more accessible and less dependent on intricate synthetic procedures. This availability from natural sources also suggests they may have lower toxicity profiles, as many plant derive compounds are often biocompatible and exhibit minimal harmful effects on cells in the absence of light.

To the results of our research, PAF1 and PAF2 both showed negligible dark toxicity, which means that when there was no light present, they barely killed any cells. In order to minimize unintentional side effects in surrounding tissues, this feature is essential for an excellent photosensitizer (Kubrak.,2022). This ensures that the compounds remain inactive and non-toxic until exposed to light. Moreover, these photosensitizers are only activated by light, which effectively produces reactive oxygen species (ROS) such as singlet oxygen or radicals that cause cell death in the targeted regions. Because it permits precise control over their cytotoxic effects, this

selective activation under light exposure improves the safety profile of PAF1 and PAF2 in PDT applications.

Morphological analysis in our study reveals clear signs of cytotoxicity induced by photodynamic therapy (PDT), with notable changes in cell shape and structure. These changes suggest that apoptosis, a programmed and controlled form of cell death, may be the underlying mechanism. Apoptosis is characterized by specific morphological alterations, such as cell shrinkage, membrane blebbing, and nuclear condensation. This observation aligns with findings from other research studies, which have shown that natural compounds used in PDT often induce apoptosis as a primary mode of cell death (Warowicka., 2019, Berlanda.,2006).

The morphological analysis done in our research indicates distinct indications of cytotoxicity caused by PDT, including alterations in the form and structure of the cells. These modifications imply that the underlying mechanism might be apoptosis, a regulated and controlled type of cell death. Certain morphological changes, like nuclear condensation, membrane blebbing, and shrinking of the cell, are indicative of apoptosis. This conclusion is consistent with earlier research studies that have demonstrated that one of the main modes of cell death induced by natural chemicals used in PDT happens to be apoptosis.

In the vast majority of applications, the primary role of PDT is to kill unwanted cells. Since the term “apoptosis” was introduced in 1972, (Kerr *et al*.,1972) cell killing mechanisms are generally

classified as occurring through apoptosis or necrosis. Apoptosis is a normal physiological process essential for the control of tissue development and involution and for tissue homeostasis (Ashkenazi *et al*.,1998). Apoptosis is a tightly regulated process of cell suicide, controlled by both intracellular and extracellular signals, terminating in a characteristic sequence of morphological and biochemical changes for the systematic dismantling of the cell and preparation of the residual cell components, known as apoptotic bodies, for engulfment by tissue macrophages or other neighbouring cells. The process limits leakage of intracellular material to the immediate environment, and thereby prevents tissue inflammation. The loss of ability to regulate apoptosis can lead to disease (Evan *et al*.,1998, Kromer *et al*.,2000, Reed *et al*.,2000). Although PDT can produce apoptosis or necrosis, or a combination of the two mechanisms, in many cases PDT is highly efficient in inducing apoptosis (Kroemer *et al*.,1998).

The results of our study demonstrate the preferential accumulation of photosensitizers, including ALA within the mitochondrial fraction of cells. This finding is particularly significant considering the crucial role of mitochondria in cellular apoptosis. Mitochondria are often referred to as the "powerhouses of the cell" due to their role in ATP production. However, they also play a pivotal role in initiating programmed cell death. A key event in this process is the release of cytochrome c from the mitochondrial intermembrane space into the cytosol. This release is triggered by the activation of pro-apoptotic Bcl-2 family proteins, such as Bax and Bak, which form pores in the mitochondrial outer membrane (Ruddon,2007). The

accumulation of photosensitizers within mitochondria suggests a potential mechanism of action involving the induction of mitochondrial dysfunction after the light treatment. There are reports indicating that photosensitizers accumulate within mitochondria, leading to a loss of mitochondrial membrane potential. This finding is consistent with the results of our study (Saneesh *et al*.,2017). These compounds may directly damage the mitochondrial membrane, leading to increased permeability and cytochrome c release. Alternatively, they may generate reactive oxygen species (ROS) within mitochondria, which can further contribute to oxidative stress and cell death. The production of ROS during PDT treatment is also revealed in our study.

While subcellular fractionation is a valuable technique for studying organelle-specific localization, it has inherent limitations. These limitations include the potential for organelle damage during the fractionation process, cross-contamination between fractions, and the loss of soluble proteins. To address these limitations and obtain more precise information about mitochondrial localization, staining with a mitochondrial-specific dye like MitoTracker Deep red FM and lase scanning microscope could be employed in future studies. This approach would allow for direct visualization of photosensitizer localization within intact cells, providing a more accurate and reliable assessment of their subcellular distribution.

Reactive oxygen species (ROS) are highly reactive molecules derived from oxygen, including superoxide anion (O2•-), hydroxyl radical (•OH), and hydrogen peroxide (H_2O_2). Mitochondria are a major source of ROS, particularly from the electron transport chain

and enzymes like monoamine oxidase (MAO) (Halliwell and Gutteridge 2007; Valko et al. 2007; Halliwell and Cross 1994; Matés et al. 2012; Farrugia and Balzan 2012; Orrenius et al. 2007; Circu and Aw 2010; Andreyev et al. 2005; Migliaccio et al. 2006; Lambert and Brand 2004; Korshunov et al. 1997; De Grey 2002; Aikens and Dix 1991). These ROS can damage cellular components, leading to oxidative stress and various diseases (Valko et al. 2005). Mitochondria, being the primary source of ROS, are particularly vulnerable to oxidative stress. This can lead to severe consequences, such as damage to mitochondrial DNA (mtDNA) (Circu *et al*.,2009, Rachek *et al*., 2009, Orrenius *et al*.,2007). We believe that this mitochondrial damage, induced by excessive ROS production, can lead to the release of cytochrome c from the intermembrane space into the cytosol. Cytochrome c plays a critical role in initiating the apoptotic cascade.

Figure 5.13 describes the extrinsic and intrinsic pathway. In the intrinsic pathway, mitochondrial damage leads to the release of cytochrome c, which activates caspase-9. Caspase-9, in turn, activates caspase-3. In the extrinsic pathway, death receptors such as TNF receptor and Fas receptor activate caspase-8, which can directly activate caspase-3 or indirectly through caspase-9 (Tsai *et al*., 2018). Caspase-3, a crucial member of the caspase family, plays a pivotal role in the execution phase of apoptosis (Hu *et al*., 2020). It is activated by both intrinsic and extrinsic apoptotic pathways (Reed, 2000). In our study the observed increase in caspase-3 activity in the PDT groups suggests that apoptosis is a primary mechanism underlying the inhibition of cell growth.

Figure 5.13 Extrinsic and intrinsic apoptotic pathways

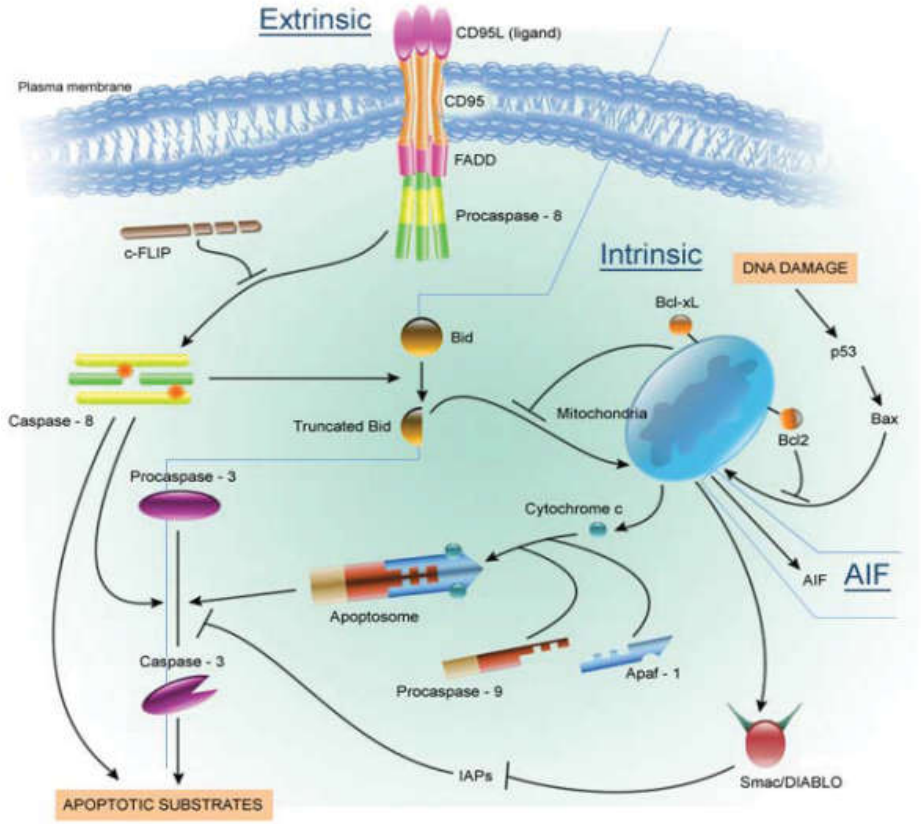

The extrinsic apoptotic pathway is initiated by the binding of a ligand (e.g., CD95L) to its receptor (CD95). This activation leads to the activation of FADD and DED, which in turn activates caspase 8. Caspase 8 can initiate apoptosis either directly or through effector caspases like caspase 3. Active caspase 8 also cleaves BID to tBID, which translocates to the mitochondria and releases SMAC/DIABLO. SMAC/DIABLO sequesters IAPs, leading to apoptotic induction through caspase 3. The intrinsic apoptotic pathway is initiated at the mitochondria by various stimuli, including irreparable DNA damage signaling through p53 proteins. This signaling removes suppression of apoptosis by BCL2, leading to membrane permeabilization and the release of cytochrome c, SMAC/DIABLO, and AIF. Cytochrome c interacts with APAF1 to recruit and activate caspase 9, forming the apoptosome, which activates downstream executioner caspases 3 and 7. AIF causes DNA degradation. The figure was taken from an article by Hejmadi. (Hejmadi., 2014).

The cellular response to DNA damage is a complex interplay of various mechanisms, primarily focused on DNA repair and cell cycle

arrest. Key players in this response include lesion sensors like MMR, signal transducers like ATM, and transcription factors like p53 and p73. While these factors are crucial for regulating apoptosis, their primary role is to protect the damaged cell. Apoptosis, a secondary response, is activated when DNA damage is severe and irreparable. The decision to induce apoptosis or enforce growth arrest is influenced by the extent of damage and the cellular context. The p53-dependent transcriptional response plays a pivotal role in this decision-making process (Wang.,2001). In our study we found DNA damage to the PDT groups and also S phase cell cycle arrest. The observation of cell cycle arrest at the S phase in response to DNA damage is consistent with the cell's strategy to prioritize DNA repair. During the S phase, DNA replication occurs, and any damage to the DNA template can lead to errors in replication and genomic instability. By arresting the cell cycle at this stage, the cell buys time for DNA repair mechanisms to correct the damage before proceeding to the next phase of the cell cycle. This response is crucial for maintaining genomic integrity and preventing the propagation of damaged cells, which could lead to cancer and other diseases. The activation of DNA repair pathways, such as those involving proteins like ATM and p53, is essential for efficient repair and the subsequent release of the cell cycle arrest.

Apoptotic cells exhibit a characteristic set of morphological changes, including cell shrinkage, membrane blebbing, chromatin condensation, nuclear fragmentation, and the formation of apoptotic bodies (Doonan., 2008). These observations were found during

ethidium bromide acridine orange dual staining and DAPI staining also.

Our results suggest that photodynamic therapy (PDT) primarily induces apoptosis in the experimental model. While necrosis or a combination of apoptosis and necrosis may occur in some cases, our findings predominantly support an apoptotic mechanism. The observed mitochondrial accumulation points to an intrinsic apoptotic pathway. However, further investigation is required to definitively confirm the specific apoptotic pathway and the involvement of various caspase markers. Future studies should include gene and protein expression analysis to gain deeper insights into the molecular mechanisms underlying PDT-induced cell death. Consistent with our findings, previous studies on PDT with hypericin and other photosensitizers have also implicated mitochondrial-mediated apoptosis as a major mechanism of cell death (Zhang *et al*.,2015, Li D *et al*.,2015, Saneesh *et al*., 2017).

Chapter 6

Cytotoxicity assessment of PAF 1 and PAF 2 on L929 cells

6.1 Introduction

Primarily via causing apoptosis, PAF 2 and PAF 1 have demonstrated promise as possible photodynamic treatment (PDT) agents against A431 skin cancer cells. This has shown to happen. This makes it likely that they could be utilised as a therapy method for skin cancer. Nevertheless, it is crucial to assess their safety profile before they are used in clinical environments, especially with relation to the possible damage they might cause on normal cells. By looking at their effects on cell viability, proliferation, and general cellular health in normal cell lines such L929, researchers are able to identify possible side effects and hence can optimize the formulation and administration of these drugs to maximise therapeutic efficacy, while concurrently reducing adverse reactions. This approach guarantees the creation of medications that are safe and efficient for usage in clinical environments in next generations. The cytotoxic effects of PAF 1 and PAF 2 on L929 normal cells are investigated in this chapter, presenting a thorough study of the results. Two main tools that we employed to reach this aim were the MTT assay and morphological analysis. Unlike the morphological assessment, which lets one observe clearly cellular alterations including changes in cell form, size, and quantity, the MTT assay measures cell viability by counting metabolic activity of the

cells. We think that by combining these approaches, we will be able to get understanding of the possible toxicity of PAF 2 and PAF 1 on regular cells. This will provide essential data to assess the safety profile of these drugs and direct next projects on research and development.

6.2 Materials and Methods

6.2.1 Materials

L929 mouse fibroblast cells were procured from the National Centre for Cell Science (NCCS), Pune. For cell culture experiments, essential materials, including Dulbecco's Modified Eagle Medium (DMEM), 0.25% Trypsin - EDTA, and Antibiotic-antimycotic solutions and 3-(4,5-dimethylthiazol-2-yl)-2,5-diphenyltetrazolium bromide (MTT) were purchased from Himedia, India. Fetal Bovine serum (FBS) was purchased from Gibco, Life Technologies Limited, UK. 5-Amino Levulinic acid (ALA) was acquired from Sisco Research Laboratories Pvt. Ltd, Mumbai, India.

6.2.2 *In vitro* cytotoxicity assay

In vitro cytotoxicity assessment of samples was done using MTT assay.The IC_{50} of each samples and their multiple concentrations (1X-4X) were used for the treatment. And checking whether our IC_{50} concentration shows significant cytotoxicity.

- **MTT assay and analysis of cell morphology**

The procedures for MTT assay and cell analysis have already been described in the previous chapter (5.2.2.5 and 5.2.2.6)

6.3 Results

6.3.1 MTT Assay

The results of MTT assay is given in Figures 6.1, Figure 6.2 and Figure 6.3.

Figure 6.1 Percentage inhibition of L929 cell growth during 24 h

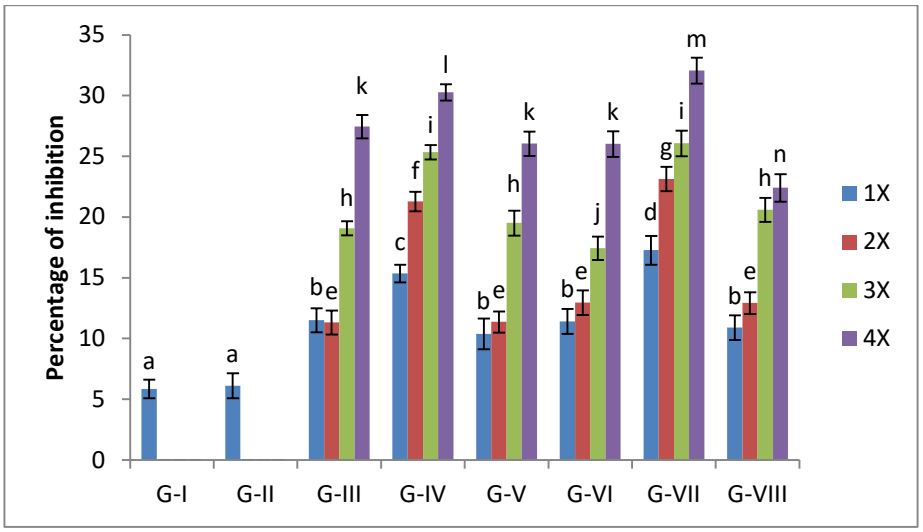

Percentage inhibition of L929 cell growth was determined for different experimental groups. Values are mean of three estimations. Different alphabets indicates significant difference between the groups. F value for 1X,2X,3X and 4X is 45.289,137.074,223.363 and 337.672 respectively. P<0.05

Figure 6.2 Percentage inhibition of L929 cell growth during 48 h

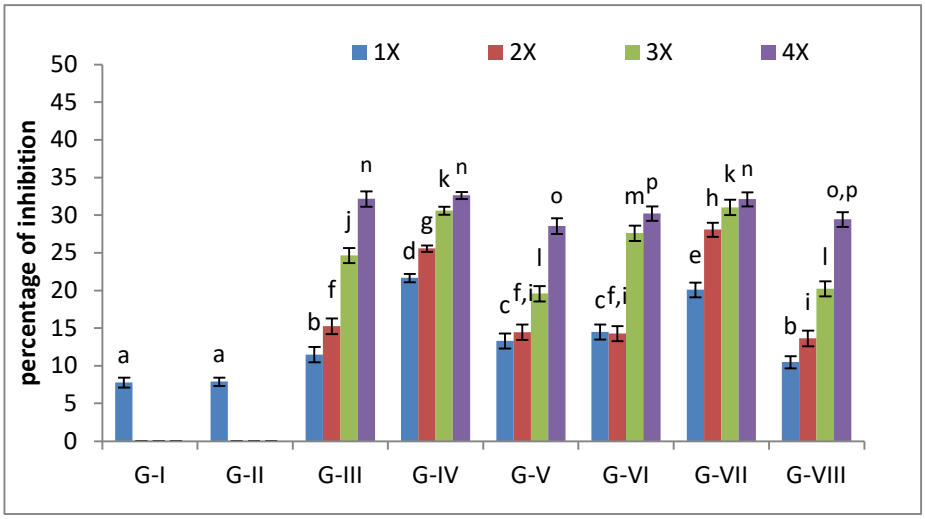

Percentage inhibition of L929 cell growth was determined for different experimental groups. Values are mean of three estimations. Different alphabets indicates significant difference between the groups. F value for 1X,2X,3X and 4X is 112.153,202.966,373.044 and 495.299 respectively. P<0.05.

Figure 6.3 Percentage inhibition of L929 cell growth during 72 h

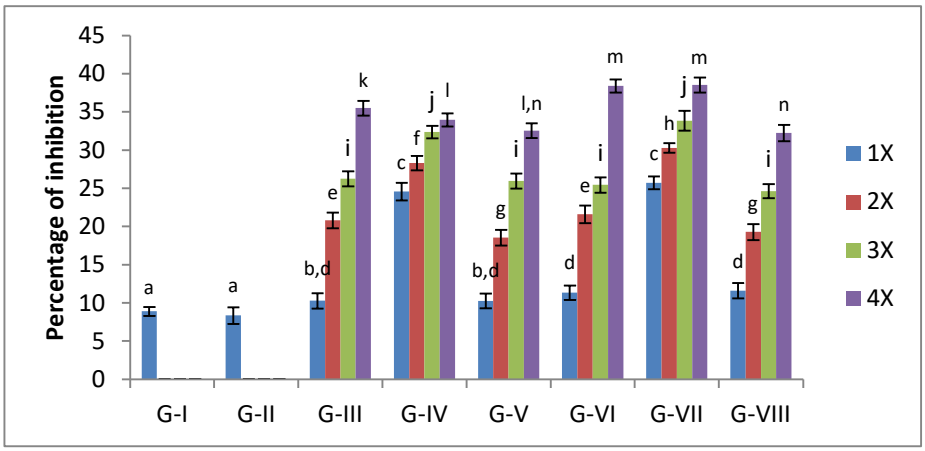

Percentage inhibition of L929 cell growth was determined for different experimental groups. Values are mean of three estimations. Different alphabets indicates significant difference between the groups. F value for 1X,2X,3X and 4X is 160.123,204.707,287.767 and 588.727 respectively. P<0.05.

The results of Figures 6.1, 6.2, and 6.3 indicate that the percentage of inhibition was lower for the samples. This suggests that the samples had a lower toxicity towards the normal cells.

6.3.2 Morphological Analysis

Through the use of morphological analysis, we attempted to determine how the structure and integrity of L929 cells were impacted by the different experimental settings that were used. Control groups I and II demonstrated normal cellular shape; these groups served as benchmarks for the baseline values. Characteristics of this form include the integrity of cell membranes, the presence of nuclei that can be identified, and a regular cellular shape. It is important to note that the experimental groups, consisting of people who were receiving PDT in addition to other therapies, did not exhibit any discernible aberrations from the form of the control group. In spite of the fact that the experimental settings might have had an effect on other cellular processes, this evidence suggests that the L929 cells did not undergo any significant morphological changes as a consequence of the conditions involved. The fact that the usual form of the cells has been kept is indicative of the absence of overt cytotoxicity or significant cellular damage within the cells.

Figure 6.4 Morphological analysis of L929

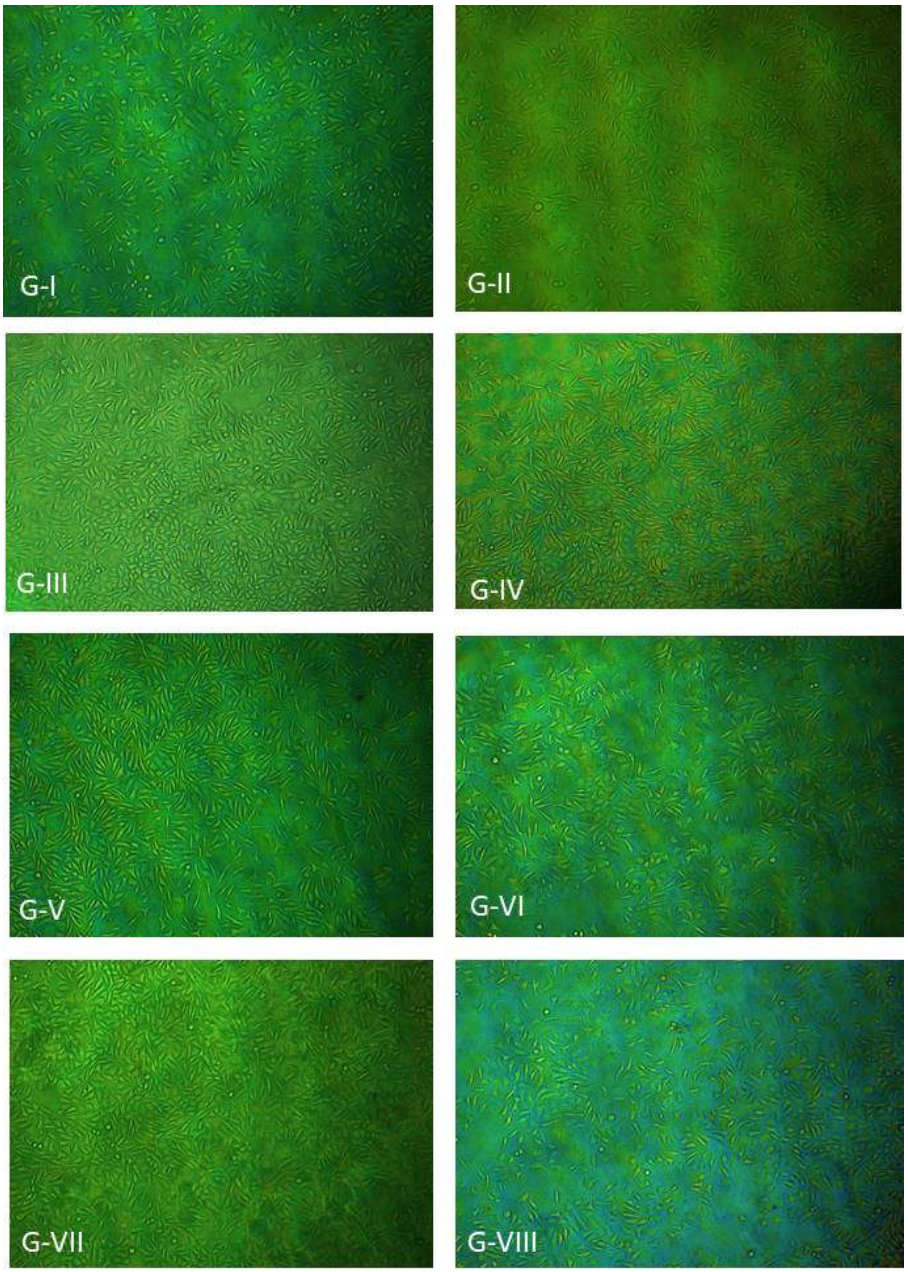

The morphological changes that were observed in control groups I and II were shown to be insignificant, according to the observations. The cell shape of other groups did not demonstrate any significant differentiating characteristics. Cells were observed under 10 x magnification.

6.4 Discussion

The vitality of cells can be quantified by the use of viability tests, which involve the measurement of metabolic processes, such as those related with cellular survival and maintenance. The quantity of viable cells that are still present after a treatment time is regarded to be directly related to the activities that are being discussed here, which are frequently associated with "housekeeping" enzymes. The MTT assay is a colorimetric approach which measures the reduction of the yellow tetrazolium dye MTT to a purple formazan product. This allows the assay to quantify the viability of cells as well as their proliferation. MTT is transformed into formazan by metabolically active cells, particularly those cells that have mitochondrial dehydrogenases that are performing their function. In order to provide a precise evaluation of cell proliferation and cytotoxicity, the amount of formazan that is produced is directly related to the number of live cells. The outcomes of the MTT assay and the morphological evaluation indicated that the photosensitizers exhibited a level of toxicity to L929 cells that was so low that it was considered inconsequential under normal conditions. The absence of cytotoxicity that was seen in L929 cells is an important discovery because it has the potential to suggest that these photosensitizers may have a therapeutic window that is favourable, hence minimising the possibility of adverse effects.

For a drug candidate to be considered successful, it must exhibit efficacy without causing any adverse effects that are deemed undesirable. For the purpose of optimising drug development, researchers give priority to candidates who contain desired features

similar to those of drugs. Beginning the process of drug discovery and development with an early screening for drug toxicity has become an essential component of the process. It is generally accepted to use cytotoxicity endpoints in concert with other cellular tests in order to screen for organ-specific toxicity. These endpoints include evaluations of membrane integrity, cellular metabolite content, mitochondrial function, and lysosomal function. Researchers have the ability to dramatically improve the effectiveness of drug discovery and development by employing these screening tests in a methodical manner and doing thorough data analysis. Assessing the integrity of membranes, for example, can assist in the identification of substances that disrupt cellular membranes, which ultimately results in the death of cells. A better understanding of the metabolic disturbances that drug candidates generate can be gained through the monitoring of cellular metabolite content. The evaluation of mitochondrial activity enables researchers to determine the impact of compounds on the creation of cellular energy, whereas the examination of lysosomal function assists in the identification of compounds that interfere with the systems that are responsible for the disposal of waste in cells. By incorporating these cytotoxicity endpoints into the early stages of drug discovery, researchers are able to prioritise compounds that have favourable toxicity profiles. This helps decrease the likelihood of failures in the later stages of the drug discovery process and speeds up the development of treatments that are both safe and effective.

Research on normal cells *in vivo* is crucial for the aim of doing a thorough assessment of the toxicity of a possible pharmacological

candidate. The medicine is given to animal models, such as mice, in several dosages in order to reach this aim. Scientists are able to assess the degree of toxicity connected to the drug and spot strong negative side effects. Blood tests are meant to be used for monitoring changes in vital components such the existence or absence of blood cells, the functioning of the kidneys and liver, and the electrolyte distribution. Furthermore enabled by the histological study of organs for the purpose of characterising them is the microscopic evaluation of tissue damage, inflammation, and other cellular anomalies. This multifarious approach offers a thorough knowledge of the toxicity profile of the medication and helps in the identification of any safety issues before moving forward with clinical research.

Having indicated that previous research have revealed that similar photosensitisers had a low cytotoxicity in non-cancerous cells, and our findings are consistent with their findings. The potential of skyrin, which is a precursor to the anticancer drug hypericin, was studied in a study that was conducted by Terezia Zajikova in the year 2022. Within the scope of this investigation, the genotoxic and DNA-protective properties of skyrin were investigated. These effects were more prominent in human lymphocytes that did not have cancer, despite the fact that skyrin demonstrated DNA-protective capacities of a moderate degree. Particularly noteworthy is the fact that the chemical did not exhibit any genotoxic potential. These findings indicate that skyrin may be a good candidate for anticancer therapy, particularly due to the fact that it selectively protects cells that are not malignant (Zajikova *et al*., 2022). The cytotoxic effects of methanolic and

aqueous extracts of *Hypericum pseudolaeve*, which contained hypericin, were assessed on fibroblast cells. According to İğci, *et al*.'s 2020 study, the researchers discovered that these extracts did not demonstrate any harmful effects even when exposed to concentrations as high as 500 µg/mL. A study that was conducted in 2021 by Ahmed M. Abdelsalam and colleagues involved the development and evaluation of novel hypericin formulations. According to Abdelsalam *et al*.'s research from 2021, these formulations showed a lower phototoxicity profile in murine fibroblast L929 cells, which suggests that they may be safe for use in normal cells.

According to the findings of our research, the chemical targets A431 skin cancer cells in a selective manner while leaving normal cells unaffected. Nevertheless, additional studies need to be carried out in order to completely understand the processes that are responsible for the compound's cytotoxicity against cancer cells and its lack of toxicity towards normal cells within the body. In addition to this, it is essential to do more exhaustive toxicity testing on normal cells, which should also include *in vivo* models, in order to ensure that the molecule is safe for usage in clinical settings.

Chapter 7

Identification of photosensitizers in PAF1 and PAF 2

7.1 Introduction

In 1942, Klaber discovered that people could get sunburned from sun exposure after the contact with several species of plants (Klaber *et al*.,1942). Based on this observation, researchers began investigating various plants and their chemical compounds, which become toxic under the influence of sunlight. They discovered that these "phototoxic" substances can cause a variety of harmful skin reactions, including irritation, allergies, increased sensitivity and genetic changes. These compounds contain light-absorbing elements called chromophores. Interestingly, plants sometimes produce these compounds as a natural defense mechanism against excessive sun exposure, making them ingredients in sunscreens and cosmetic products (Kubrak *et al*., 2022). In this chapter we will examine the photoactive components of photoactive fractions PAF1 and PAF 2 from *F.tataricum* and *F. auriculata*. Although the genus Fagopyrum includes many species, *Fagopyrum esculentum*, *Fagopyrum tataricum* and *Fagopyrum cymosum* are the most widely used and studied. Fagopyrins are a class of natural compounds found in plants of the genus Fagopyrum. Parts of these plants are consumed globally by humans and animals. The other genus Ficus which include in the

family of Moraceae consists of medicinal and ornamental plants. *Ficus carica* was reported to have furan compounds (Chunyan *et al*.,2008).

7.2 Materials and Methods

7.2.1 Materials

In the case of PAF1 our investigation focused specifically on fagopyrin, as existing literature identifies it as the primary photosensitizer in *F.tataricum* (Kim *et al*., 2020) fagopyrin, in pure form is not commercially available. Hence due to its structural similarity with hypericin, a compound found in St. John's wort (*Hypericum perforatum* L.), and hypericin is commonly used as a standard for detecting fagopyrin in samples. Furan compounds are present in Ficus species, as shown in existing literature (Caporale *et al*., 1970). In the study of PAF 2, we used psoralen, a well-established furan compound, as a reference standard. Hypericin is procured from HWI pharma services GmbH,Ruelzheim,Germany.Psoralen procured from Sigma –Aldrich,USA.

7.2.2 HPLC

HPLC analysis was conducted in the Central Sophisticated Instrumentation facility (CSIF) University of Calicut. It was performed using Agilent 6100 Series equipped with Edwards vacuum pump. C18 column (Agilent, Poroshell 120 EC-C 18, 4.6 mm X 50 mm, 2.7 μ) was used for the separation. The injection volume was 20 μL, flow rate was 1 mL/min, and detection wavelength was 590nm. Water (A) and acetonitrile (B) made up the mobile phase, with the elution gradient

being 0–1 min at 0% B, 1-2 min at 0–60% B, 2–8 min at 60–100% B, 8–15 min at 100% B, and 15–18 min at 0% B (Stojilkovski *et al*.,2013). To detect furan compounds, the mobile phase was a mixture of water (Solvent A) and methanol (solvent B) in a ratio of 45:55 (v/v) for the first 8 min. The composition was then linearly increased to a ratio of 0:100 (A: B) over 20 min and maintained at this ratio for another 5 min. The column was then re-equilibrated with the original mobile phase composition (45:55, A: B) for 5 min. The total time was 30 min, and detection occurred at a wavelength of 246 nm (Jeong *et al*., 2015).

7.2.3 HR-LCMS

The compounds in PAF1 and PAF2 were detected in the Sophisticated Analytical Instrument Facility (SAIF) at IIT Bombay.

7.2.4 GCMS

The compounds in PAF 1 were analyzed and identified at CAI-K, Kerala Forest Research Institute (KFRI), Peechi. The components of PAF 2 were characterized by GC-MS at the Central Instruments Laboratory, College of Veterinary and Animal Sciences, Mannuthy.

7.3 Results

For better clarity, the results have been divided into two sections: the first contains the analysis of PAF1, the second that of PAF 2.

7.3.1 Identification of photosensitizers present in PAF 1

7.3.1.1 HPLC

The results of the HPLC analysis of Hypericin and PAF 1 are given in Figure 7.1.

Figure 7.1. HPLC chromatogram of hypericin and PAF 1

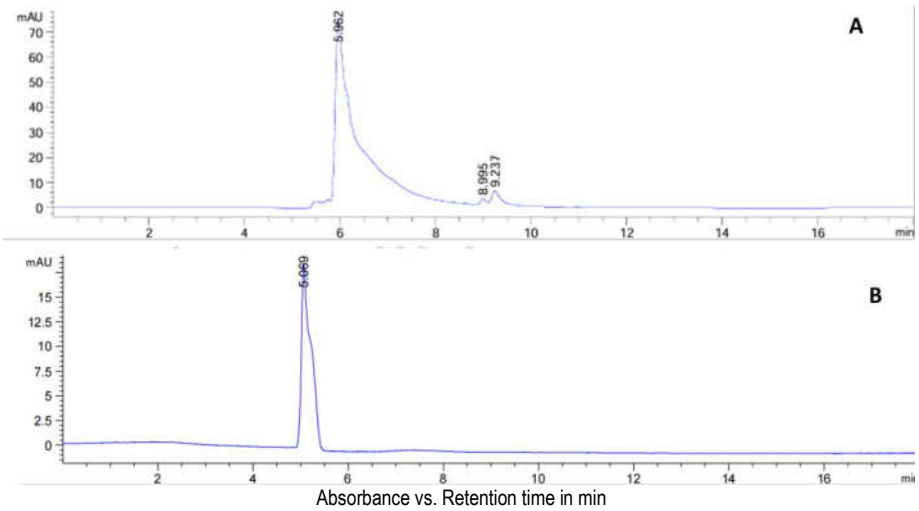

(A) hypericin (B) PAF 1. Retention time of Hypericin 97 % at 5.962. retention time of PAF1 100 % at 5.069.

A distinct, high-intensity peak at a retention time of 5.962 min on chromatogram A indicates the presence of the major compound, Hypericin. At retention times of 8.995 and 9.237 min, smaller peaks indicate the presence of minor components, possibly impurities. Chromatogram B exhibits a single, sharp peak at a retention time of 5.069 min, indicating the presence of fagopyrin in the PAF1 sample.

7.3.1.2 HRLCMS

The chromatograms of HRLCMS are given in Figure 7.2 and Figure 7.4.

Figure 7.2 Positive ion chromatogram of PAF1

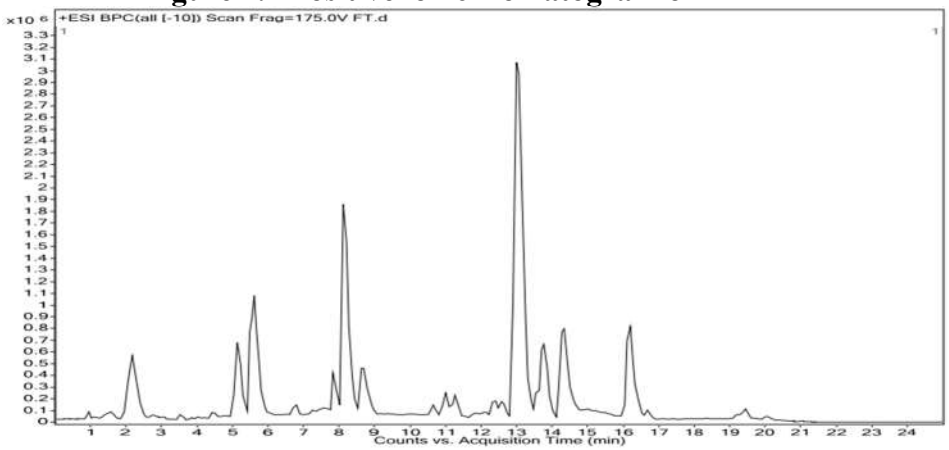

Table 7.1 Compounds detected in positive ion chromatogram of PAF 1

Compound label	RT	Mass	Abundance	Formula
L-1,2,3,4-Tetrahydro beta-carboline-3-carboxylic acid	4.54	216.0895	60886	$C_{12}H_{12}N_2O_2$
Betavulgarin	5.673	312.0622	50068	$C_{17}H_{12}O_6$
Genistin	5.837	432.1039	343253	$C_{21}H_{20}O_{10}$
Maritimetin	5.933	286.0463	37077	$C_{15}H_{10}O_6$
Adlumidiceine	6.824	399.1301	92006	$C_{21}H_{21}NO_7$
Tirofiban	7.283	440.2341	47719	$C_{22}H_{36}N_2O_5S$
Citpressine II	7.859	315.1115	46455	$C_{17}H_{17}NO_5$
Cavinine	7.864	347.1376	175147	$C_{18}H_{21}NO_6$
[4]-Gingerdiol 3,5-diacetate	8.086	352.1863	16974	$C_{19}H_{28}O_6$
3-Acetylnerbowdine	8.141	361.1532	838544	$C_{19}H_{23}NO_6$
Melicopicine	8.153	329.1272	102620	$C_{18}H_{19}NO_5$
Haemanthidine	8.388	317.1269	85903	$C_{17}H_{19}NO_5$
Ezetimibe	8.388	409.1505	96997	$C_{24}H_{21}F_2NO_3$
Papaveraldine	8.636	353.1251	261655	$C_{20}H_{19}NO_5$
2-O-Acetylpseudolycorine	9.028	331.1429	107174	$C_{18}H_{21}NO_5$
Phytosphingosine	10.646	317.2915	58594	$C_{18}H_{39}NO_3$
Oleic acid (d5)	11.308	287.2816	131383	$C_{18}H_{29}D_5O_2$
Kuwanon V	11.581	646.2566	31396	$C_{40}H_{38}O_8$
Terminaline	12.946	363.3124	85621	$C_{23}H_{41}NO_2$
Fagopyrine	15.327	670.2283	91086	$C_{40}H_{34}N_2O_8$

Figure 7.3 MS spectra of fagopyrin

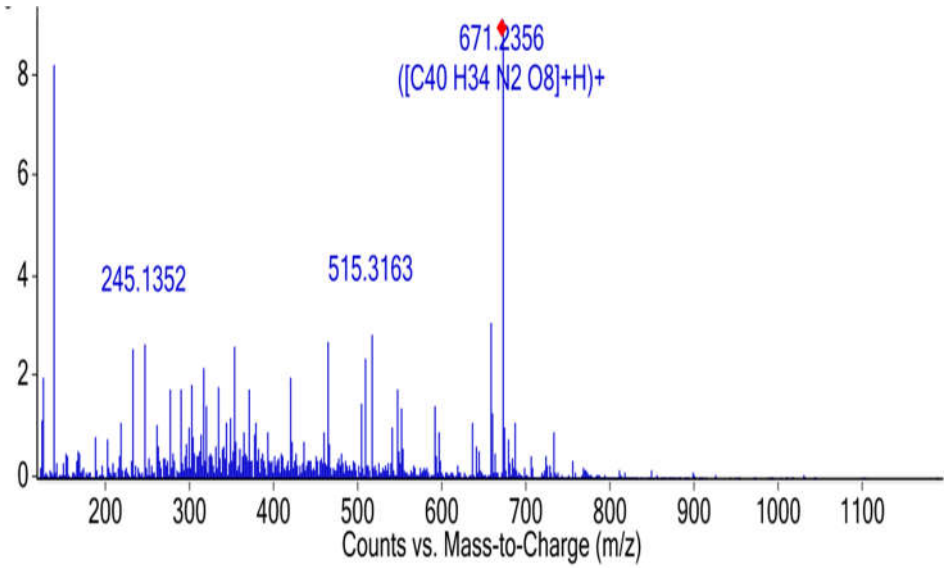

Figure 7.4 Negative ion chromatogram of PAF1

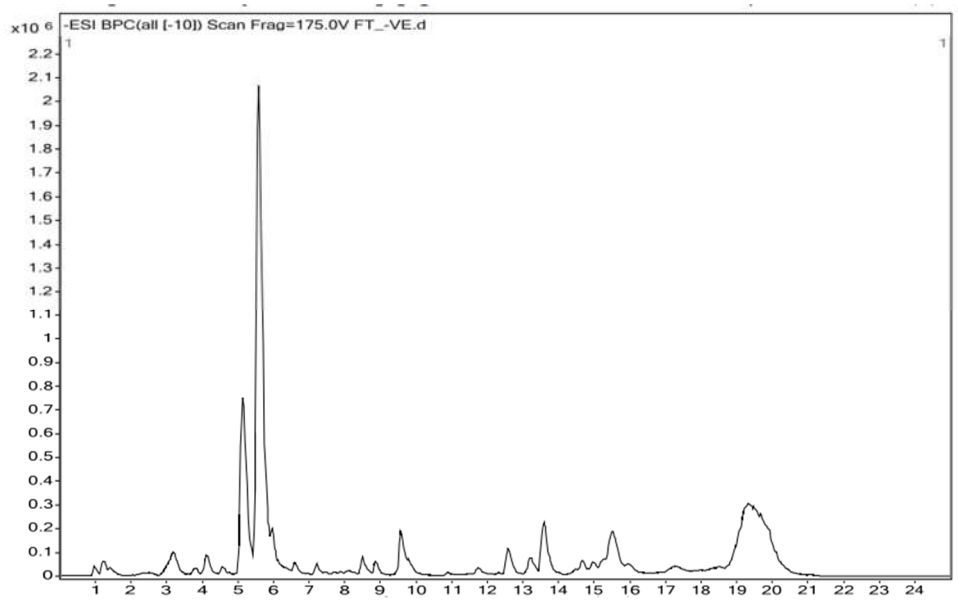

Table 7.2 Compounds detected in negative ion chromatogram of PAF1

Compound Label	RT	Mass	Abundance	Formula
L-Malic acid	1.29	134.0216	1638	$C_4 H_6 O_5$
2,6-dihydroxybenzoic acid	2.779	154.0265	1121	$C_7 H_6 O_4$
Chlorogenic acid	3.186	354.0956	51497	$C_{16} H_{18} O_9$
Monomethyl phthalate	4.126	180.0417	1195	$C_9 H_8 O_4$
Benzoic acid	4.299	122.0366	866	$C_7 H_6 O_2$
Altersolanol A	4.892	336.0849	1219	$C_{16} H_{16} O_8$
Kaempferol 7-O-glucoside	5.134	448.1018	340276	$C_{21} H_{20} O_{11}$
Resorcinol	5.262	110.0371	1149	$C_6 H_6 O_2$
o-Cresol	5.417	108.0576	1713	$C_7 H_8 O$
Guajavarin	5.986	434.0863	98617	$C_{20} H_{18} O_{11}$
2,3-Dihydroxy-p-cumate	6.45	196.0734	524	$C_{10} H_{12} O_4$
Kaempferol	6.57	286.0487	374	$C_{15} H_{10} O_6$
Enol-phenylpyruvate	8.019	164.0472	2513	$C_9 H_8 O_3$
Genistein	11.933	270.0535	849	$C_{15} H_{10} O_5$
Mupirocin	13.415	500.3001	47206	$C_{26} H_{44} O_9$
10-Oxo-11-octadecen-13-olide	14.09	294.22	1928	$C_{18} H_{30} O_3$
Hexazinone	15.426	252.1557	65954	$C_{12} H_{20} N_4 O_2$

The base peak chromatogram obtained from ESI in positive (figure 7.3) and negative (Figure 7.4) mode shows several distinct peaks eluting between 1 to 21 min. In positive ion mode at 15 min shows the presence of Fagopyrin. The analysis of the mass-to-charge ratio (m/z) fagopyrin peak, which exhibited an m/z of 671.2356 in positive ion mode (Figure 7.3). Numerous smaller peaks with varying intensities are also present throughout the chromatogram, indicating the presence of multiple components in the analyzed sample.

7.3.1.3 GCMS

The GCMS chromatogram is given in Figure 7.5.

Figure 7.5 GCMS chromatogram of PAF1

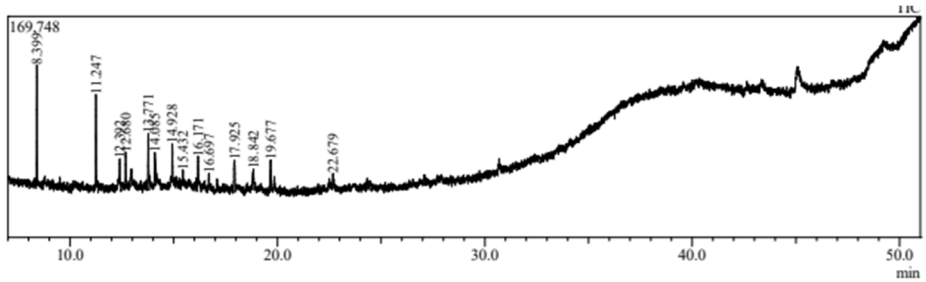

Table 7.3 compounds identified in PAF1 by using GCMS

Compound Label	RT	Area %	MW	Formula
Dodecane	8.399	17.29	170	$C_{12}H_{26}$
Hexadecane	11.247	14.62	226	$C_{16}H_{34}$
Heneicosane	12.392	3.79	296	$C_{21}H_{44}$
2,4-Di-tert-butylphenol	12.680	5.82	206	$C_{14}H_{22}O$
Heptadecane	13.771	11.24	240	$C_{17}H_{36}$
1-(2-Hydroxyethyl)-2,2,6,6-tetramethyl-4-piperidinol	14.085	10.96	201	$C_{11}H_{23}NO_2$
Eicosane	14.928	5.92	282	$C_{20}H_{42}$
Hexadecane, 2,6,10,14-tetramethyl-	15.432	2.16	282	$C_{20}H_{42}$
Octadecane	16.171	4.38	254	$C_{18}H_{38}$
2-Hexadecen-1-ol, 3,7,11,15-tetramethyl-, acetate, [R-[R*,R*-(E)]]-	16.697	2.25	338	$C_{22}H_{42}O_2$
Silane, trichlorooctadecyl-	17.925	10.67	386	$C_{18}H_{37}Cl_3Si$
Dibutyl phthalate	18.842	2.01	278	$C_{16}H_{22}O_4$
Benzenepropanoic acid, 3,5-bis(1,1-dimethylethyl)-4-hydroxy-, ethyl ester	19.677	7.49	306	$C_{19}H_{30}O_3$
11-Methyltricosane	22.679	1.40	338	$C_{24}H_{50}$

There are several peaks observed in GCMS analysis of PAF 1. The compounds were eluted from 8.399 to 22.679 min. The list of compounds is given in table 7.3.

7.3.2 Identification of photosensitizers present in PAF 2

7.3.2.1 HPLC

The results of HPLC analysis of Psoralen and PAF2 are given in Figure 7.6.

Figure 7.6 HPLC chromatogram of psoralen (A) PAF2 (B).

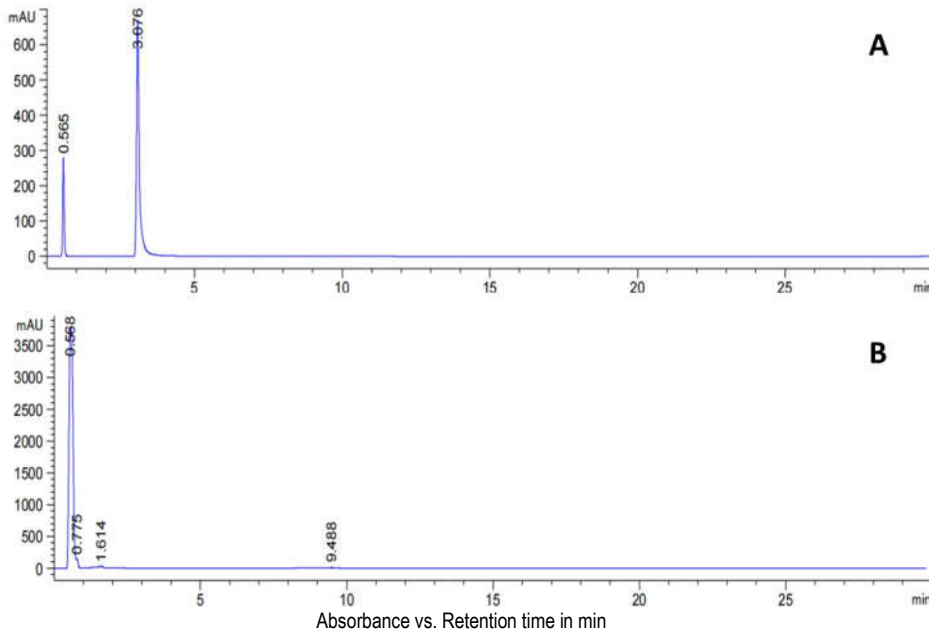

Chromatogram of Psoralen exhibits a major peak eluted at approximately 3.076 min with high absorbance, as well as a minor peak at 0.565 min. For Psoralen, two peaks were observed at retention times of 0.565 and 3.076 min, indicating the presence of multiple isomers or degradation products. Chromatogram of PAF 2 exhibits a

very large peak at 0.568 min, which is significantly more intense than all peaks in chromatogram A and it corresponds to a similar peak in the chromatogram of psoralen, at 0.565 min. In addition, chromatogram B contains minor peaks at 0.775, 1.614, and 9.488 min.

7.3.2.2 HRLCMS

The HRLCMS positive ion and negative ion chromatograms are given in Figure 7.7 and Figure 7.8. The compounds identified are given in tables 7.4 and 7.5.

Figure 7.7 Positive ion chromatogram of PAF 2

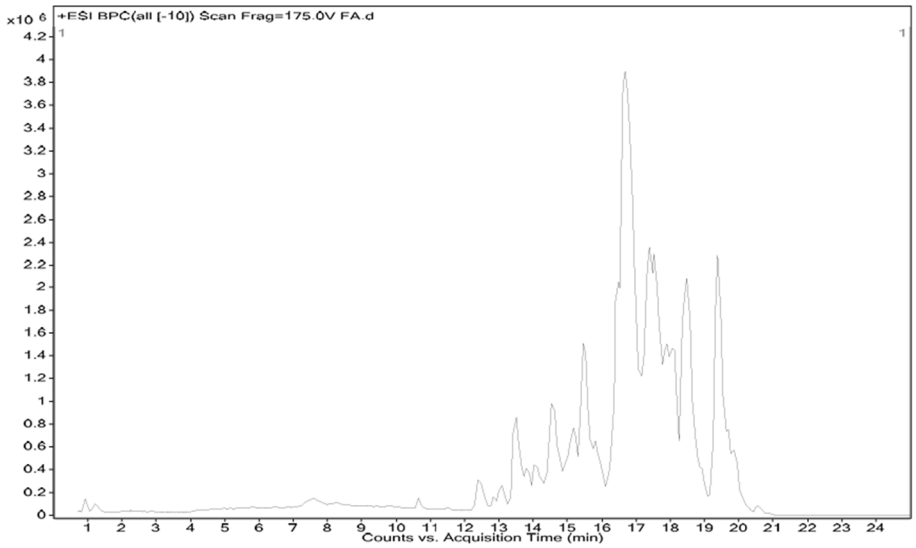

Table 7.4 Compounds identified in positive ion chromatogram of PAF 2

Compound Label	RT	Mass	Abund	Formula
Austalide A	13.366	516.2335	366145	C_{28} H_{36} O_9
AFN911	13.75	511.278	179450	C_{29} H_{33} N_7 O_2
12,15-cis-Squamostatin A	13.982	638.4726	258239	C_{37} H_{66} O_8
PE(16:0/14:1(9Z))	14.13	660.4547	152575	C_{35} H_{68} N O_8 P
cis-Annonacin-10-one	16.282	594.4467	473545	C_{35} H_{62} O_7
Squamostatin E	16.343	622.4778	989856	C_{37} H_{66} O_7
Mosinone A	17.965	620.4618	155656	C_{37} H_{64} O_7
Isomurisolenin	18.954	578.4515	354582	C_{35} H_{62} O_6
cis-Reticulatacin-10-one	19.181	606.483	395922	C_{37} H_{66} O_6

.

Figure 7.8 Negative ion chromatogram of PAF 2

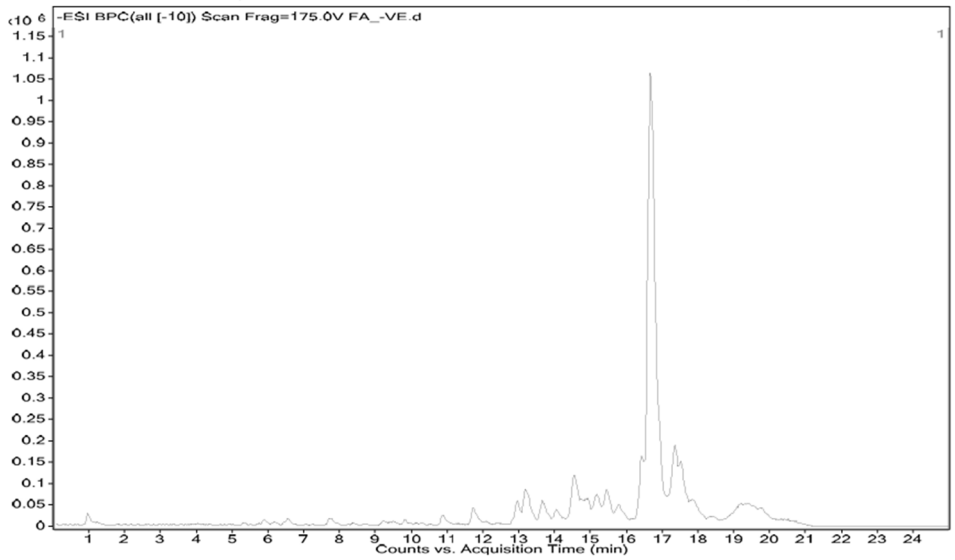

Table 7.5 Compounds identified in negative ion chromatogram of PAF2

Compound Label	RT	Mass	Abundance	Formula
L-Malic acid	1.233	134.0214	4362	$C_4 H_6 O_5$
(1R,6R)-6-Hydroxy-2 succinylcyclohexa-2,4-diene-1 carboxylate	4.109	240.0627	1018	$C_{11} H_{12} O_6$
Caffeic acid	4.109	180.0416	975	$C_9 H_8 O_4$
Ellagic acid	5.556	302.0055	618	$C_{14} H_6 O_8$
Quercitrin	5.829	448.101	2399	$C_{21} H_{20} O_{11}$
Benzoic acid	6.69	122.0364	991	$C_7 H_6 O_2$
Genistein	8.351	270.0528	3283	$C_{15} H_{10} O_5$
Kaempferol	8.6	286.0478	1113	$C_{15} H_{10} O_6$
Luteolin	8.6	286.0478	1113	$C_{15} H_{10} O_6$
[7]-Paradol	12.554	292.2042	462	$C_{18} H_{28} O_3$
10-Oxo-11-octadecen-13 olide	12.966	294.22	26706	$C_{18} H_{30} O_3$
Dinoseb	13.175	240.075	42351	$C_{10} H_{12} N_2 O_5$
12,15-cis-Squamostatin A	15.185	638.4784	49342	$C_{37} H_{66} O_8$
cis-Annonacin-10 one	16.349	594.4541	28349	$C_{35} H_{62} O_7$
Asitrilobin B	16.669	596.4669	27746	$C_{35} H_{64} O_7$
Squamostatin E	17.615	622.4837	118912	$C_{37} H_{66} O_7$

The base peak chromatogram obtained from ESI in positive (figure 7.7) and negative (Figure 7.8) mode shows several distinct peaks eluting between 11 to 21 min. Numerous smaller peaks with varying intensities are also present throughout the chromatogram, indicating the presence of multiple components in the analyzed sample.

7.3.2.3 GCMS

GCMS chromatogram of PAF 2 is given in Figure 7.9.

Figure 7.9 GCMS chromatogram of PAF 2

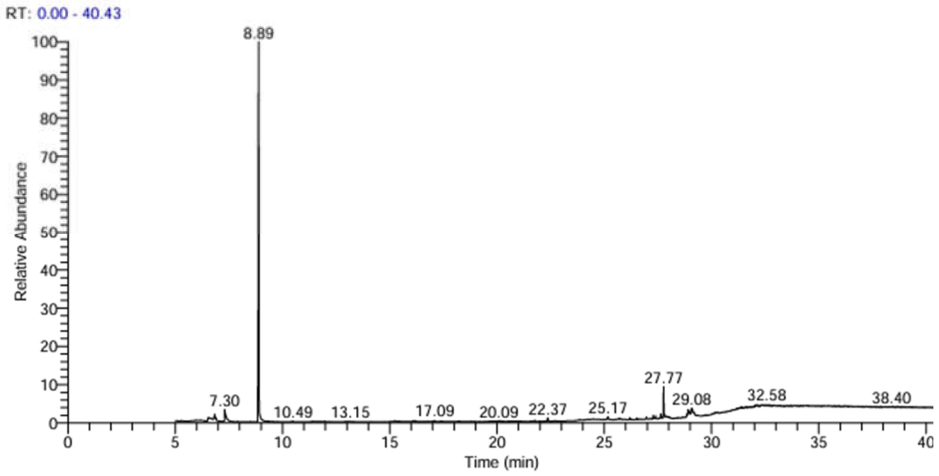

Table 7.6 Compounds identified in GCMS of PAF 2

Compound Label	RT	MW
Phenol, 2,4-bis(1,1-dimethylethyl)-	22.37	206
Nonadecane, 2-methyl-	25.17	282
Tetradecane, 2,6,10-trimethyl-	25.68	240
i-Propyl 12-methyl-tridecanoate	26.52	270
Phthalic acid, hex-3-yl isobutyl ester	26.97	306
Heptadecane, 2,6,10,15-tetramethyl-	27.28	296
7,9-Di-tert-butyl-1-oxaspiro(4,5)deca-6,9-diene-2,8-dione	27.40	276
Benzo[e]isobenzofuran-1,4-dione,1,3,4,5,5a,6,7,8,9,9a-decahydro-6,6,9a-trimethyl	27.40	248
n-Hexadecanoic acid	27.64	256
Phthalic acid, butyl undecyl ester	27.77	376
Hexadecanoic acid, ethyl ester	27.85	284
Adamantane, 2-[2-(pentamethyldisilanyl)-2-(phenylthio)ethylidene]-	28.04	400

Coumatetralyl isomer-2 ME	28.04	306
9,12,15-Octadecatrienoic acid, 2,3-bis[(trimethylsilyl)oxy]propyl ester, (Z,Z,Z)-	28.86	496
9,12-Octadecadienoic acid (Z,Z)-	28.91	280
Ethyl 9.cis.,11.trans.-octadecadienoate	29.08	308
2-Bromotetradecanoic acid	29.19	306
9,12,15-Octadecatrienoic acid, 2,3-bis[(trimethylsilyl)oxy]propyl ester, (Z,Z,Z)-	31.35	496
Chromone, 5-hydroxy-6,7,8-trimethoxy-2,3-dimethyl-	31.35	280
6-Amino-5-cyano-4-(5-cyano-2,4-dimethyl-1H-pyrrol-3-yl)-2-methyl-4H-pyran-3	31.39	326
9,12,15-Octadecatrienoic acid, 2,3-bis[(trimethylsilyl)oxy]propyl ester, (Z,Z,Z)-	31.42	496
Octasiloxane, 1,1,3,3,5,5,7,7,9,9,11,11,13,13,15,15-hexadecamethyl-	31.62	578
1-Naphthoic acid, 2-hydroxy-, monoanhydride with 1-butaneboronic acid, cyclic ester	32.04	254
9,10-Anthracenedione, 1-hydroxy-2-(hydroxymethyl)-	32.04	254
Columbin	32.13	358
1-Monolinoleoylglycerol trimethylsilyl ether	32.58	498

The gas chromatogram displays a profile of separated compounds over 40 min analysis period. Several peaks of varying intensity are observed, indicating the presence of different phytochemical compounds.

7.4 Discussion

This chapter describes some analytical strategy for the identification of photosensitizers in fractions PAF1 and PAF 2. This includes High-resolution liquid chromatography-mass spectrometry (HR-LCMS), gas chromatography-mass spectrometry (GCMS), high-performance thin layer chromatography (HPTLC), and High-performance liquid chromatography (HPLC). The various methods were strategically used to obtain additional insights into the chemical composition of the fractions. GCMS and LCMS were primarily used to identify volatile and non-volatile compounds in these fractions.

When HR LC-MS analysis was performed on the fraction collected from the TLC plate of *F. tataricum*, several compounds were detected. This may have been influenced by minor manual handling errors during the scraping of the silica gel, potentially incorporating surrounding spots into the fraction. However, we made every effort to carefully collect the spots that specifically contained fagopyrin and psoralen-like compounds.

In the case of PAF1 our investigation focused specifically on fagopyrin, as existing literature identifies it as the primary photosensitizer in F.tataricum. We detected fagopyrin in fraction PAF1. Furthermore, the detection of other phytochemicals in PAF 1 indicates that this fraction does not contain isolated fagopyrin, but rather a mixture containing fagopyrin along with their components.

There are six possible chemical structures of fagopyrins, among which three types of fagopyrins (fagopyrin A, E, and F) have been

identified using LC–MS/ MS and NMR. The analysis of the mass-to-charge ratio (m/z) in our study closely aligns with the findings reported by Benković *et al*. (2014) and Jacheol (2020) regarding the fagopyrin peak, which exhibited an m/z of 671.2356 in positive ion mode, consistent with the reported m/z of fagopyrin F (671.2401 [M+H]+). Other fagopyrin peaks did not correlate with any known fagopyrins (A–E), which may be attributed to insufficient sample amounts for LC-MS detection or the presence of unknown fagopyrin derivatives, similar to the conclusions drawn by Jacheol in 2020. This consistency reinforces the validity of the identification of fagopyrin F and highlights its significance in the study of tatary buckwheat extracts. Due to its structural similarity to hypericin (Figure 7.10), a compound found in St. John's wort (*Hypericum perforatum* L.), hypericin is commonly used as a standard for detecting fagopyrin in samples (Hinnburg *et al*., 2005, Ožbolt *et al*.,2008).

Figure 7.10 Structure of hypericin (A) fagopyrin F (B)

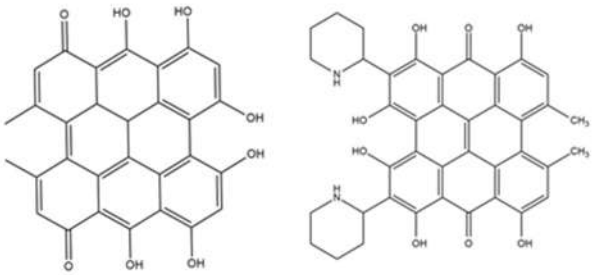

Furan compounds are present in Ficus species, as shown in existing literature (Chunyan *et al*.,2008). In the study of PAF 2, we used psoralen, a well-established furan compound, as a reference

standard. GC-MS analysis of complex biological and environmental samples often faces the challenge of incomplete chromatographic separations, leading to co-elution of compounds at the same retention time. This occurs when multiple compounds overlap in chromatographic peaks, making it difficult to extract pure component spectra and accurately identify individual compounds. As a result, distinguishing between co-eluting compounds becomes challenging, especially in samples with hundreds of chemical components, such as those found in studies of *Arabidopsis thaliana* leaf tissue extracts by Likic and team. The overlap of peaks complicates the extraction of unambiguous mass spectra, hindering accurate identification (Likic *et al*., 2009). The presence of 7,9-Di-tert-butyl-1-oxaspiro(4,5)deca-6,9-diene-2,8-dione in the methanol latex extract of *Ficus sycomorous* was previously reported by Abdel and team in 2019. In the present study, we have also identified the presence of this spiro-compound in the leaf extract of *F. auriculata*. Columbin, a compound identified in the PAF2, contains fused oxygenated rings, possibly resembling furocoumarins. 9,10-Anthracenedione, 1-hydroxy-4-methoxy has a conjugated polycyclic structure with oxygenation. Benzo[e]isobenzofuran-1,4-dione contains a fused benzofuran and quinone system. More structurally similar to psoralen due to the oxygenated fused rings. Chromone, 5-hydroxy-6,7,8-trimethoxy-2,3-dimethyl- contains a chromone core, similar to psoralen's oxygenated fused-ring system.

Figure 7.11 structure of Psoralen (A) 7,9-Di-tert-butyl-1-oxaspiro(4,5)deca-6,9-diene-2,8-dione (B) Benzo[e]isobenzofuran-1,4-dione (C) 9,10-Anthracenedione, 1-hydroxy-4-methoxy (D) Chromone, 5-hydroxy-6,7,8-trimethoxy-2,3-dimethyl- (E) Columbin (F)

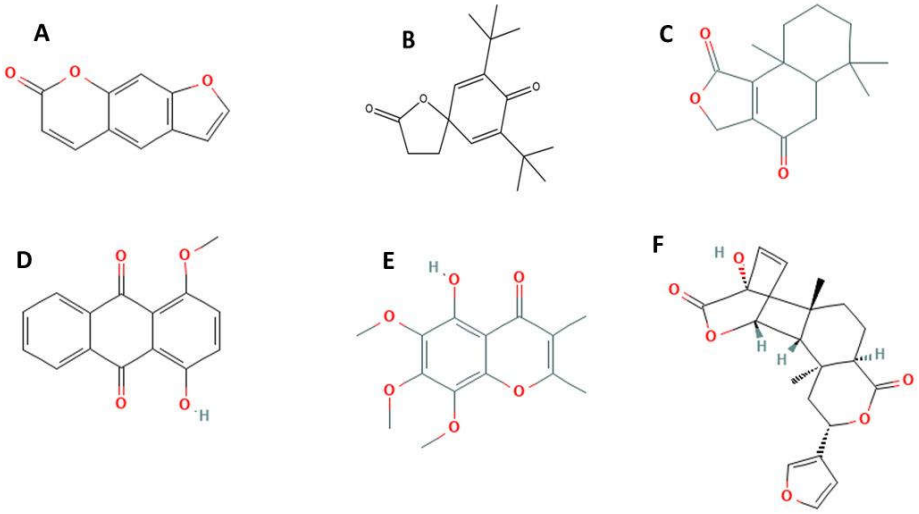

In addition to the known photosensitizers, the plant fraction also contains other phytochemicals (Figure 7.11). Therefore, further purification of these photosensitizers is required to further understand their effectiveness and accurately assess their anti-cancer activity. This could expand their potential applications in other areas.

Chapter 8

In silico Analysis of PAF1 and PAF2

8.1 Introduction

One of the most important members of the human epidermal receptor (HER) family is the epidermal growth-factor receptor, often known as EGFR. This family of proteins is accountable for a significant part of the process of cell growth and proliferation. When EGFR is overexpressed on the surface of tumor cells, it immediately becomes a primary target for the development of cancer therapies. Through the process of growth factors binding to EGFR, intracellular signaling pathways are activated, which in turn promotes the growth and division of cells. The EGFR gene has been the subject of intensive research as a possible therapeutic target (Byrne *et al*. 2008; Creixell et al. 2010; Laskin and Sandler 2004). This is because of the significant role that it plays in the development of cancer. According to Laskin and Sandler (2004), EGFR engages in interactions with six widely recognised endogenous ligands, including EGF, TGF-α, amphiregulin, betacellulin, HB-EGF, and epiregulin. EGF is the most common choice for targeting EGFR because it is frequently detected in people and because it strikes the perfect balance between molecular size (6.1 kDa) and binding affinity (Byrne *et al*. 2008). However, any of these ligands can be implemented to target EGFR. In this chapter, we have done an analysis of the tumor site-targeting efficacy of the identified photosensitizers in PAF1 and PAF2 through *in silico* methods.

We have shown that the photosensitizers from the studied plants have the ability to bind EGFR, which is overexpressed on A431 cells. Whenever the photosensitiser is exposed to light, an activation process happens; this action produces reactive oxygen species (ROS). Reactive oxygen species have the ability to trigger cellular stress, which could finally cause the organism to die as well as cells to perish. This chapter aims to quantify the photosensitiser's binding affinity to EGFR by means of molecular docking simulations primarily. Way2Drug was used to identify photoactive compounds in PAF1 and PAF2 beyond the previously investigated photosensitizers. The resulting list of compounds was then subjected to a docking study with EGFR.

8.2 Materials and methods

8.2.1 Materials

For the objective of carrying out PASS online drug prediction, website such as https://www.way2drug.com/passonline and https://pubchem.ncbi.nim.nih.gov are vital resources. In addition, in order to perform molecular docking investigations, it is necessary to install software tools that include Discovery Studio Visualizer v24.1.0.23298, Avogadro 1.100.0, UCSF CHimeraX 1.9 and AutoDock 4.2.6. Both the evaluation of molecular interactions and the prediction of drug-target affinities are crucial steps in the procedure of drug discovery research. These programs provide assistance for advanced computational modelling, which helps complete these tasks.

8.2.2 PASS online

Utilising specialised drug prediction tools, we can analyse and compare the photosensitising potential of the targeted chemicals that were found within the photoactive fractions. Using this approach, we can determine the likelihood that each compound would be able to produce a photosensitising effect when it is exposed to light. This is vital for applications in fields such as photodynamic treatment. We succeeded to obtain probability ratings for the photosensitiser activity of each compound, by implementing predictive software techniques. These scores furnished us with significant insights into the possible effectiveness and selectivity of the compounds. The procedure consisted of the following steps:

- PASS Online can be accessed by going to https://www.way2drug.com/passonline. After logging in to the website we can utilise the drug prediction tools that are available on PASS Online.

- In order to prepare the compound data, one must first get the chemical structures of the compounds that you need to analyse in the SMILES format. This format is compatible with PASS Online. You are able to identify and convert chemical structures into SMILES format by utilising resources that include PubChem (https://pubchem.ncbi.nim.nih.gov). This simplifies the process of entering the information into the PASS Online platform.

- In the PASS online interface, locate the input field for SMILES strings. Choose the types of biological activity you wish to predict. PASS online provides a variety of activity classes, ranging from the therapeutic effects to specific molecular targets.

- Click “Predict” to start the prediction. PASS online will process the input and proven an output with predicted activities. Each activity will be accompanied by “Pa” and “Pi” values, representing the likelihood of the compound being active or inactive, respectively.

The PASS user receives output as a list of predicted activity types, each with an estimated probability for "active" (Pa) and "inactive" (Pi) status, ranging from zero to one. These probabilities, Pa and Pi, also represent the estimated probabilities of errors of the first and second kind, respectively. These values can be understood as indicators of the likelihood that the predicted compound belongs to fuzzy categories of active or inactive compounds (Filimonov *et al*.,2014).

8.2. 3 Molecular Docking

The assessment of the chemical compounds' capability to bind to the Epidermal Growth Factor Receptor (EGFR) was carried out with the assistance of AutoDock 4.2.6 in collaboration with Discovery Studio. The structure of EGFR was downloaded from RCSB Protein Data Bank (PDB ID: 1NQL) (Sun *et al*.,2015). Ligands were

downloaded from Pubchem using Pubchem ID. In order to guarantee that the docking investigation has only the atoms that are pertinent to the problem at hand, removed water molecules from the EGFR structure. Ensured that receptor is adequately prepared by adding polar hydrogen atoms and Kollman charges to the protein. Prepared the ligand in a similar manner, which involves the addition of polar hydrogen atoms. Ligand preparation was done using Avogadro 1.100.0.The middle of the grid was set to be found using the following coordinates: X: 169, Y: 183, and Z: 237. These coordinates should coincide with the active site of the EGFR protein, where ligands will attach to the protein. Receptor preparation was done using UCSF Chimerax 1.9,CHARMM-GUI, Autodock and AGFR. Docking was done by using Autodock 4.2.6. By means of critical analysis of the expected binding energy values incorporated in the results, one can better appreciate the strength and stability of the ligand-receptor interaction. Usually, lower binding energy values indicate the presences of greater affinities. The docked structures were visualized using Discovery Studio Visualizer v24.1.0.23298.

8.3 Results

8.3.1 PASS online analysis

The results of PASS online are given in table 8.1 for PAF1 and table 8.2 PAF2.

Table 8.1 List of compounds that possess photoactivity in PAF1

Compound name	Pa	Pi
Betavulgarin	0.353	0.023
Maritimetin	0.347	0.025
Melicopicine	0.310	0.044
Fagopyrin	0.347	0.025
2,6-dihydroxybenzoic acid	0.369	0.017
Monomethyl phthalate	0.403	0.009
Resorcinol	0.407	0.008
O-Cresol	0.389	0.012
Kaempferol	0.396	0.010
Enol - phenylpyruvate	0.362	0.019
Genistein	0.445	0.005
2,4-Di-tert-butylphenol	0.396	0.010
Dibutyl phthalate	0.425	0.006
Benzenepropanoic acid, 3,5-bis(1,1-dimethylethyl)-4-hydroxy-, ethyl ester	0.524	0.003

Table 8.2 list of compounds that possess photoactivity in PAF2

Compound Name	Pa	Pi
(1R,6R)-6-Hydroxy-2 succinylcyclohexa-2,4-diene-1 carboxylate	0.388	0.012
Caffeic acid	0.348	0.025
Ellagic acid	0.479	0.004
Genistein	0.445	0.005
Kaempferol	0.396	0.010
Luteolin	0.357	0.021
[7]-Paradol	0.443	0.005
Dinoseb	0.337	0.030
Phenol, 2,4-bis(1,1-dimethylethyl)-	0.396	0.010
7,9-Di-tert-butyl-1-oxaspiro(4,5)deca-6,9-diene-2,8-dione	0.350	0.024
1-Naphthoic acid, 2-hydroxy-, monoanhydride with 1-butaneboronic acid, cyclic ester	0.305	0.47
9,10-Anthracenedione, 1-hydroxy-4-methoxy	0.471	0.004
Chromone, 5-hydroxy-6,7,8-trimethoxy-2,3-dimethyl-	0.403	0.009

Table 8.1 and 8.2 provided a list of compounds predicted to exhibit photoactivity by using PASS online. In each of the fractions PAF1 and PAF2, 14 compounds were identified, that are predicted to have photo-activity.

8.3.2 Docking

The binding energy with EGFR, of compounds present in PAF 1 and PAF 2 are given in table 8.3 and 8.4. Among the analysed 14

compounds from each fraction, 11 in PAF1 and 9 in PAF2 show binding with EGFR.

Table 8.3 Binding energy of predicted compounds in PAF1

Compound name	Binding energy (KCal)
O-cresol	-4.00
Kaempferol	-4.43
Genistein	-4.82
Resorcinol	-3.92
Fagopyrin	-5.76
2-(Methoxycarbonyl)benzoic_acid	-4.18
2,6-dihydroxybenzoic_acid	-3.89
Melicopicine	-4.11
Maritimetin	-5.31
enol-phenylpyruvate	-4.75
Betavulgarin	-4.65

Table 8.4 Binding energy of predicted compounds in PAF 2

Compound name	Binding energy KCal
Kaempferol	-4.45
Caffeic_acid	-4.38
Chromone,_5-hydroxy-6,7,8-trimethoxy-2,3-dimethyl-	-3.80
luteolin	-4.69
Genistein	-4.82
DINOSEB	-5.04
7,9-Di-tert-butyl-1-oxaspiro[4.5]deca-6,9-diene-2,8-dione	-5.30
9,10-Anthracenedione, 1-hydroxy-4-methoxy	-5.06
Ellagic acid	-4.61

Most intense binding is exhibited by fagopyrin (-5.76 KCal) in PAF1 whereas 2-Pentanone, _4-hydroxy-4-methyl-1, 1, 1-triphenyl (-5.39 KCal) shows the same in PAF2. Other compounds also show binding with EGFR, but to a lesser extent.

The structural representation of EGFR is given in Figure 8.1. Figures 8.2 and 8.3 depict the molecular interactions of EGFR with the photoactive compounds in PAF1 and PAF2, respectively.

Figure 8.1 Structure of EGFR

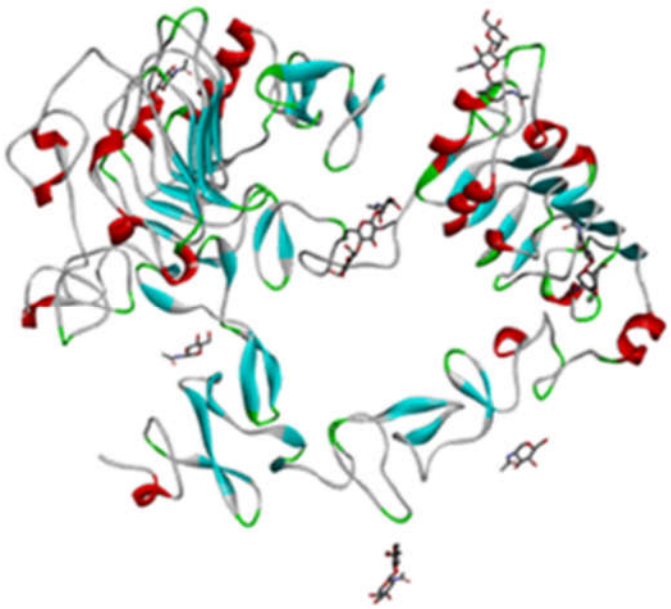

Figure 8.2 Molecular interactions of Fagopyrin and EGFR

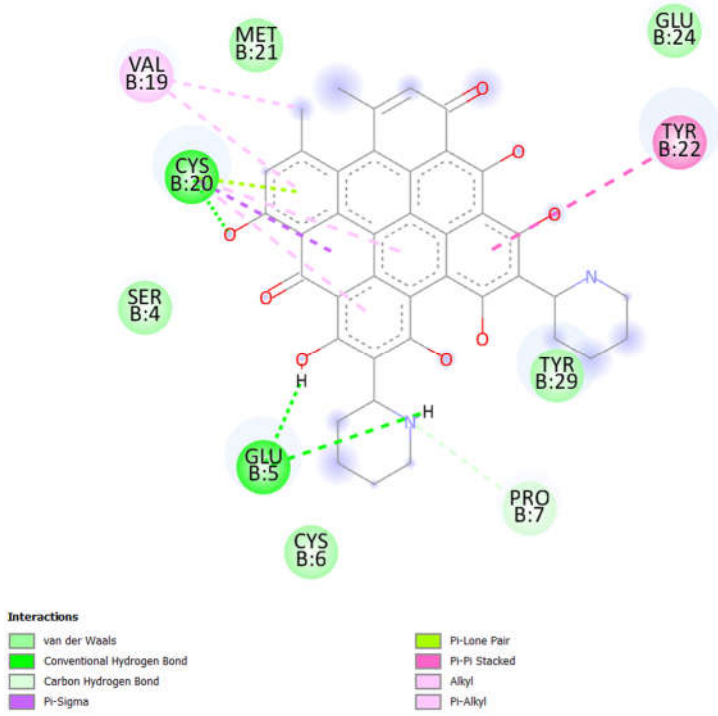

2D illustration of the interactions within the optimal binding pose of Fagopyrin F at the EGFR binding site, demonstrating a binding affinity of -5.76 kcal/mol.

Fagopyrin's interaction with EGFR involves several key residues of the B chain. A π-π stacking interaction is observed with TYR B:22, while VAL B:19 exhibits a pi-alkyl interaction. Conventional hydrogen bonds are formed between GLU B:5 and CYS B:20. Van der Waals forces also contribute to binding via residues CYS B:6, SER B:4, MET B:21, GLU B:24, and TYR B:29. A carbon-hydrogen bond also exists with PRO B:7, which overall indicates a multifaceted binding mode of fagopyrin to EGFR.

Figure 8.3 Molecular interactions of 7,9-Di-tert-butyl-1-oxaspiro[4.5]deca-6,9-diene-2,8-dione and EGFR

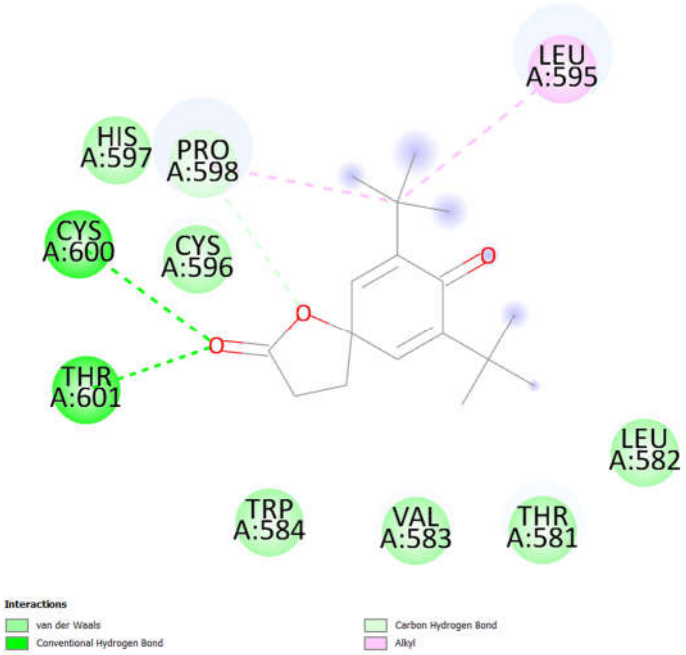

2D illustration of the interactions within the optimal binding pose of 7,9-Di-tert-butyl-1-oxaspiro[4.5]deca-6,9-diene-2,8-dione at the EGFR binding site, demonstrating a binding affinity of -5.30 kcal/mol.

The docking of 7,9-Di-tert-butyl-1-oxaspiro[4.5]deca-6,9-diene-2,8-dione with EGFR reveals alkyl interactions with LEU A:595 and PRO A:598. Vander Waals forces are contributed by PRO A:598, HIS A:597, CYS A:596, TRP A:584, VAL A:583, THR A:581, and LEU A:582. Furthermore, hydrogen bonds are established with LYS A:600 and THR A:601, indicating a combination of hydrophobic and polar interactions in the binding of this compound to EGFR.

8.4 Discussion

An important protein tyrosine kinase associated with signal transduction pathways is EGFR, or epidermal growth factor receptor.

Some essential physiological events, including cell survival and proliferation, are under control by these channels. Among the most exciting breakthroughs in cancer treatments aimed at the molecular level are EGFR-targeted approaches. Currently among the most clinically advanced, these techniques show great promise in precision oncology by selectively disrupting signalling pathways linked with tumor growth and resistance mechanisms (Tortora *et al*., 2001, Albanell *et al*., 2001, Chinnaiyan *et al*., 2006, Cerea *et al*., 2006, Saba *et al*., 2006). EGFR thus has the possibility to be a therapeutic target. Nonetheless, to confirm the EGFR binding capabilities of these compounds, additional validation through wet lab experiments is essential.

The *in silico* analysis described here gives evidences for the photo activity and tumor-targeting efficacy of compounds from PAF1 and PAF2. Apart from fagopyrin, many other compounds show the probability to act as photosensitizers, in PAF1. However, when comparing their ability to target tumor cells, fagopyrin shows maximum efficacy. The compound 7,9-Di-tert-butyl-1-oxaspiro [4.5] deca-6,9-diene-2,8-dione with a lactone ring, which is also present in psoralen shows maximum binding affinity to EGFR, when the cyclic compounds from PAF2 were subjected to *in silico* analysis.

Chapter 9
Summary and Conclusion

The cold extraction of *F. auriculata* and *F. tataricum* using ethanol yielded stable crude extracts, analyzed for potential photosensitizers. The photodynamic activity of photosensitizers from *these plants* was confirmed by uric acid degradation, with *F. auriculata* showing stronger singlet oxygen generation. Photoactive fractions (PAF1 and PAF2) were obtained from plant extracts by thin-layer chromatography (TLC). Their phototoxicity was subsequently confirmed using the uric acid and linoleic acid assays.

MTT assay confirmed the dose and time-dependent cytotoxicity of PAF1 (29.08 ± 0.234) and PAF2 (46.45 ± 1.192) on A431 cells, with increased effects under light exposure. PDT-treated groups showed reduced IC_{50} values and higher cell death (40–45%) compared to non-light-treated groups (2–5%), as revealed by trypan blue test. Morphological analysis showed apoptosis-specific changes in PDT-treated cells, confirming the selective phototoxicity of light-activated PAF1 and PAF2.

PAF1 and PAF2 preferentially accumulated in mitochondria, triggering apoptosis. PDT-treated groups showed apoptotic features, ROS generation, DNA damage, elevated caspase-3 activity, chromatin condensation, and nuclear fragmentation. Cell cycle arrest (S-phase for PAF1/PAF2, G2-phase for ALA) and reduced cell adhesion further confirmed PDT-induced apoptosis and impaired cell viability.

MTT assay revealed that PAF1 and PAF2 had minimal effects on L929 cell viability over 24, 48, and 72 h, indicating low toxicity. Morphological analysis further supported these findings, showing no significant structural changes in treated L929 cells across all groups, with control and experimental cells maintaining normal shape, size, and membrane integrity, confirming the less-toxic nature of PAF1 and PAF2 on normal cells.

Using HPLC, HR-LCMS and GCMS, the photosensitizers in PAF1 and PAF2 were identified. Additional PASS online analyses predicted 14 and 13 photoactive compounds in PAF1 and PAF2 respectively. Docking studies revealed that fagopyrin and pentanone compounds exhibited high affinity for the EGFR. This suggests that the photoactive compounds contained in the fractions contribute to the observed photoactivity against A431 cells. Future research should focus on the individual purification and potency testing of these compounds, as well as *in vitro* and *in vivo* studies, to identify the most promising photosensitizer.

PDT with photosensitizers from *F. tataricum* and *F. auriculata* shows promise for cancer treatment. Future research may enhance cancer therapy, dental infection treatment, and thrombolysis, while exploring applications in viral infections, vaccine development, and vitiligo. PDT could also provide antibiotic-free solutions in veterinary medicine, improve antimicrobial resistance, and offer benefits in agriculture by controlling pathogens and reducing contamination. Additionally, it could help purify air and water and accelerate plastic

degradation, making PDT a powerful tool for health and environmental sustainability.

In conclusion, PDT using photosensitizers from *F. auriculata* and *F. tataricum* shows significant potential for medical applications. The study confirmed the presence of active compounds like fagopyrin and psoralen-like molecules through various analytical methods. PDT using these plant derived photo active fractions demonstrated photodynamic activity, with selective cytotoxic effects on cancer cells and minimal toxicity to normal cells. Molecular docking and predictions support their use in cancer therapy.

Chapter 10
Recommendations

The results of our research on photodynamic therapy (PDT) with natural photosensitizers from *F. tataricum* and *F. auriculata* provide a basis for future bio-medical and environmental applications of natural photosensitizers. There are some potential approaches for further research, leveraging the high efficacy of PDT to target specific cells and pathogens. The intention of these proposals is to expand the use of PAF1- and PAF2-mediated PDT, increase its efficiency, and contribute to solving significant environmental and health problems on a global level. In future works, we have to purify fagopyrin and 7,9-Di-tert-butyl-1-oxaspiro[4.5]deca-6,9-diene-2,8-dione to further explore their efficacy in A431 cells *in vitro*, as well as their application for the treatment of skin cancer *in vivo* and in clinical trials. In addition, *in silico* studies might include molecular dynamics (MD) simulations and other relevant tests. This preliminary work forms the basis for further investigations. PDT (photodynamic therapy) has numerous medical and therapeutic applications, including improving molecular docking studies to directly target EGFR, advancing its use in dental infection control, and investigating its potential in treating strokes through blood clot dissolution. PDT is also being investigated in veterinary medicine to combat viral infections, support vaccine development, and improve infection control. PDT also shows promise in the treatment of vitiligo, combating antimicrobial resistance, and applying advanced light therapy systems. PDT is being investigated in the cosmetics industry to make treatments more effective. In food

safety and agriculture, PDT is used to sterilize food and protect plants from pathogens. Finally, PDT is used in environmental engineering to purify air and water by killing microbes and degrading plastics, thus contributing to the reduction of environmental pollution. The natural photosensitizers identified in the present study can be explored further in all these aspects.

References

AlGhamdi, A. S., Alsalhi, H., Almutairi, N., Alotaibi, B., Barakat, A. A., Khanam, H. K., & Alawfi, A. A. (2023). Push out bond strength of fiber post to radicular dentin using Q-mix, lemon/garlic extract, and riboflavin activated by photodynamic therapy as a final canal irrigant. *European Review for Medical & Pharmacological Sciences*, *27*(9).

Alvarez, N., & Sevilla, A. (2024). Current advances in photodynamic therapy (PDT) and the future potential of PDT-combinatorial cancer therapies. *International Journal of Molecular Sciences*, *25*(2), 1023.

Benković, E. T., Žigon, D., Friedrich, M., Plavec, J., & Kreft, S. (2014). Isolation, analysis and structures of phototoxic fagopyrins from buckwheat. *Food chemistry*, *143*, 432-439.

Benković, E.T., Žigon, D., Friedrich, M., Plavec, J., Kreft, S., 2014. Isolation, analysis and structures of phototoxic fagopyrins from buckwheat. Food Chem. 143, 432–439.

Berg, C. C., & Corner, E. J. H. (2005). Moraceae: ficeae. *Flora Malesiana-Series 1, Spermatophyta*, *17*(2), 1-702.

Bromfield, J. I., Hugenholtz, P., Frazer, I. H., Khosrotehrani, K., & Chandra, J. (2023). Targeting Staphylococcus aureus dominated skin dysbiosis in actinic keratosis to prevent the onset of cutaneous squamous cell carcinoma: Outlook for future therapies?. *Frontiers in Oncology*, *13*, 1091379.

Correia, J. H., Rodrigues, J. A., Pimenta, S., Dong, T., & Yang, Z. (2021). Photodynamic therapy review: principles, photosensitizers, applications, and future directions. *Pharmaceutics*, *13*(9), 1332.

Eguchi, K., Anase, T., & Osuga, H. (2009). Development of a high-performance liquid chromatography method to determine the fagopyrin content of tartary buckwheat (Fagopyrum tartaricum Gaertn.) and common buckwheat (F. esculentum Moench). *Plant Production Science*, *12*(4), 475-480.

Harborne, A. J. (1998). *Phytochemical methods a guide to modern techniques of plant analysis*. springer science & business media.

Hasan, T., Ortel, B., Solban, N., & Pogue, B. (2003). Photodynamic therapy of cancer. *Cancer medicine*, *7*, 537-48.

J.C.Reed,Mechanisms of apoptosis,Am.J.Pathol.,2000,157,1415-1430

Kirveliene, V., Grazeliene, G., Dabkeviciene, D., Micke, I., Kirvelis, D., Juodka, B., & Didziapetriene, J. (2006). Schedule-dependent interaction between Doxorubicin and mTHPC-mediated photodynamic therapy in murine hepatoma in vitro and in vivo. *Cancer chemotherapy and pharmacology*, *57*, 65-72.

Kubrak, T. P., Kołodziej, P., Sawicki, J., Mazur, A., Koziorowska, K., & Aebisher, D. (2022). Some natural photosensitizers and their medicinal properties for use in photodynamic therapy. *Molecules*, *27*(4), 1192.

Liu, K., Liu, P. C., Liu, R., & Wu, X. (2015). Dual AO/EB staining to detect apoptosis in osteosarcoma cells compared with flow cytometry. *Medical science monitor basic research*, *21*, 15.

Nandhakumar S, Parasuraman S, Shanmugam M, Rao Kr, Chand P and Bhat Bv: Evaluation of DNA damage using single-cell gel electrophoresis (Comet Assay). Journal of Pharmacology and Pharmacotherapeutics 2: 107, 2011.

Orrenius S, Gogvadze V, Zhivotovsky B (2007) Mitochondrial oxidative stress: implications for cell death. Annu Rev Pharmacol Toxicol 47:143–183

Rocha, L. G. B. (2016). *Development of a novel photosensitizer for photodynamic therapy of cancer* (Doctoral dissertation, Universidade de Coimbra (Portugal)).

Santhi, K., & Sengottuvel, R. (2016). Qualitative and quantitative phytochemical analysis of Moringa concanensis Nimmo. *International Journal of Current Microbiology and Applied Sciences*, *5*(1), 633-640.

Saxena, M., van der Burg, S. H., Melief, C. J., & Bhardwaj, N. (2021). Therapeutic cancer vaccines. *Nature Reviews Cancer*, *21*(6), 360-378.

Segun, A. F (2024). Advances in Personalized Medical Therapeutics: Leveraging Genomics for Targeted Treatments.*International Journal of Research Publication and Reviews,*5(10),2921-2933.

Stojilkovski, K., Glavač, N. K., Kreft, S., & Kreft, I. (2013). Fagopyrin and flavonoid contents in common, Tartary, and cymosum buckwheat. *Journal of Food Composition and Analysis*, *32*(2), 126-130.

Sytar, O., Kotta, K., Valasiadis, D., Kosyan, A., Brestic, M., Koidou, V., ... & Hilioti, Z. (2021). The effects of photosensitizing dyes fagopyrin and hypericin on planktonic growth and multicellular life in budding yeast. *Molecules*, *26*(16), 4708.

Vivek, R., Thangam, R., Muthuchelian, K., Gunasekaran, P., Kaveri, K., & Kannan, S. (2012). Green biosynthesis of silver nanoparticles from Annona squamosa leaf extract and its in vitro cytotoxic effect on MCF-7 cells. *Process Biochemistry*, *47*(12), 2405-2410.

Weller, M., Trepel, M., Grimmel, C., Schabet, M., Bremen, D., Krajewski, S., & Reed, J. (1997). Hypericin-induced apoptosis of human malignant glioma cells is light-dependent, independent of bcl-2 expression, and does not require wild-type p53. *Neurological research*, *19*(5), 456-470.

A.Ashkenazi and V. M. Dixit, Death receptors: signaling and modulation, *Science*, 1998, **281**, 1305–1308

Abdel-Aty, A. M., Hamed, M. B., Salama, W. H., Ali, M. M., Fahmy, A. S., & Mohamed, S. A. (2019). Ficus carica, Ficus sycomorus and Euphorbia tirucalli latex extracts: Phytochemical screening, antioxidant and cytotoxic properties. *Biocatalysis and Agricultural Biotechnology*, *20*, 101199.

Abdelsalam, A. M., Somaida, A., Ambreen, G., Ayoub, A. M., Tariq, I., Engelhardt, K., ... & Bakowsky, U. (2021). Surface tailored zein as a novel delivery system for hypericin: Application in photodynamic therapy. *Materials Science and Engineering: C*, *129*, 112420.

Abrahamse, H., & Hamblin, M. R. (2016). New photosensitizers for photodynamic therapy. *Biochemical Journal*, *473*(4), 347-364.

Aebisher, D., Czech, S., Dynarowicz, K., Misiołek, M., Komosińska-Vassev, K., Kawczyk-Krupka, A., & Bartusik-Aebisher, D. (2024). Photodynamic therapy: past, current, and future. *International Journal of Molecular Sciences*, *25*(20), 11325.

Agostinis, P., Berg, K., Cengel, K. A., Foster, T. H., Girotti, A. W., Gollnick, S. O., ... & Golab, J. (2011). Photodynamic therapy of cancer: an update. *CA: a cancer journal for clinicians*, *61*(4), 250-281.

Aharoni, N., Afek, U., Finkelstein, E., Orenstein, J., Dvir, O., Nuriel, E., & Carmeli, S. (1996). Impact of celery age and infection by Botrytis cinerea on linear furanocoumarin (psoralens) content in stored celery. *Phytoparasitica*, *24*, 195-197.

Aikens J, Dix TA (1991) Perhydroxyl radical (HOO·) Initiated lipid-peroxidation-The role of fatty-acid hydroperoxides. J Biol Chem 266:15091–15098

Akasov, R. A., Sholina, N. V., Khochenkov, D. A., Alova, A. V., Gorelkin, P. V., Erofeev, A. S., & Khaydukov, E. V. (2019). Photodynamic therapy of melanoma by blue-light photoactivation of flavin mononucleotide. *Scientific reports*, *9*(1), 9679.

Al Deeb, L., Almohareb, T., Al Ahdal, K., Maawadh, A., Alshamrani, A. S., & Alrahlah, A. (2023). The impact of PEEK pretreatment using H. *European Review for Medical and Pharmacological Sciences*, *27*, 9639-9647.

Albanell J, Rojo F, Baselga J. Pharmacodynamic studies with the epidermal growth factor receptor tyrosine kinase inhibitor ZD1839. Semin Oncol 2001;28:56–66.

Alekseeva, P., Makarov, V., Efendiev, K., Shiryaev, A., Reshetov, I., & Loschenov, V. (2024). Devices and Methods for Dosimetry of Personalized Photodynamic Therapy of Tumors: A Review on Recent Trends. *Cancers*, *16*(13), 2484.

Alkhudhairy, F., & Aljamhan, A. S. (2023). Surface conditioning of PEEK post using Nd: YVO4 laser, photodynamic therapy, and sulfuric acid on the pushout bond strength to canal dentin. *Photodiagnosis and Photodynamic Therapy*, *42*, 103601.

Allison, R. R., & Moghissi, K. (2013). Photodynamic therapy (PDT): PDT mechanisms. *Clinical endoscopy*, *46*(1), 24-29.

Ambreen, G., Duse, L., Tariq, I., Ali, U., Ali, S., Pinnapireddy, S. R., ... & Mandic, R. (2020). Sensitivity of papilloma virus-associated cell lines to photodynamic therapy with curcumin-loaded liposomes. *Cancers*, *12*(11), 3278.

American Cancer Society. (2014). Cancer treatment and survivorship facts & figures 2014–2015. *Atlanta: American Cancer Society; 2014.*

Andreyev AY, Kushnareva YE, Starkov AA (2005) Mitochondrial metabolism of reactive oxygen species. Biochemistry 70:200–214

Armstrong, B. K., & Kricker, A. (2001). The epidemiology of UV induced skin cancer. *Journal of photochemistry and photobiology B: Biology*, *63*(1-3), 8-18.

Ashkbar, A., Rezaei, F., Attari, F., & Ashkevarian, S. (2020). Treatment of breast cancer in vivo by dual photodynamic and photothermal approaches with the aid of curcumin photosensitizer and magnetic nanoparticles. *Scientific reports*, *10*(1), 21206.

Athikkavil, F. M., Aiswarya, S. U., Johny, R., Sudhesh, M., Nisthul, A. A., Lankalapalli, R. S., & Bava, S. V. (2023). A potent bioactive fraction against colon cancer from Plectranthus vettiveroides. *Exploration of Targeted Anti-tumor Therapy*, *4*(2), 227.

Aubert, L., & Quinet, M. (2022). Comparison of heat and drought stress responses among twelve Tartary buckwheat (*Fagopyrum tataricum*) varieties. Plants, 11(11), 1517.

Aye, M. M., Aung, H. T., Sein, M. M., & Armijos, C. (2019). A review on the phytochemistry, medicinal properties and pharmacological activities of 15 selected Myanmar medicinal plants. *Molecules*, *24*(2), 293.

Bagnardi, V., Rota, M., Botteri, E., Tramacere, I., Islami, F., Fedirko, V., ... & La Vecchia, C. (2015). Alcohol consumption and site-specific cancer risk: a comprehensive dose–response meta-analysis. *British journal of cancer*, *112*(3), 580-593.

Bao, Z., Xie, Y., Xu, C., Zhang, Z., & Zhu, D. (2023). Biotechnological production and potential applications of hypocrellins. *Applied Microbiology and Biotechnology*, *107*(21), 6421-6438.

BarileARILE, F. A. (1996). Drug Toxicity Assessment. *In vitro methods in pharmaceutical research*, 33.

Bartusik-Aebisher, D., Woźnicki, P., Dynarowicz, K., & Aebisher, D. (2023). Photosensitizers for Photodynamic Therapy of Brain Cancers—A Review. *Brain Sciences*, *13*(9), 1299.

Beier, R. C., Ivie, G. W., & Oertli, E. H. (1994). Linear furanocoumarins and graveolone from the common herb parsley. *Phytochemistry*, *36*(4), 869-872.

Benković, E. T., Žigon, D., Friedrich, M., Plavec, J., & Kreft, S. (2014). Isolation, analysis and structures of phototoxic fagopyrins from buckwheat. *Food chemistry*, *143*, 432-439.

Berg, K., Luksiene, Z., Moan, J., & Ma, L. (1995). Combined treatment of ionizing radiation and photosensitization by 5-aminolevulinic acid-induced protoporphyrin IX. *Radiation research*, *142*(3), 340-346.

Bergstrom, L. C., Vucenik, I., Hagen, I. K., Chernomorsky, S. A., & Poretz, R. D. (1994). In-vitro photocytotoxicity of lysosomotropic immunoliposomes containing pheophorbide a with human bladder carcinoma cells. *Journal of Photochemistry and Photobiology B: Biology*, *24*(1), 17-23.

Berlanda, J., Kiesslich, T., Oberdanner, C. B., Obermair, F. J., Krammer, B., & Plaetzer, K. (2006). Characterization of apoptosis induced by photodynamic treatment with hypericin in A431 human epidermoid carcinoma cells. *Journal of Environmental Pathology, Toxicology and Oncology*, *25*(1-2).

Berr, F., Wiedmann, M., Tannapfel, A., Halm, U., Kohlhaw, K. R., Schmidt, F., ... & Mössner, J. (2000). Photodynamic therapy for advanced bile duct cancer: evidence for improved palliation and extended survival. *Hepatology*, *31*(2), 291-298.

Berridge, M. V., & Tan, A. S. (1993). Characterization of the cellular reduction of 3-(4, 5-dimethylthiazol-2-yl)-2, 5-diphenyltetrazolium bromide (MTT): subcellular localization, substrate dependence, and involvement of mitochondrial electron transport in MTT reduction. *Archives of biochemistry and biophysics*, *303*(2), 474-482.

Bertoletti, L. L., Skoronski, E., Schittler, L., & Kempka, A. P. (2018). Extracts of Leaves of Ficus auriculata Lour.: antioxidant, antimicrobial and phytotoxic activity. *Agriculturae Conspectus Scientificus*, *83*(4), 321-328.

Berwick, M., Reiner, A. S., Paine, S., Armstrong, B. K., Kricker, A., Goumas, C., ... & GEM Study Group. (2014). Sun exposure and melanoma survival: a GEM study. *Cancer Epidemiology, Biomarkers & Prevention*, *23*(10), 2145-2152.

Bhinder, S., Singh, N., & Kaur, A. (2022). Impact of germination on nutraceutical, functional and gluten free muffin making properties of Tartary buckwheat (*Fagopyrum tataricum*). *Food Hydrocolloids*, *124*, 107268.

Bhuvaneswari, R., Gan, Y. Y., Soo, K. C., & Olivo, M. (2009). Targeting EGFR with photodynamic therapy in combination with Erbitux enhances in vivo bladder tumor response. *Molecular cancer*, *8*, 1-11.

Bibi, N., Shah, M. H., Khan, N., Al-Hashimi, A., Elshikh, M. S., Iqbal, A., ... & Abbasi, A. M. (2022). Variations in total phenolic, total flavonoid contents, and free radicals' scavenging potential of onion varieties planted under diverse environmental conditions. *Plants*, *11*(7), 950.

Bonafaccia, G., Gambelli, L., Fabjan, N., & Kreft, I. (2003). Trace elements in flour and bran from common and tartary buckwheat. *Food Chemistry*, *83*(1), 1-5.

Bonafaccia, G., Marocchini, M., & Kreft, I. (2003). Composition and technological properties of the flour and bran from common and tartary buckwheat. *Food chemistry*, *80*(1), 9-15.

Borovaya, S. A., & Klykov, A. G. (2020). Some aspects of flavonoid biosynthesis and accumulation in buckwheat plants. Plant Biotechnology Reports, 14(2), 213-225.

Bosch, F. X., Broker, T. R., Forman, D., Moscicki, A. B., Gillison, M. L., Doorbar, J., & de Sanjose, S. (2013). Comprehensive control of human papillomavirus infections and related diseases. *Vaccine*, *31*, H1-H31.

Brand-Williams, W., Cuvelier, M. E., & Berset, C. L. W. T. (1995). Use of a free radical method to evaluate antioxidant activity. *LWT-Food science and Technology*, *28*(1), 25-30.

Bredell, M. G., Besic, E., Maake, C., & Walt, H. (2010). The application and challenges of clinical PD–PDT in the head and neck region: A short review. *Journal of Photochemistry and Photobiology B: Biology*, *101*(3), 185-190.

Brockmann, H., Weber, E., & Pampus, G. (1952). Protofagopyrin und Fagopyrin, die photodynamisch wirksamen Farbstoffe des Buchweizens (Fagopyrum esculentum). *Justus Liebigs Annalen der Chemie*, *575*(1), 53-83.

Byrne JD, Betancourt T, Brannon-Peppas L (2008) Active targeting schemes for nanoparticle systems in cancer therapeutics. Adv Drug Deliv Rev 60:1615–1626. doi:10.1016/j.addr.2008.08.005

Caffrey, M. (2023). Coverage From the 2023 NCCN Annual Conference. *Evidence-Based Oncology*, NA-NA.

Caporale, G., Dall'Acqua, F., Marciani, S., & Capozzi, A. (1970). Studies on the biosynthesis of psoralen and bergapten in the leaves of Ficus carica. *Zeitschrift für Naturforschung B*, *25*(7), 700-703.

Castell, J. V., Gomez-Lechon, M. J., Grassa, C., Martinez, L. A., Miranda, M. A., & Tarrega, P. (1994). Photodynamic lipid peroxidation by the photosensitizing nonsteroidal antiinflammatory drugs suprofen and tiaprofenic acid. *Photochemistry and photobiology*, *59*(1), 35-39.

Castilho, M. L., Jesus, V. P., Vieira, P. F., Hewitt, K. C., & Raniero, L. (2021). Chlorin e6-EGF conjugated gold nanoparticles as a nanomedicine based therapeutic agent for triple negative breast cancer. *Photodiagnosis and Photodynamic Therapy*, *33*, 102186.

Čellárová, E., Kimáková, K., Halušková, J., & Daxnerová, Z. (1994). The variability of the hypericin content in the regenerants of Hypericum perforatum. *Acta biotechnologica*, *14*(3), 267-274.

Cerea G, Ricotta R, Schiavetto I, et al. Cetuximab for treatment of metastatic colorectal cancer. Ann Oncol 2006;17(Suppl 7):vii66–7.

Chehelgerdi, M., Chehelgerdi, M., Khorramian-Ghahfarokhi, M., Shafieizadeh, M., Mahmoudi, E., Eskandari, F., & Mokhtari-Farsani, A. (2024). Comprehensive review of CRISPR-based gene editing: mechanisms, challenges, and applications in cancer therapy. *Molecular cancer*, *23*(1), 9.

Chick, H., & Ellinger, P. (1941). The photosensitizing action of buckwheat (Fagopyrum esculentum). *The Journal of Physiology*, *100*(2), 212.

Chilakamarthi, U., & Giribabu, L. (2017). Photodynamic therapy: past, present and future. *The Chemical Record*, *17*(8), 775-802.

Chinnaiyan P, Harari PM. Clinical advancement of EGFR inhibitors in cancer therapy. Methods Mol Biol 2006;327:189–202.

Cho, M., Park, G. M., Kim, S. N., Amna, T., Lee, S., & Shin, W. S. (2014). Glioblastoma-specific anticancer activity of pheophorbide a from the

edible red seaweed Grateloupia elliptica. *Journal of Microbiology and Biotechnology*, *24*(3), 346-353.

Chung, P. S., He, P., Shin, J. I., Hwang, H. J., Lee, S. J., & Ahn, J. C. (2009). Photodynamic therapy with 9-hydroxypheophorbide α on AMC-HN-3 human head and neck cancer cells: Induction of apoptosis via photoactivation of mitochondria and endoplasmic reticulum. *Cancer biology & therapy*, *8*(14), 1343-1351.

Chunyan, C., Bo, S., Ping, L., Jingmei, L., & Ito, Y. (2008). Isolation and purification of psoralen and bergapten from Ficus carica L. leaves by high-speed countercurrent chromatography. *Journal of liquid chromatography & related technologies*, *32*(1), 136-143.

Circu ML, Aw TY (2010) Reactive oxygen species, cellular redox systems, and apoptosis. Free Radic Biol Med 48:749–762

Circu ML, Moyer MP, Harrison L, Aw TY (2009) Contribution of glutathione status to oxidant-induced mitochondrial DNA damage in colonic epithelial cells. Free Radic Biol Med 47:1190–1198

Comini, L. R., Fernandez, I. M., Vittar, N. R., Montoya, S. N., Cabrera, J. L., & Rivarola, V. A. (2011). Photodynamic activity of anthraquinones isolated from Heterophyllaea pustulata Hook f.(Rubiaceae) on MCF-7c3 breast cancer cells. *Phytomedicine*, *18*(12), 1093-1095.

Compagnin, C., Mognato, M., Celotti, L., Canti, G., Palumbo, G., & Reddi, E. (2010). Cell proliferation and cell cycle alterations in oesophageal p53‐mutated cancer cells treated with cisplatin in combination with photodynamic therapy. *Cell Proliferation*, *43*(3), 262-274.

Conforti, F., Marrelli, M., Menichini, F., Bonesi, M., Statti, G., Provenzano, E., & Menichini, F. (2009). Natural and synthetic furanocoumarins as treatment for vitiligo and psoriasis. *Current Drug Therapy*, *4*(1), 38-58.

Conforti, F., Menichini, G., Zanfini, L., Tundis, R., Statti, G. A., Provenzano, E., & Alfano, C. (2012). Evaluation of phototoxic potential of aerial components of the fig tree against human melanoma. *Cell Proliferation*, *45*(3), 279-285.

Correia, J. H., Rodrigues, J. A., Pimenta, S., Dong, T., & Yang, Z. (2021). Photodynamic therapy review: principles, photosensitizers, applications, and future directions. *Pharmaceutics*, *13*(9), 1332.

Craythorne, E., & Al-Niami, F. (2017). Skin cancer. *Medicine*, *45*(7), 431-434.

Creixell M, Herrera AP, Ayala V, Latorre-Esteves M, Perez-Torres M, Torres-Lugo M, Rinaldi C (2010) Preparation of epidermal growth factor (EGF) conjugated iron oxide nanoparticles and their internalization into colon cancer cells. J Magn Magn Mater 322:2244–2250. doi:10.1016/j.jmmm.2010.02.019

Crescenzi, E., Varriale, L., Iovino, M., Chiaviello, A., Veneziani, B. M., & Palumbo, G. (2004). Photodynamic therapy with indocyanine green complements and enhances low-dose cisplatin cytotoxicity in MCF-7 breast cancer cells. *Molecular cancer therapeutics*, *3*(5), 537-544.

Dąbrowski, J. M. (2017). Reactive oxygen species in photodynamic therapy: mechanisms of their generation and potentiation. In *Advances in inorganic chemistry* (Vol. 70, pp. 343-394). Academic Press.

Datta, S. N., Allman, R., Loh, C., Mason, M., & Matthews, P. N. (1997). Effect of photodynamic therapy in combination with mitomycin C on a mitomycin-resistant bladder cancer cell line. *British journal of cancer*, *76*(3), 312-317.

De Grey AD (2002) HO2·: the forgotten radical. DNA Cell Biol 21:251–257

Derraik, J. G., & Rademaker, M. (2007). Phytophotodermatitis caused by contact with a fig tree (Ficus carica). *The New Zealand Medical Journal (Online)*, *120*(1259).

Deveoglu, O., Karadag, R., & Yurdun, T. (2011). Qualitative HPLC determination of main anthraquinone and lake pigment contents from Dactylopius coccus dye insect. *Chemistry of Natural Compounds*, *47*, 103-104.

Dizon, D. S., & Kamal, A. H. (2024). Cancer statistics 2024: All hands on deck. *CA: a cancer journal for clinicians*, *74*(1).

Doll, R., & Peto, R. (1981). The causes of cancer: quantitative estimates of avoidable risks of cancer in the United States today. *JNCI: Journal of the National Cancer Institute*, *66*(6), 1192-1308.

Dolmans, D. E., Fukumura, D., & Jain, R. K. (2003). Photodynamic therapy for cancer. *Nature reviews cancer*, *3*(5), 380-387.

Doonan, F., & Cotter, T. G. (2008). Morphological assessment of apoptosis. *Methods*, *44*(3), 200-204.

Driscoll, T., Steenland, K., Nelson, D. I., Prüss-Ustün, A., Campbell-Lendrum, D. H., Corvalán, C. F., ... & World Health Organization. (2004). *Occupational carcinogens: assessing the environmental burden of disease at national and local levels*. World Health Organization.

Eguchi, K., Anase, T., & Osuga, H. (2009). Development of a high-performance liquid chromatography method to determine the fagopyrin content of tartary buckwheat (Fagopyrum tartaricum Gaertn.) and common buckwheat (F. esculentum Moench). *Plant Production Science*, *12*(4), 475-480.

El-Serag, H. B. (2012). Epidemiology of viral hepatitis and hepatocellular carcinoma. *Gastroenterology*, *142*(6), 1264-1273.

Endosc. 46 (2013) 24, https://doi.org/10.5946/ce.2013.46.1.24.

Eom, T., Kim, E., & Kim, J. S. (2020). In vitro antioxidant, antiinflammation, and anticancer activities and anthraquinone content from Rumex crispus root extract and fractions. *Antioxidants*, *9*(8), 726.

Fabjan, N., Rode, J., Košir, I. J., Wang, Z., Zhang, Z., & Kreft, I. (2003). Tartary buckwheat (*Fagopyrum tataricum* Gaertn.) as a source of dietary rutin and quercitrin. *Journal of agricultural and food chemistry*, *51*(22), 6452-6455.

Farrugia G, Balzan R (2012) Oxidative stress and programmed cell death in yeast. Front Oncol 2:64

Filimonov, D. A., Lagunin, A. A., Gloriozova, T. A., Rudik, A. V., Druzhilovskii, D. S., Pogodin, P. V., & Poroikov, V. V. (2014). Prediction of the biological activity spectra of organic compounds using the PASS online web resource. *Chemistry of Heterocyclic Compounds*, *50*, 444-457.

Fischer, F., Graschew, G., Sinn, H. J., Maier-Borst, W., Lorenz, W. J., & Schlag, P. M. (1998). A chemical dosimeter for the determination of the photodynamic activity of photosensitizers. *Clinica chimica acta*, *274*(1), 89-104.

Foote, C. S. (1968). Mechanisms of photosensitized oxidation: there are several different types of photosensitized oxidation which may be important in biological systems. *Science*, *162*(3857), 963-970.

Friedenreich, C. M., Neilson, H. K., Farris, M. S., & Courneya, K. S. (2016). Physical activity and cancer outcomes: a precision medicine approach. *Clinical Cancer Research*, *22*(19), 4766-4775.

Fu, P. P., Xia, Q., Zhao, Y., Wang, S., Yu, H., & Chiang, H. M. (2013). Phototoxicity of herbal plants and herbal products. *Journal of Environmental Science and Health, Part C*, *31*(3), 213-255.

G. Kroemer, B. Dallaporta and M. Resche-Rigon, The mitochondrial death/life regulator in apoptosis and necrosis, *Annu. Rev. Physiol.*, 1998, **60**, 619–642

G.Evan and T.littlewood, A matter of life and cell death, science, 1998, 281, 1317-1322

G.Kromer and J.C.Reed,Mitochondrial control of cell death, nat.med., 2000, 6, 513-519

Gantchev, T. G., Brasseur, N., & Van Lier, J. E. (1996). Combination toxicity of etoposide (VP-16) and photosensitisation with a water-soluble aluminium phthalocyanine in K562 human leukaemic cells. *British journal of cancer*, *74*(10), 1570-1577.

Germ, M., Árvay, J., Vollmannová, A., Tóth, T., Kreft, I., & Golob, A. (2020). Hydrothermal treatments affecting the concentration of neochlorogenic acid in dough of Tartary buckwheat. *Agriculture*, *10*(12), 601.

Ghemrawi, R., Abuamer, L., Kremesh, S., Hussien, G., Ahmed, R., Mousa, W., ... & Khair, M. (2024). Revolutionizing Cancer Treatment: Recent Advances in Immunotherapy. *Biomedicines*, *12*(9), 2158.

Gijsens, A., & De Witte, P. E. T. E. R. (1998). Photocytotoxic action of EGF-PVA-Sn (IV) chlorin e6 and EGF-dextran-Sn (IV) chlorin e6 internalizable conjugates on A431 cells. *International journal of oncology*, *13*(6), 1171-1178.

Gijsens, A., Missiaen, L., Merlevede, W., & de Witte, P. (2000). Epidermal growth factor-mediated targeting of chlorin e6 selectively potentiates its photodynamic activity. *Cancer Research*, *60*(8), 2197-2202.

Glavač, N. K., Stojilkovski, K., Kreft, S., Park, C. H., & Kreft, I. (2017). Determination of fagopyrins, rutin, and quercetin in Tartary buckwheat products. *LWT-Food Science and Technology*, *79*, 423-427.

Halliwell B, Cross CE (1994) Oxygen-derived species: their relation to human disease and environmental stress. Environ Health Perspect 10:5–12

Halliwell B, Gutteridge JMC (2007) Free radicals in biology and medicine, 4th edn. Oxford University Press, Oxford

Harborne, A. J. (1998). *Phytochemical methods a guide to modern techniques of plant analysis*. springer science & business media.

Hashemikamangar, S. S., Alsaedi, R. J. F., Chiniforush, N., & Motevaselian, F. (2022). Effect of antimicrobial photodynamic therapy with different photosensitizers and adhesion protocol on the bond strength of resin composite to sound dentin. *Clinical Oral Investigations*, *26*(5), 4011-4019.

Hassan, I., Chibber, S., & Naseem, I. (2013). Vitamin B2: a promising adjuvant in cisplatin based chemoradiotherapy by cellular redox management. *Food and chemical toxicology*, *59*, 715-723.

Hassan, I., Chibber, S., Khan, A. A., & Naseem, I. (2012). Riboflavin ameliorates cisplatin induced toxicities under photoillumination. *PLoS One*, *7*(5), e36273.

Hassouni, A. E., Bachiri, A. E., & Belbachir, C. (2019). Lavandula dentata solid residue from essential oil industry. *Journal of Essential Oil Bearing Plants*, *22*(6), 1601-1613.

He, P., Ahn, J. C., Shin, J. I., Hwang, H. J., Kang, J. W., Lee, S. J., & Chung, P. S. (2009). Enhanced apoptotic effect of combined modality of 9-hydroxypheophorbide α-mediated photodynamic therapy and carboplatin on AMC-HN-3 human head and neck cancer cells. *Oncology reports*, *21*(2), 329-334.

Hejmadi, M. (2014). *Introduction to cancer biology*. Bookboon.

Hinneburg, I., & Neubert, R. H. (2005). Influence of extraction parameters on the phytochemical characteristics of extracts from buckwheat (Fagopyrum esculentum) herb. *Journal of Agricultural and Food Chemistry*, *53*(1), 3-7.

Hong, M., Clubb, J. D., & Chen, Y. Y. (2020). Engineering CAR-T cells for next-generation cancer therapy. *Cancer cell*, *38*(4), 473-488.

Hu, C., Zhang, X., Zhang, N., Wei, W. Y., Li, L. L., Ma, Z. G., & Tang, Q. Z. (2020). Osteocrin attenuates inflammation, oxidative stress,

apoptosis, and cardiac dysfunction in doxorubicin‐induced cardiotoxicity. *Clinical and Translational Medicine*, *10*(3), e124.

Hussen, E. M., & Endalew, S. A. (2023). In vitro antioxidant and free-radical scavenging activities of polar leaf extracts of Vernonia amygdalina. *BMC Complementary Medicine and Therapies*, *23*(1), 146.

İğci, B. K., & Aytac, Z. (2020). An investigation on the in vitro wound healing activity and phytochemical composition of Hypericum pseudolaeve N. Robson growing in Turkey. *Turkish Journal of Pharmaceutical Sciences*, *17*(6), 610.

Ismail, A., & Cheah, S. F. (2003). Determination of vitamin C, β-carotene and riboflavin contents in five green vegetables organically and conventionally grown. *Malaysian journal of nutrition*, *9*(1), 31-39.

Jagadeesan, G., Muniyandi, K., Manoharan, A. L., Thamburaj, S., Sathyanarayanan, S., & Thangaraj, P. (2019). Optimization of phenolic compounds extracting conditions from Ficus racemosa L. fruit using response surface method. *Journal of Food Measurement and Characterization*, *13*, 312-320.

Jemal A, Murray T, Samuels A, Ghafoor A, Ward E, Thun MJ (2003) Cancer statistics, 2003. CA Cancer J Clin 53:5–26

Jeong, M., Hong, T., Lee, K., Hwangbo, H., Kim, M., Ma, W., & Zahn, M. (2015). HPLC method for simultaneous quantification of bakuchiol and minor furocoumarins in bakuchiol extract from Psoralea corylifolia. *Journal of AOAC International*, *98*(4), 902-906.

Jiang, Y., Leung, A. W., Wang, X., Zhang, H., & Xu, C. (2013). Inactivation of Staphylococcus aureus by photodynamic action of hypocrellin B. *Photodiagnosis and photodynamic therapy*, *10*(4), 600-606.

Jiang, Y., Xia, X., Leung, A. W., Xiang, J., & Xu, C. (2012). Apoptosis of breast cancer cells induced by hypocrellin B under light-emitting diode irradiation. *Photodiagnosis and Photodynamic Therapy*, *9*(4), 337-343.

Joshi, B. D. (1999). Status of buckwheat in India.

Juarez, A. V., Sosa, L. D. V., De Paul, A. L., Costa, A. P., Farina, M., Leal, R. B., & Pons, P. (2015). Riboflavin acetate induces apoptosis in

squamous carcinoma cells after photodynamic therapy. *Journal of Photochemistry and Photobiology B: Biology*, *153*, 445-454.

Kacerovská, D., Pizinger, K., Majer, F., & Šmíd, F. (2008). Photodynamic therapy of nonmelanoma skin cancer with topical hypericum perforatum extract—a pilot study. *Photochemistry and photobiology*, *84*(3), 779-785.

Kala, C. P. (2007). Prioritization of cultivated and wild edibles by local people in the Uttaranchal hills of Indian Himalaya.

Karges, J., Heinemann, F., Jakubaszek, M., Maschietto, F., Subecz, C., Dotou, M., & Gasser, G. (2020). Rationally designed long-wavelength absorbing Ru (II) polypyridyl complexes as photosensitizers for photodynamic therapy. *Journal of the American Chemical Society*, *142*(14), 6578-6587.

Kazantzis, K. T., Koutsonikoli, K., Mavroidi, B., Zachariadis, M., Alexiou, P., Pelecanou, M., & Sagnou, M. (2020). Curcumin derivatives as photosensitizers in photodynamic therapy: photophysical properties and in vitro studies with prostate cancer cells. *Photochemical & Photobiological Sciences*, *19*, 193-206.

Kerr, J. F., Wyllie, A. H., & Currie, A. R. (1972). Apoptosis: a basic biological phenomenon with wideranging implications in tissue kinetics. *British journal of cancer*, *26*(4), 239-257.

Khalaf, S. D., Mahdi, M. M., & Mahmood, R. S. (2024). The Cancer: Types, The Mechanism of Caner Growth and Diagnosis: A. *World*, *3*(3).

Kim, B. R., Kim, M., Na, J. I., Huh, C. H., & Shin, J. W. (2023). A Randomized Split-Face Study of Photodynamic Therapy With St. John's Wort and Indole-3-Acetic Acid for the Treatment of Acne. *Dermatologic Surgery*, *49*(5), 483-488.

Kim, E. J., Mangold, A. R., DeSimone, J. A., Wong, H. K., Seminario-Vidal, L., Guitart, J., & Poligone, B. (2022). Efficacy and safety of topical hypericin photodynamic therapy for early-stage cutaneous T-cell lymphoma (Mycosis fungoides): the FLASH phase 3 randomized clinical trial. *JAMA dermatology*, *158*(9), 1031-1039.

Kim, J., & Hwang, K. T. (2020). Fagopyrins in different parts of common buckwheat (*Fagopyrum esculentum*) and Tartary buckwheat (*F. tataricum*) during growth. *Journal of Food Composition and Analysis*, *86*, 103354.

Kim, J., & Hwang, K. T. (2020). Fagopyrins in different parts of common buckwheat (Fagopyrum esculentum) and Tartary buckwheat (F. tataricum) during growth. *Journal of Food Composition and Analysis*, *86*, 103354.

Kim, J., & Hwang, K. T. (2020). Fagopyrins in different parts of common buckwheat (Fagopyrum esculentum) and Tartary buckwheat (F. tataricum) during growth. *Journal of Food Composition and Analysis*, *86*, 103354

Kim, J., Kim, S., Lee, K., Kim, R. H., & Hwang, K. T. (2021). Antibacterial photodynamic inactivation of fagopyrin f from tartary buckwheat (Fagopyrum tataricum) flower against streptococcus mutans and its biofilm. *International Journal of Molecular Sciences*, *22*(12), 6205.

Kim, S. M., Lee, E. J., Lee, J. H., Yang, W. M., Nam, D., Lee, J. H., ... & Ahn, K. S. (2016). Simvastatin in combination with bergamottin potentiates TNF-induced apoptosis through modulation of NF-κB signalling pathway in human chronic myelogenous leukaemia. *Pharmaceutical biology*, *54*(10), 2050-2060.

King, M. C., Marks, J. H., & Mandell, J. B. (2003). Breast and ovarian cancer risks due to inherited mutations in BRCA1 and BRCA2. *Science*, *302*(5645), 643-646.

Kirkwood, J. M., Butterfield, L. H., Tarhini, A. A., Zarour, H., Kalinski, P., & Ferrone, S. (2012). Immunotherapy of cancer in 2012. *CA: a cancer journal for clinicians*, *62*(5), 309-335.

Klaber, R. (1942). Phyto-photo-dermatitis. *British Journal of Dermatology*, *54*(7), 193-211.

Korshunov SS, Skulachev VP, Starkov AA (1997) High protonic potential actuates a mechanism of production of reactive oxygen species in mitochondria. FEBS Lett 416:15–18

Kubrak, T. P., Kołodziej, P., Sawicki, J., Mazur, A., Koziorowska, K., & Aebisher, D. (2022). Some natural photosensitizers and their medicinal properties for use in photodynamic therapy. *Molecules*, *27*(4), 1192.

Kumari, A., Verma, R., Sharma, M., Chauhan, P., & Kumar, A. (2018). Evaluation of phytochemical, antioxidant, antibacterial and anti-cancerous activity of Ficus auriculata Lour. and Osyris wightiana Wall. ex Wight. *Bull. Environ. Pharmacol. Life Sci*, *7*, 64-70.

Kunwar, A., Barik, A., Mishra, B., Rathinasamy, K., Pandey, R., & Priyadarsini, K. I. (2008). Quantitative cellular uptake, localization and cytotoxicity of curcumin in normal and tumor cells. *Biochimica et Biophysica Acta (BBA)-General Subjects*, *1780*(4), 673-679.

Kwiatkowski, S., Knap, B., Przystupski, D., Saczko, J., Kędzierska, E., Knap-Czop, K., & Kulbacka, J. (2018). Photodynamic therapy–mechanisms, photosensitizers and combinations. *Biomedicine & pharmacotherapy*, *106*, 1098-1107.

Kyriazi M, Yova D, Rallis M, Lima A (2006) Cancer chemopreventive effects of Pinus Maritima bark extract on ultraviolet radiation and ultraviolet radiation-7,12, dimethylbenz(a) anthracene induced skin carcinogenesis of hairless mice. Cancer Lett 237:234–241

Labban, N., Al Taweel, S. M., ALRabiah, M. A., Alfouzan, A. F., Alshiddi, I. F., & Assery, M. K. (2021). Efficacy of Rose Bengal and Curcumin mediated photodynamic therapy for the treatment of denture stomatitis in patients with habitual cigarette smoking: A randomized controlled clinical trial. *Photodiagnosis and photodynamic therapy*, *35*, 102380.

Lambert AJ, Brand MD (2004) Superoxide production by NADH: ubiquinone oxidoreductase (complex I) depends on the pH gradient across the mitochondrial inner membrane. Biochem J 382:511–517

Laskin JJ, Sandler AB (2004) Epidermal growth factor receptor: a promising target in solid tumours. Cancer Treat Rev 30:1–17. doi:10.1016/j.ctrv.2003.10.002

Lee, C. N., Hsu, R., Chen, H., & Wong, T. W. (2020). Daylight photodynamic therapy: An update. *Molecules*, *25*(21), 5195.

Lee, H. J., Kang, S. M., Jeong, S. H., Chung, K. H., & Kim, B. I. (2017). Antibacterial photodynamic therapy with curcumin and Curcuma xanthorrhiza extract against Streptococcus mutans. *Photodiagnosis and photodynamic therapy*, *20*, 116-119.

Lee, W. Y., Lim, D. S., Ko, S. H., Park, Y. J., Ryu, K. S., Ahn, M. Y., ... & Cho, C. W. (2004). Photoactivation of pheophorbide a induces a mitochondrial-mediated apoptosis in Jurkat leukaemia cells. *Journal of Photochemistry and Photobiology B: Biology*, *75*(3), 119-126.

Leite, D. P. V., Paolillo, F. R., Parmesano, T. N., Fontana, C. R., & Bagnato, V. S. (2014). Effects of photodynamic therapy with blue light and

curcumin as mouth rinse for oral disinfection: a randomized controlled trial. *Photomedicine and laser surgery*, *32*(11), 627-632.

Leu, Y. L., Hwang, T. L., Hu, J. W., & Fang, J. Y. (2008). Anthraquinones from Polygonum cuspidatum as tyrosinase inhibitors for dermal use. *Phytotherapy Research: An International Journal Devoted to Pharmacological and Toxicological Evaluation of Natural Product Derivatives*, *22*(4), 552-556.

Li, D., Li, L., Li, P., Li, Y., & Chen, X. (2015). Apoptosis of HeLa cells induced by a new targeting photosensitizer-based PDT via a mitochondrial pathway and ER stress. *OncoTargets and therapy*, 703-711.

Li, L., Li, Y., Dong, H., Yan, J., Zhang, Y., Zhang, C., & Xu, X. (2024). Therapeutic and fluorescence evaluation of 20% 5-aminolevulinic acid-mediated photodynamic therapy in actinic keratosis. *Photodiagnosis and Photodynamic Therapy*, *47*, 104100.

Li, S. Q., & Zhang, Q. H. (2001). Advances in the development of functional foods from buckwheat. *Critical reviews in food science and nutrition*, *41*(6), 451-464.

Likić, V. A. (2009). Extraction of pure components from overlapped signals in gas chromatography-mass spectrometry (GC-MS). *BioData Mining*, *2*, 1-11.

Lim, D. S., Ko, S. H., & Lee, W. Y. (2004). Silkworm-pheophorbide a mediated photodynamic therapy against B16F10 pigmented melanoma. *Journal of photochemistry and photobiology B: Biology*, *74*(1), 1-6.

Lin, H.-Y.; Lin, J.-N.; Ma, J.-W.; Yang, N.-S.; Ho, C.-T.; Kuo, S.-C.; Way, T.-D. Demethoxycurcumin induces autophagic and apoptotic responses on breast cancer cells in photodynamic therapy. *J. Funct. Foods* **2015**, *12*, 439–449.

Liu, C. D., Kwan, D., Saxton, R. E., & McFadden, D. W. (2000). Hypericin and photodynamic therapy decreases human pancreatic cancer in vitro and in vivo. *Journal of Surgical Research*, *93*(1), 137-143.

Ma, L. W., Steen, H. B., Moan, J., Berg, K., Peng, Q., Saether, H., & Rimington, C. (1992). Cytotoxicity and cytokinetic effects of mitomycin C and/or photochemotherapy in a human colon

adenocarcinoma cell line. *The International Journal of Biochemistry*, *24*(11), 1807-1813.

Ma, L., Iani, V., & Moan, J. (1993). Combination therapy: photochemotherapy; electric current; and ionizing radiation. Different combinations studied in a WiDr human colon adenocarcinoma cell line. *Journal of Photochemistry and Photobiology B: Biology*, *21*(2-3), 149-154.

Mäbert, K., Cojoc, M., Peitzsch, C., Kurth, I., Souchelnytskyi, S., & Dubrovska, A. (2014). Cancer biomarker discovery: current status and future perspectives. *International journal of radiation biology*, *90*(8), 659-677.

Maennling, A. E., Tur, M. K., Niebert, M., Klockenbring, T., Zeppernick, F., Gattenlöhner, S., ... & Hussain, A. F. (2019). Molecular targeting therapy against EGFR family in breast cancer: progress and future potentials. *Cancers*, *11*(12), 1826.

Mage, M. E. (1963). Histochemical localization of phenols in healthy and diseased banana roots. *Physiologia plantarum*, *16*(4).

Manojlović, T. N., Solujić, S., Sukdolak, S., & Krstić, L. J. (1998). Anthraquinones from the lichen Xanthoria parietina. *J Serb Chem Soc*, *63*, 7-11.

Mastrangelopoulou, M., Grigalavicius, M., Berg, K., Menard, M., & Theodossiou, T. A. (2019). Cytotoxic and photocytotoxic effects of cercosporin on human tumor cell lines. *Photochemistry and photobiology*, *95*(1), 387-396.

Matés JA, Segura FJ, Alonso JM, Javier M (2012) Oxidative stress in apoptosis and cancer: an update. Arch Toxicol. doi:10.1007/s00204-012-0906-3

Matsui, K., & Walker, A. R. (2020). Biosynthesis and regulation of flavonoids in buckwheat. Breeding science, 70(1), 74-84.

Maurer, T. H. (1987). Phototoxicity testing—in vivo and in vitro. *Food and Chemical Toxicology*, *25*(5), 407-414.

Menichini, F., Tundis, R., Loizzo, M. R., Bonesi, M., Provenzano, E., Cindio, B. D., & Menichini, F. (2010). In vitro photo-induced cytotoxic activity of Citrus bergamia and C. medica L. cv. Diamante peel essential oils and identified active coumarins. *Pharmaceutical Biology*, *48*(9), 1059-1065.

Mew, D., Wat, C. K., Towers, G. H., & Levy, J. G. (1983). Photoimmunotherapy: treatment of animal tumors with tumor-specific monoclonal antibody-hematoporphyrin conjugates. *Journal of immunology (Baltimore, Md.: 1950)*, *130*(3), 1473-1477.

Migliaccio E, Giorgio M, Pelicci PG (2006) Apoptosis and aging: role of p66Shc redox protein. Antioxid Redox Signal 8:600–608

Miller, G. G., Brown, K., Ballangrud, Å. M., Barajas, O., Xiao, Z., Tulip, J., ... & Moore, R. B. (1997). Preclinical assessment of hypocrellin B and hypocrellin B derivatives as sensitizers for photodynamic therapy of cancer: progress update. *Photochemistry and Photobiology*, *65*(4), 714-722.

Miller, N. J., & Rice-Evans, C. A. (1996). Spectrophotometric determination of antioxidant activity. *Redox report*, *2*(3), 161-171.

Miranda, M. A., Castell, J. V., Gómez-Lechón, M. J., & Martinez, L. A. (1993). In vitro photoperoxidation as an indicator of the potential phototoxicity of non-steroidal anti-inflammatory 2-arylpropionic acids. *Toxicology in vitro*, *7*(4), 523-526.

Monfrecola, G., Fabbrocini, G., & Pinton, P. C. (2009). Photodynamic Therapy For Non-Melanoma Skin Cancers. *Current Cancer Therapy Reviews*, *5*(4), 271-280.

Montoya, S. C. N., Comini, L. R., Sarmiento, M., Becerra, C., Albesa, I., Argüello, G. A., & Cabrera, J. L. (2005). Natural anthraquinones probed as Type I and Type II photosensitizers: singlet oxygen and superoxide anion production. *Journal of Photochemistry and Photobiology B: Biology*, *78*(1), 77-83.

Mugas, M. L., Calvo, G., Marioni, J., Céspedes, M., Martinez, F., Sáenz, D., ... & Casas, A. (2021). Photodynamic therapy of tumour cells mediated by the natural anthraquinone parietin and blue light. *Journal of Photochemistry and Photobiology B: Biology*, *214*, 112089.

Mukkukada Ravi, R., Mani, A., Rahim, S., & Anirudhan, T. S. (2024). A Self-Skin Permeable Doxorubicin Loaded Nanogel Composite as a Transdermal Device for Breast Cancer Therapy. *ACS Applied Materials & Interfaces*, *16*(38), 50407-50429.

Mustafa, K., Yu, S., Zhang, W., Mohamed, H., Naz, T., Xiao, H., & Song, Y. (2021). Screening, characterization, and in vitro-ROS dependent

cytotoxic potential of extract from Ficus carica against hepatocellular (HepG2) carcinoma cells. *South African Journal of Botany*, *138*, 217-226.

Nagatani, T., Matsuzaki, T., Kim, S., Baba, N., Ichiyama, S., Miyamoto, H., & Nakajima, H. (1990). Treatment of cutaneous T-cell lymphoma (CTCL) by extracorporeal photochemotherapy. *Journal of Dermatological Science*, *1*(3), 226.

National Cancer Institute. (n.d.). Office of Cancer Survivorship Statistics and Graphs. Retrieved from cancercontrol.cancer.gov: https:// cancercontrol. cancer.gov/ocs/statistics

Nonaka, M., Ikeda, H., & Inokuchi, T. (2002). Effect of combined photodynamic and chemotherapeutic treatment on lymphoma cells in vitro. *Cancer letters*, *184*(2), 171-178.

Noratto, G., Porter, W., Byrne, D., & Cisneros-Zevallos, L. (2009). Identifying peach and plum polyphenols with chemopreventive potential against estrogen-independent breast cancer cells. *Journal of agricultural and food chemistry*, *57*(12), 5219-5226.

Noronha, V., Rao, A. R., Ramaswamy, A., Kumar, A., Pillai, A., Dhekale, R., ... & Prabhash, K. (2023). The current status of geriatric oncology in India. *ecancermedicalscience*, *17*.

Oh, D. Y., & Bang, Y. J. (2020). HER2-targeted therapies—a role beyond breast cancer. *Nature reviews Clinical oncology*, *17*(1), 33-48.

Orrenius S, Gogvadze V, Zhivotovsky B (2007) Mitochondrial oxidative stress: implications for cell death. Annu Rev Pharmacol Toxicol 47:143–183

Ožbolt, L., Kreft, S., Kreft, I., Germ, M., & Stibilj, V. (2008). Distribution of selenium and phenolics in buckwheat plants grown from seeds soaked in Se solution and under different levels of UV-B radiation. *Food Chemistry*, *110*(3), 691-696.

Pal, S., & Monica Subashini, M. (2020). Skin Cancer Detection Using Advanced Imaging Techniques. In *Smart Computing Paradigms: New Progresses and Challenges: Proceedings of ICACNI 2018, Volume 1* (pp. 229-237). Springer Singapore.

Panno, M. L., Giordano, F., Palma, M. G., Bartella, V., Rago, V., Maggiolini, M., & Ando, S. (2009). Evidence that bergapten, independently of its photoactivation, enhances p53 gene expression and induces apoptosis

in human breast cancer cells. *Current cancer drug targets*, *9*(4), 469-481.

Panno, M. L., Giordano, F., Rizza, P., Pellegrino, M., Zito, D., Giordano, C., & Andò, S. (2012). Bergapten induces ER depletion in breast cancer cells through SMAD4-mediated ubiquitination. *Breast cancer research and treatment*, *136*, 443-455.

Park, C. H., Yeo, H. J., Park, Y. J., Morgan, A. M., Valan Arasu, M., Al-Dhabi, N. A., & Park, S. U. (2017). Influence of indole-3-acetic acid and gibberellic acid on phenylpropanoid accumulation in common buckwheat (Fagopyrum esculentum Moench) sprouts. Molecules, 22(3), 374.

Parvez, M. K., Al‐Dosari, M. S., Alam, P., Rehman, M., Alajmi, M. F., & Alqahtani, A. S. (2019). The anti‐hepatitis B virus therapeutic potential of anthraquinones derived from Aloe vera. *Phytotherapy research*, *33*(11), 2960-2970.

Patel, D., Shah, Y., Thakkar, N., Shah, K., & Shah, M. (2020). Implementation of artificial intelligence techniques for cancer detection. *Augmented Human Research*, *5*, 1-10.

Pattayil, L., & Balakrishnan-Saraswathi, H. T. (2019). In vitro evaluation of apoptotic induction of butyric acid derivatives in colorectal carcinoma cells. *Anticancer research*, *39*(7), 3795-3801.

Peng, C. L., Lai, P. S., Lin, F. H., Wu, S. Y. H., & Shieh, M. J. (2009). Dual chemotherapy and photodynamic therapy in an HT-29 human colon cancer xenograft model using SN-38-loaded chlorin-core star block copolymer micelles. *Biomaterials*, *30*(21), 3614-3625.

Peroutka, R., Schulzová, V., Botek, P., & Hajšlová, J. (2007). Analysis of furanocoumarins in vegetables (Apiaceae) and citrus fruits (Rutaceae). *Journal of the Science of Food and Agriculture*, *87*(11), 2152-2163.

Pinheiro, S. L., Bonadiman, A. C., Borges Lemos, A. L. D. A., Annicchino, B. M., Segatti, B., Pucca, D. S., ... & Leal, F. (2019). Photobiomodulation therapy in cancer patients with mucositis: A clinical evaluation. *Photobiomodulation, photomedicine, and laser surgery*, *37*(3), 142-150.

Podolska, G., Gujska, E., Klepacka, J., & Aleksandrowicz, E. (2021). Bioactive compounds in different buckwheat species. *Plants*, *10*(5), 961.

Price, R. B., Ehrnford, L., Andreou, P., & Felix, C. A. (2003). Comparison of quartz-tungsten-halogen, light-emitting diode, and plasma arc curing lights. *composites*, *12*, 40.

Qumseya, B. J., David, W., & Wolfsen, H. C. (2013). Photodynamic therapy for Barrett's esophagus and esophageal carcinoma. *Clinical endoscopy*, *46*(1), 30-37.

R.R. Allison, K. Moghissi, Photodynamic therapy (PDT): PDT mechanisms, Clin.

Rachek LI, Yuzefovych LV, Ledoux SP, Julie NL, Wilson GL (2009) Troglitazone, but not rosiglitazone, damages mitochondrial DNA and induces mitochondrial dysfunction and cell death in human hepatocytes. Toxicol Appl Pharmacol 240:348–354

Rana, J. C., Chauhan, R. C., Sharma, T. R., & Gupta, N. (2012). Analyzing problems and prospects of buckwheat cultivation in India.

Rasch, E., & SWIFT, H. (1960). Microphotometric analysis of the cytochemical Millon reaction. *Journal of Histochemistry & Cytochemistry*, *8*(1), 4-17.

Recknagel, R. O., & Glende Jr, E. A. (1984). [40] Spectrophotometric detection of lipid conjugated dienes. In *Methods in enzymology* (Vol. 105, pp. 331-337). Academic Press.

Reed, J. C. (2000). Mechanisms of apoptosis. *The American journal of pathology*, *157*(5), 1415-1430.

Ren, R., Zeng, H., Mei, Q., Xu, Z., Mazhar, M., & Qin, L. (2022). Effects of Monascus purpureus-fermented tartary buckwheat extract on the blood lipid profile, glucose tolerance and antioxidant enzyme activities in KM mice. *Journal of Cereal Science*, *105*, 103465.

Ricci Donato, H. A., Pratavieira, S., Grecco, C., Brugnera-Junior, A., Bagnato, V. S., & Kurachi, C. (2017). Clinical comparison of two photosensitizers for oral cavity decontamination. *Photomedicine and Laser Surgery*, *35*(2), 105-110.

Rishton, G. M. (2008). Natural products as a robust source of new drugs and drug leads: past successes and present day issues. *The American journal of cardiology*, *101*(10), S43-S49.

Robinson, J. P., Suriya, K., Subbaiya, R., & Ponmurugan, P. (2017). Antioxidant and cytotoxic activity of Tecoma stans against lung cancer cell line (A549). *Brazilian Journal of Pharmaceutical Sciences*, *53*, e00204.

Rocha, L. G. B. (2016). *Development of a novel photosensitizer for photodynamic therapy of cancer* (Doctoral dissertation, Universidade de Coimbra (Portugal)).

Ruddon, R. W. (2007). *Cancer biology*. Oxford University Press.

Ruigrok, T. (2015, June). *Temperature response of duckweed growth at the Ecoferm greenhouse*.

Saba NF, Khuri FR, Shin DM. Targeting the epidermal growth factor receptor. Trials in head and neck and lung cancer. Oncology (Williston Park) 2006;20:153–61, discussion 162, 166, 169 passim.

Saini, M., Barakat, A., Qamar, Z., Shenoy, M., Alotaibi, R. J., Alotaibi, A. M., & Niazi, F. (2022). Use of photosensitizers activated by photodynamic therapy on the canal disinfection of radicular dentin bonded to Dimethacrylate-based glass fiber post: an assessment of pushout bond strength. *European Review for Medical & Pharmacological Sciences*, *26*(21).

Saneesh Babu, P. S., Manu, P. M., Dhanya, T. J., Tapas, P., Meera, R. N., Surendran, A., ... & Pillai, M. R. (2017). Bis (3, 5-diiodo-2, 4, 6-trihydroxyphenyl) squaraine photodynamic therapy disrupts redox homeostasis and induce mitochondria-mediated apoptosis in human breast cancer cells. *Scientific reports*, *7*(1), 42126.

Sanjeevan Lekshmi, R., Kodinattumkunnel Abraham, M., Madanan Anju, S., Omana Aswathy, A., Varghese, S., Nettaichuvilakom Subha, V., & George, S. (2023). Europium (III) Incorporated Bovine Serum Albumin Stabilized Gold Nanoclusters as Fluorescent Probes for the Detection of Sarcosine, a Prostate Cancer Biomarker. *ChemistrySelect*, *8*(5), e202204649.

Sarkar, T., Sahoo, S., Neekhra, S., Paul, M., Biswas, S., Babu, B. N., ... & Hussain, A. (2023). A dipyridophenazine Ni (II) dithiolene complex as a dual-acting cancer phototherapy agent activatable within the

phototherapeutic window. *European Journal of Medicinal Chemistry*, *261*, 115816.

Saxena, M., van der Burg, S. H., Melief, C. J., & Bhardwaj, N. (2021). Therapeutic cancer vaccines. *Nature Reviews Cancer*, *21*(6), 360-378.

Schulz, J. B., Lindenau, J., Seyfried, J., & Dichgans, J. (2000). Glutathione, oxidative stress and neurodegeneration. *European journal of biochemistry*, *267*(16), 4904-4911.

Shahinuzzaman, M., Akhtar, P., Amin, N., Ahmed, Y., Anuar, F. H., Misran, H., & Akhtaruzzaman, M. (2021). New insights of phenolic compounds from optimized fruit extract of Ficus auriculata. *Scientific Reports*, *11*(1), 12503.

Shia, C. S., Juang, S. H., Tsai, S. Y., Chang, P. H., Kuo, S. C., Hou, Y. C., & Chao, P. D. L. (2009). Metabolism and pharmacokinetics of anthraquinones in Rheum palmatum in rats and ex vivo antioxidant activity. *Planta medica*, *75*(13), 1386-1392.

Siegel, R. L., Kratzer, T. B., Giaquinto, A. N., Sung, H., & Jemal, A. (2025). Cancer statistics, 2025. *CA: A Cancer Journal for Clinicians*.

Simone, C. B., Friedberg, J. S., Glatstein, E., Stevenson, J. P., Sterman, D. H., Hahn, S. M., & Cengel, K. A. (2012). Photodynamic therapy for the treatment of non-small cell lung cancer. *Journal of thoracic disease*, *4*(1), 63.

Singh, B., & Sharma, R. A. (2023). Updated review on Indian Ficus species. *Arabian Journal of Chemistry*, *16*(8), 104976.

Sitki Copur, M. (2019). State of Cancer Research Around the Globe. *Oncology (08909091)*, *33*(5).

Soltanian, S., Mohamadi, N., Rajaei, P., Khodami, M., & Mohammadi, M. (2019). Phytochemical composition, and cytotoxic, antioxidant, and antibacterial activity of the essential oil and methanol extract of Semenovia suffruticosa. *Avicenna journal of phytomedicine*, *9*(2), 143.

Sonar, A., Amre, B., Advankar, Y., Babar, S., & Furia, T. M. (2021). Calibration of Lux Meter Using Comparison Method. *International Journal of Engineering Research & Technology*, *9*, 720-4.

Soni, A., & Sosa, S. (2013). Phytochemical analysis and free radical scavenging potential of herbal and medicinal plant extracts. *Journal of Pharmacognosy and phytochemistry*, *2*(4), 22-29.

Sontsa-Donhoung, A. M., Bahdjolbe, M., Hawaou, & Nwaga, D. (2022). Selecting endophytes for rhizome production, curcumin content, biocontrol potential, and antioxidant activities of turmeric (Curcuma longa). *BioMed Research International*, *2022*(1), 8321734.

Sterner, R. C., & Sterner, R. M. (2021). CAR-T cell therapy: current limitations and potential strategies. *Blood cancer journal*, *11*(4), 69.

Stojilkovski, K., Glavač, N. K., Kreft, S., & Kreft, I. (2013). Fagopyrin and flavonoid contents in common, Tartary, and cymosum buckwheat. *Journal of Food Composition and Analysis*, *32*(2), 126-130.

Stratton, M. R., Campbell, P. J., & Futreal, P. A. (2009). The cancer genome. *Nature*, *458*(7239), 719-724.

Strober, W. (1997). Trypan blue exclusion test of cell viability. *Current protocols in immunology*, *21*(1), A-3B.

Sumiyoshi, M., Sakanaka, M., Taniguchi, M., Baba, K., & Kimura, Y. (2014). Anti-tumor effects of various furocoumarins isolated from the roots, seeds and fruits of Angelica and Cnidium species under ultraviolet A irradiation. *Journal of natural medicines*, *68*, 83-94.

Sun, C. Y., Young, G. H., Hsieh, Y. T., Chen, Y. H., Wu, M. S., Wu, V. C., & Lee, C. C. (2015). Protein-bound uremic toxins induce tissue remodeling by targeting the EGF receptor. *Journal of the American Society of Nephrology*, *26*(2), 281-290.

Sung, H., Ferlay, J., Siegel, R. L., Laversanne, M., Soerjomataram, I., Jemal, A., & Bray, F. (2021). Global cancer statistics 2020: GLOBOCAN estimates of incidence and mortality worldwide for 36 cancers in 185 countries. *CA: a cancer journal for clinicians*, *71*(3), 209-249.

Sytar, O., Kotta, K., Valasiadis, D., Kosyan, A., Brestic, M., Koidou, V., & Hilioti, Z. (2021). The effects of photosensitizing dyes fagopyrin and hypericin on planktonic growth and multicellular life in budding yeast. *Molecules*, *26*(16), 4708.

Sytar, O., Švedienė, J., Ložienė, K., Paškevičius, A., Kosyan, A., & Taran, N. (2016). Antifungal properties of hypericin, hypericin tetrasulphonic

acid and fagopyrin on pathogenic fungi and spoilage yeasts. *Pharmaceutical Biology*, *54*(12), 3121-3125.

Tang, P. M. K., Chan, J. Y. W., Au, S. W. N., Kong, S. K., Tsui, S. K. W., Waye, M. M. Y., & Fung, K. P. (2006). Pheophorbide a, an active compound isolated from Scutellaria barbata, possesses photodynamic activities by inducing apoptosis in human hepatocellular carcinoma. *Cancer biology & therapy*, *5*(9), 1111-1116.

Tang, P. M. K., Liu, X. Z., Zhang, D. M., Fong, W. P., & Fung, K. P. (2009). Pheophorbide a based photodynamic therapy induces apoptosis via mitochondrial-mediated pathway in human uterine carcinosarcoma. *Cancer biology & therapy*, *8*(6), 533-539.

Tavčar Benković, E., & Kreft, S. (2015). Fagopyrins and protofagopyrins: Detection, analysis, and potential phototoxicity in buckwheat. *Journal of agricultural and food chemistry*, *63*(24), 5715-5724.

Theurer, C., Gruetzner, K. I., Freeman, S. J., & Koetter, U. (1997). In vitro phototoxicity of hypericin, fagopyrin rich, and fagopyrin free buckwheat herb extracts. *Pharmaceutical and Pharmacological Letters*, *7*(2), 113-115.

Thurow, T. (2012). Effect of chlorogenic acid and neochlorogenic acid on human colon cancer cells.

Tortora G, Caputo R, Damiano V, et al. Oral administration of a novel taxane, an antisense oligonucleotide targeting protein kinase A, and the epidermal growth factor receptor inhibitor Iressa causes cooperative antitumor and antiangiogenic activity. Clin Cancer Res 2001;7:4156–63.

Tracey, M. V., & Paech, K. (Eds.). (1955). *Modern methods of plant analysis*. Springer.

Trease, G. E., & Evans, W. C. (1983). *Pharmacognosy*.

Tsai, M. J., Chang, W. A., Jian, S. F., Chang, K. F., Sheu, C. C., & Kuo, P. L. (2018). Possible mechanisms mediating apoptosis of bronchial epithelial cells in chronic obstructive pulmonary disease–a next-generation sequencing approach. *Pathology-Research and Practice*, *214*(9), 1489-1496.

Tsai, W. H., Yu, K. H., Huang, Y. C., & Lee, C. I. (2018). EGFR-targeted photodynamic therapy by curcumin-encapsulated chitosan/TPP nanoparticles. *International journal of nanomedicine*, 903-916.

Uemura, N., Okamoto, S., Yamamoto, S., Matsumura, N., Yamaguchi, S., Yamakido, M., & Schlemper, R. J. (2001). Helicobacter pylori infection and the development of gastric cancer. *New England journal of medicine*, *345*(11), 784-789.

Upchurch, R. G., Walker, D. C., Rollins, J. A., Ehrenshaft, M., & Daub, M. E. (1991). Mutants of Cercospora kikuchii altered in cercosporin synthesis and pathogenicity. *Applied and Environmental Microbiology*, *57*(10), 2940-2945.

Valko M, Leibfritz D, Moncola J, Cronin Mark TD, Mazura M, Telser J (2007) Free radicals and antioxidants in normal physiological functions and human disease. Int J Biochem Cell Biol 39:44–84

Valko M, Morris H, Cronin MTD (2005) Metals, toxicity and oxidative stress. Curr Med Chem 12:1161–1208

Vantieghem, A., Assefa, Z., Vandenabeele, P., Declercq, W., Courtois, S., Vandenheede, J. R., & Agostinis, P. (1998). Hypericin-induced photosensitization of HeLa cells leads to apoptosis or necrosis: Involvement of cytochrome c and procaspase-3 activation in the mechanism of apoptosis. *FEBS letters*, *440*(1-2), 19-24.

Varghese, S., Madanan, A. S., Abraham, M. K., Shkhair, A. I., Indongo, G., Rajeevan, G., & George, S. (2024). Highly sensitive lanthanide complex as a probe for l‐kynurenine: A cancer biomarker. *Luminescence*, *39*(4), e4740..

Villacorta, R. B., Roque, K. F. J., Tapang, G. A., & Jacinto, S. D. (2017). Plant extracts as natural photosensitizers in photodynamic therapy: in vitro activity against human mammary adenocarcinoma MCF-7 cells. *Asian Pacific Journal of Tropical Biomedicine*, *7*(4), 358-366.

Vogelstein, B., & Kinzler, K. W. (2004). Cancer genes and the pathways they control. *Nature medicine*, *10*(8), 789-799.

Vujanović, M., Zengin, G., Đurović, S., Mašković, P., Cvetanović, A., & Radojković, M. (2019). Biological activity of extracts of traditional wild medicinal plants from the Balkan Peninsula. *South African Journal of Botany*, *120*, 213-218.

Wagner, H. (1993). Pharmazeutische Biology AUFI. 15 BN 3-437-20 498-X. *Gustav fisher Vwelag. Stuttgart. Germany*, *184*.

Wang, H. K., Hyde, K. D., Soytong, K., & Lin, F. C. (2008). Fungal diversity on fallen leaves of Ficus in northern Thailand. *Journal of Zhejiang University Science B*, *9*(10), 835-841.

Wang, H., Ewetse, M. P., Ma, C., Pu, W., Xu, B., He, P., ... & Chen, H. (2022). The "light knife" for gastric cancer: photodynamic therapy. *Pharmaceutics*, *15*(1), 101.

Wang, J. Y. J. (2001). DNA damage and apoptosis. *Cell Death & Differentiation*, *8*(11), 1047-1048.

Wang, S. W., Gao, C., Zheng, Y. M., Yi, L., Lu, J. C., Huang, X. Y., & Ke, A. W. (2022). Current applications and future perspective of CRISPR/Cas9 gene editing in cancer. *Molecular cancer*, *21*(1), 5

Wang, Y., Guan, Z., Liang, C., Liao, K., Xiang, D., Huang, J., & Chen, Q. (2022). Agronomic and metabolomics analysis of rice-Tartary buckwheat (*Fagopyrum tataricum* Gaertn) bred by hybridization. Scientific Reports, 12(1), 11986.

Warowicka, A., Popenda, Ł., Bartkowiak, G., Musidlak, O., Litowczenko-Cybulska, J., Kuźma, D., & Goździcka-Józefiak, A. (2019). Protoberberine compounds extracted from Chelidonium majus L. as novel natural photosensitizers for cancer therapy. *Phytomedicine*, *64*, 152919.

World Cancer Research Fund. (2018). Diet, Nutrition, Physical Activity and Cancer: A Global Perspective. World Cancer Research Fund International

Woźniak, M., & Nowak-Perlak, M. (2023). Hypericin-based photodynamic therapy displays higher selectivity and phototoxicity towards melanoma and squamous cell cancer compared to normal keratinocytes in vitro. *International Journal of Molecular Sciences*, *24*(23), 16897.

Woźniak, M., Nowak, M., Lazebna, A., Więcek, K., Jabłońska, I., Szpadel, K., ... & Ziółkowski, P. (2021). The comparison of in vitro photosensitizing efficacy of curcumin-loaded liposomes following photodynamic therapy on melanoma MUG-Mel2, squamous cell carcinoma SCC-25, and normal keratinocyte HaCaT cells. *Pharmaceuticals*, *14*(4), 374.

Wu, D., Liu, Z., Fu, Y., Zhang, Y., Tang, N., Wang, Q., & Tao, L. (2013). Efficacy of 2-(1-hexyloxyethyl)-2-devinyl pyropheophorbide-a in photodynamic therapy of human esophageal squamous cancer cells. *Oncology letters*, *6*(4), 1111-1119.

Xu, C. S., & Leung, A. W. N. (2009). Light-activated hypericin induces cellular destruction of nasopharyngeal carcinoma cells. *Laser Physics Letters*, *7*(1), 68.

Xu, D. D., Lam, H. M., Hoeven, R., Xu, C. B., Leung, A. W. N., & Cho, W. C. S. (2013). Photodynamic therapy induced cell death of hormone insensitive prostate cancer PC-3 cells with autophagic characteristics. *Photodiagnosis and Photodynamic Therapy*, *10*(3), 278-287.

Yaghobee, S., Pourhajibagher, M., Bahrami, R., & Isaabadi, M. (2024). Nano-emodin mediated photodynamic therapy for wound healing of donor site after free gingival graft: A parallel clinical trial. *Photodiagnosis and Photodynamic Therapy*, *45*, 103958.

Yan, T., Alimu, G., Zhu, L., Fan, H., Zhang, L., Du, Z., & Zhang, X. (2022). PpIX/IR-820 dual-modal therapeutic agents for enhanced PDT/PTT synergistic therapy in cervical cancer. *ACS omega*, *7*(49), 44643-44656.

Yang, G., Tian, J., Chen, C., Jiang, D., Xue, Y., Wang, C., & Zhang, W. (2019). An oxygen self-sufficient NIR-responsive nanosystem for enhanced PDT and chemotherapy against hypoxic tumors. *Chemical science*, *10*(22), 5766-5772.

Yang, M. Y., Chang, C. J., & Chen, L. Y. (2017). Blue light induced reactive oxygen species from flavin mononucleotide and flavin adenine dinucleotide on lethality of HeLa cells. *Journal of Photochemistry and Photobiology B: Biology*, *173*, 325-332.

Yang, T., Tan, Y., Zhang, W., Yang, W., Luo, J., Chen, L., & Lei, X. (2020). Effects of ALA-PDT on the healing of mouse skin wounds infected with Pseudomonas aeruginosa and its related mechanisms. *Frontiers in cell and developmental biology*, *8*, 585132.

Yang, Y., Wang, L., Cao, H., Li, Q., Li, Y., Han, M., & Li, J. (2019). Photodynamic therapy with liposomes encapsulating photosensitizers with aggregation-induced emission. *Nano letters*, *19*(3), 1821-1826.

Yasuma, A., & Ichikawa, T. (1953). Ninhydrin-Schiff and alloxan-Schiff staining: a new histochemical staining method for protein. *The Journal of laboratory and clinical medicine*, *41*(2), 296-299.

Zajičková, T., Horváthová, E., Kyzek, S., Šályová, E., Túryová, E., Ševčovičová, A., & Gálová, E. (2022). Comparison of cytotoxic, genotoxic, and DNA-protective effects of skyrin on cancerous vs. non-cancerous human cells. *International Journal of Molecular Sciences*, *23*(10), 5339.

Zhang, L., Li, X., Ma, B., Gao, Q., Du, H., Han, Y., & Qiao, Z. (2017). The tartary buckwheat genome provides insights into rutin biosynthesis and abiotic stress tolerance. Molecular plant, 10(9), 1224-1237.

Zhang, Q., Li, Z. H., Li, Y. Y., Shi, S. J., Zhou, S. W., Fu, Y. Y., & Lu, L. C. (2015). Hypericin-photodynamic therapy induces human umbilical vein endothelial cell apoptosis. *Scientific reports*, *5*(1), 18398.

Zhang, Y., Su, Y., Tang, Y., Qin, L., Shen, Y., Wang, B., & Zhang, M. (2022). Comparative study of topical 5-aminolevulinic acid photodynamic therapy (5-ALA-PDT) and surgery for the treatment of high-grade vaginal intraepithelial neoplasia. *Photodiagnosis and Photodynamic Therapy*, *39*, 102958.

Zhang, Y., Wang, D., Liao, C., Liu, X., Zhang, L., Wang, P., & Wang, X. (2024). Curcumin-mediated photodynamic therapy for mild to moderate Acne: A self-controlled split-face randomized study. *Photodiagnosis and Photodynamic Therapy*, *45*, 103887.

Zhao, B., & He, Y. Y. (2010). Recent advances in the prevention and treatment of skin cancer using photodynamic therapy. *Expert review of anticancer therapy*, *10*(11), 1797-1809.

Zupko, I., Kamuhabwa, A. R., D'Hallewin, M. A., Baert, L., & De Witte, P. A. (2001). In vivo photodynamic activity of hypericin in transitional cell carcinoma bladder tumors. *International journal of oncology*, *18*(5), 1099-1105.